N72-25128
NASA CR-112048

A STUDY OF PILOT MODELING IN MULTI-CONTROLLER TASKS

By: Richard F. Whitbeck and James R. Knight

CAL No. IH-3037-J-1

Prepared For:

Theoretical Mechanics Branch
Langley Research Center
National Aeronautics and Space Administration
Langley Station
Hampton, Virginia 23365

FINAL REPORT
Contract No. NAS-1-10514
March 1972

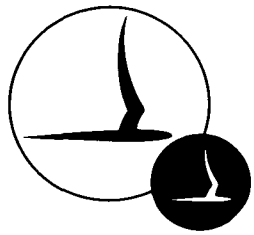

CORNELL AERONAUTICAL LABORATORY, INC.
BUFFALO, NEW YORK 14221

A STUDY OF PILOT MODELING IN MULTI-CONTROLLER TASKS

By: Richard F. Whitbeck and James R. Knight

FINAL REPORT
CAL Report No. IH-3037-J-1
Contract No. NAS-1-10514
March 1972

Prepared For:

Theoretical Mechanics Branch
Langley Research Center
National Aeronautics and Space Administration
Langley Station
Hampton, Virginia 23365

1. Report No.	2. Government Accession No.	3. Recipient's Catalog No.
NASA CR-112048		

4. Title and Subtitle	5. Report Date
A Study of Pilot Modeling in Multi-Controller Tasks	March 1972
	6. Performing Organization Code
7. Author(s)	8. Performing Organization Report No.
Richard F. Whitbeck and James R. Knight	IH-3037-J-1
	10. Work Unit No.
9. Performing Organization Name and Address	11. Contract or Grant No.
Cornell Aeronautical Laboratory, Inc. Buffalo, New York 14221	NAS-1-10514
	13. Type of Report and Period Covered
12. Sponsoring Agency Name and Address	Contractor Report
National Aeronautics and Space Administration Langley Station Hampton, Virginia 23365	14. Sponsoring Agency Code

15. Supplementary Notes

16. Abstract

A modeling approach, which utilizes a matrix of transfer functions to describe the human pilot in multiple input, multiple output control situations, is studied. The approach used was to extend a well established scalar Wiener-Hopf minimization technique to the matrix case and then study, via a series of experiments, the data requirements when only finite record lengths are available. One of these experiments was a two-controller roll tracking experiment designed to force the pilot to use rudder in order to coordinate and reduce the effects of aileron yaw.

One model was computed for the case where the signals used to generate the spectral matrix are error and bank angle while another model was computed for the case where error and yaw angle are the inputs. In general, the differences between these two models are significant.

Several anomalies were observed to be present in the experimental data. These are defined by the descriptive terms "roll up", "break up" and "roll down". Due to these algorithm induced anomalies, the frequency band over which reliable estimates of power spectra can be achieved is considerably less than predicted by the sampling theorem.

17. Key Words (Suggested by Author(s))	18. Distribution Statement
Pilot modeling Matrix model Spectral estimation	Unclassified - Unlimited

19. Security Classif. (of this report)	20. Security Classif. (of this page)	21. No. of Pages	22. Price*
Unclassified	Unclassified	135	

*For sale by the Clearinghouse for Federal Scientific and Technical Information
Springfield, Virginia 22151

TABLE OF CONTENTS

LIST OF ILLUSTRATIONS

LIST OF ILLUSTRATIONS (Cont.)

LIST OF ILLUSTRATIONS (Cont.)

LIST OF TABLES

SYMBOLS USED IN THIS REPORT

δ_a	Aileron displacement
δ_r	Rudder displacement
$\Delta\theta$	Incremental pitch angle
$\Delta\dot{\theta}$	Incremental pitch rate
ϕ	Roll angle
ψ	Yaw angle
ϕ_{XY}	Cross spectra between X and Y
ϕ_{XX}	Auto spectra between X and Y
$\hat{\phi}_{XY}$	Estimate of Cross Spectra between X and Y
$\hat{\phi}_{XX}$	Estimate of Auto Spectra between X and X
n	Noise or disturbance input
N	Noise or disturbance input
D	Reference, noise or disturbance input
R	Reference input
$W(s)$	Transfer function (may be a matrix)
$G(s)$	Transfer function
$H(s)$	Transfer function (may be a matrix)
$W_* = W'(-s)$	Transpose of W with S replaced by -S
M	A matrix or vector which depends on S
$\Phi_{(M_*,M)}$	A scalar which depends on $M(s)$ and $M'(-s)$

1. INTRODUCTION

The subject of this report is a modeling approach which utilizes a matrix of transfer functions to describe the human pilot in multiple input, multiple output control situations. It offers a theoretically consistent technique for measuring pilot activity without a priori specifying a heirarchy of sequential single (scalar) loop closures. That is, the approach is theoretically capable of operating on the available data and generating estimates of transfer functions that can be used to decide which of the pilot's loop closures are most important.

It was our intent that this modeling technique should be versatile enough to be applied to direct in-flight measurements. This requires that the model should yield reasonable results given:

1. the pilot is simultaneously manipulating more than one control in an active manner (e.g., elevator, rudder and aileron in the landing task);
2. realistic in-flight disturbances (e.g., turbulence). This dictates the use of stochastic input signals as opposed to random appearing deterministic outputs (which have no variability).
3. finite lengths of data (e.g., a landing approach may be on the order of 2 minutes).

The approach used was to extend a well established scalar Wiener Hopf minimization technique to the matrix case (a routine mathematical exercise) and then study, via a series of experiments, the data requirements when only finite record lengths are available. The experiments were four in number:

1. Identify a known network in a single input-single output task.
2. Identify a human pilot response in a single input-single output task with the controlled element $K/_S 2$. The purpose of this experiment is to check on the degree of correlation with previous results (Reference 1).
3. Identify pilot responses in a series of experiments in which the controlled element is representative of lateral response of an aircraft. The roll response time constant and the dutch roll mode characteristics were prescribed in a manner that forced a two controller task involving both the aileron and rudder. A fixed base simulator was used to obtain the necessary data.
4. Identify pilot response in the six-degree-of-freedom experiments performed under NASA Contract NAS1-8765.

In the first experiment, an instrument rated pilot flew a single controller (aileron) roll tracking experiment in which the controlled open loop dynamics were defined by $\frac{K}{S(S+2)}$.

In the second single controller experiment, the "pilot" was an analog model consisting of a linear transfer function with an added "remnant" term (the "remnant" term contained appreciable power relative to the power in the disturbance input). The open loop control dynamics were $K/S2$. The problem here is simply one of estimating the linear portion of the pilot model when it is assumed that the remnant is an unmeasurable variable. This experiment also afforded an excellent opportunity to study the problems associated with estimating the $K/S2$ control dynamics when the input power spectra varied over a dynamic range on the order of 60 dB on a power basis (120 dB on a voltage ratio basis).

The third experiment presents the opportunity to work with finite lengths of data which should, in some sense, be typical of multicontroller data. It thus affords the opportunity to examine the practical problems associated with the vector approach. As we shall see, the greatest problem is one of acquiring power spectra estimates suitable for "factorizing" a spectral matrix.

The controlled dynamics in this experiment were limited six degree-of-freedom equations of motion which permit a limited variation in velocity and altitude. The coefficients used represented a T-33 at 250 KIAS at 23000 feet while the information displayed was

1. bank angle (roll tracking error)
2. roll rate
3. pitch angle
4. pitch rate
5. sideslip angle
6. yaw rate
7. altitude
8. rate of climb
9. indicated airspeed
10. lateral acceleration without lateral "g" term
11. heading angle

This roll tracking experiment was designed to force the pilot to use rudder in order to coordinate and reduce the effects of aileron yaw.

The reason for including the fourth experiment in the present study was to use a large collation of data from a previous experiment (Reference 2) in order to estimate transfer functions for an ILS landing task.

In this previous study, four pilots performed on ILS landing approach three times for each of fifteen different aircraft configurations. However, as the present study progressed and the necessity for ensemble averaging across a "reasonable" number of estimates became clearer, it also became apparent that false impressions could be created if the fourth experiment were carried out. That is, the number of runs necessary for the ensemble averaging could only be obtained by lumping different pilots and different configurations together. For this reason, our efforts have been restricted to the first three experiments.

The report is organized in the following manner. In the second section, a derivation of the matrix modeling approach is presented, together with some illustrative examples to illustrate the type of data processing which is required.

A brief overview of the problems encountered in the estimation of power spectra, using finite length of data, is given in Section 3. In particular, several anomalies we have observed to be present in our experimental data are identified and defined by the descriptive terms "roll up", "break up" and "roll down". In this section, a theoretical base is established for a set of analytical analyses, later carried out in Appendix B, which conclusively demonstrate the presence of the aforementioned anomalies. The experimental evidence of their existence is presented in Section 4. It is shown that the frequency band over which reliable estimates of power spectra can be achieved is considerably less than predicted by the sampling theorem.

In addition, the fourth section applies the results of Section 3 to Experiments 1 and 2. It is shown that a particular combination of time domain filtering and frequency domain ensemble averaging produces an appreciable improvement in the spectral estimates.

The fifth section is concerned with Experiment 3, the two controller roll tracking task. The application of the matrix modeling approach to the analysis of the data is discussed and estimates of pilot transfer functions are presented. The dynamic ranges of the spectra encountered in the roll tracking task are an order of magnitude greater than encountered in the scalar task and consequently, there is a further reduction in the useful frequency band over which reliable estimates can be achieved.

The main body of the report concludes with a summary and conclusions section. In addition, much of the detailed material (e.g., proofs and examples) tangential to the main thrust of the report, but still important enough to document, are discussed in appendices.

This report serves two different classes of readers. The first class are, of course, those members of the manual control community who would like to overview this matrix approach to modeling in order to see what advantages and disadvantages it has relative to other techniques (such as preordaining the form of the pilot model and then estimating several parameters). The second class of readers are those who are interested in the basic problem of estimating auto and cross spectral densities using finite lengths of data. This class of reader need focus their attention primarily on Sections 3 and 4.

2. PILOT MODELING USING THE WIENER-HOPF METHOD

2.1 Introduction

Before considering the application of the Wiener-Hopf (W-H) method to the pilot modeling task, a brief overview of a variational method for deriving W-H equations will first be given, together with an illustrative example to demonstrate the approach.

After this, the variational method will be applied to the pilot modeling task and some clarifying comments will be made. An illustrative example demonstrates how the W-H equation can be solved using only experimental data (e.g., data taken from Bode plots). This example will also make it quite clear, that although the W-H technique is a "free minimization" approach in theory, in practice one is forced into making assumptions about the form and/or order of the model.

2.2 A Variational Method for Deriving W-H Equations

Consider any performance index of a form which is readily translated from the time domain to the frequency domain via the use of Parseval's theorem. For example, using two-sided LaPlace notation,

$$\int_{-\infty}^{\infty} x(t)\, y(t)\, dt = \frac{1}{2\pi j} \int_{-j\infty}^{j\infty} X(-s)\; Y(s)\, ds$$

is a typical scalar relationship that extends naturally, in the vector case, to

$$\int_{-\infty}^{\infty} x'(t)\, y(t)\, dt = \frac{1}{2\pi j} \int_{-j\infty}^{j\infty} X'(-s)\, Y(s)\, ds \quad ,$$

where $x(t)$ is an m dimensional (column) vector and x' is an m dimensional (row) vector (the transpose of x). More generally, let the performance index be represented by

$$J = \frac{1}{2\pi j} \int_{-j\infty}^{j\infty} \Phi(M_*, M)\, ds \tag{2.1}$$

where

$$M = M(s) \qquad \text{(a vector)} \tag{2.2}$$

$$M_* = M'(-s) \qquad \text{("conjugate" transpose of } M \text{)}$$

The Wiener-Hopf equation that defines the value of the vector M which minimizes Equation (2.1) is the vector equation

$$\frac{\partial \Phi}{\partial M_*} = \bar{Z}(s) \tag{2.3}$$

where Φ is a scalar and $\bar{Z}$ is a vector which is required to give rise to functions of time which exist only for negative time.* In general, it is possible for M to be a matrix instead of a vector, in which case Equation (2.3) is written as

$$\nabla_{M_*} \Phi = \bar{Z}(s) \tag{2.4}$$

where ∇ represents the gradient of Φ with respect to the matrix M_* and $\bar{Z}$ is now a matrix instead of a vector. In the event M_* is a matrix, differentiation with respect to a matrix is defined as follows. Suppose

$$\Phi = X_* H_* Y \ . \tag{2.5}$$

Then

$$\nabla_{H_*} \Phi = X'_* Y' = X(-s)\, Y'(s) \tag{2.6}$$

is a $n \times p$ matrix if X is a vector of dim n, Y is a vector of dim p, and H is a matrix of dim $n \times p$.

Example 1 - Let X be of dimension 3 and Y of dimension 2

$$\Phi = X_* H_* Y = \begin{bmatrix} X_1(-s) & X_2(-s) & X_3(-s) \end{bmatrix} \begin{bmatrix} H_{11}(-s) & H_{21}(-s) \\ H_{12}(-s) & H_{22}(-s) \\ H_{13}(-s) & H_{23}(-s) \end{bmatrix} \begin{bmatrix} Y_1(s) \\ Y_2(s) \end{bmatrix} \tag{2.7}$$

---

*This result is a straightforward extension of the scalar result given in Reference 3.

so that

$$\nabla_{H*}\,\Phi = X(-s)\,Y'(s) = \begin{bmatrix} X_1(-s) \\ X_2(-s) \\ X_3(-s) \end{bmatrix} \begin{bmatrix} Y_1(s) & Y_2(s) \end{bmatrix} = \left|\begin{array}{c|c} X_1(-s)\,Y_1(s) & X_1(-s)\,Y_2(s) \\ \hline X_2(-s)\,Y_1(s) & X_2(-s)\,Y_2(s) \\ X_3(-s)\,Y_1(s) & X_3(-s)\,Y_2(s) \end{array}\right| \tag{2.8}$$

One more case is of interest. Suppose

$$\Phi = X_* H_* H\, Y \tag{2.9}$$

then

$$\nabla_{H*}\,\Phi = X'_*\,(H\,Y)' = X(-s)\,Y'(s)\,H'(s) \tag{2.10}$$

Equations (2.9) and (2.10) usually represent the appropriate minimization condition in the pilot modeling task while Equations (2.3) and (2.4) are typical of conditions frequently used in modern control theory. Before proceeding to the application of (2.9) and (2.10) (in the next subsection), Equations (2.3) and (2.4) will be used to demonstrate the derivation of the W-H equation for the optimal regulator problem.

Example 2 - Consider the optimal regulator problem for which the performance index is

$$J = \int_0^\infty (x'\,Q\,x + u'\,R\,u)\,dt = \frac{1}{2\pi j}\int_{-j\infty}^{j\infty} \left[X'(-s)\,Q\,X(s) + U'(-s)\,R\,U(s)\right]\,ds \tag{2.11}$$

and the state equation is

$$\dot{x} = F\,x + G\,u^{\dagger} \tag{2.12}$$

---

† If, in addition, the equation $Y = Hx$ is employed, $Q \longrightarrow H'\,Q\,H$.

where x is a vector of dimension n

u is a vector of dimension p

Q is a $n \times n$ matrix

R is a $p \times p$ matrix

In this example, one wishes to find the optimal controller, so that

$$\Phi = X_* Q X + U_* R U \tag{2.13}$$

Before $\nabla_{U_*} \Phi$ is found, X and X_* must be eliminated from Equation (2.13). This done by transforming Equation (2.12) and solving for $X(s)$:

$$X(s) = \left[I S - F\right]^{-1} G\, U(s) + \left[I S - F\right]^{-1} x(0) \quad . \tag{2.14}$$

More simply,

$$X(s) = W(s) U(s) + B(s)\, x(0) \quad . \tag{2.15}$$

Equation (2.13) becomes

$$\Phi = \left[U_* W_* + x'(0) B_*\right] Q \left[W U + B x(0)\right] + U_* R U \tag{2.16}$$

Using Equation (2.4),

$$\frac{\partial \Phi}{\partial U_*} = W_* Q \left[W U + B x(0)\right] + R U = Z(s) \tag{2.17}$$

or

$$\left[R + W_* Q W\right] U(s) + W_* Q B x(0) = Z(s) \tag{2.18}$$

Equation (2.18) is the correct W-H equation, the solution of which defines the optimal control $U_0(s)$. In Equation (2.18), U_0 is a px1 vector and the spectral matrix $[R + W_* Q W]$ is a pxp matrix. Solving Equation (2.18) is vastly more complex than solving a scalar W-H problem

because, in the classical approach, the spectral matrix must be factorized into the product of two matrices, one which is analytic in the left hand plane, the other analytic in the right half plane. Algebraic techniques for solving Equation (2.18), without recourse to spectral factorization, are given in Reference 4. More general approaches can be found in References 5 and 6.

2.3 Matrix Pilot Model

In order to identify the pilot's "primary loop closures" for a complex piloting task such as an ILS Landing, it is proposed to model the pilot as a matrix of transfer functions plus additive "remnant" terms. By doing this, we expected to obtain analytical insight as to just how the pilot closes the feedback loops on the state variables (e.g., θ , $\dot{\theta}$, etc.) which define the physical entities he senses and, hopefully, get some idea as to which tasks are most important to him.

Suppose, for illustrative purposes, that an aircraft is performing an ILS approach, and its motion is restricted to that localizer plane for which $\Delta y = 0$. That is, consider only the longitudinal dynamics of the aircraft with "outer" position loops in altitude and distance covered along a line centered on the runway, (Δz) and (Δx) respectively. In this case, the state vector, x , can be represented as a vector with six components

$$x' = \left[\Delta\dot{x} \,|\, \Delta x \,|\, \Delta\dot{\theta} \,|\, \Delta\theta \,|\, \Delta\dot{z} \,|\, \Delta z\right] \tag{2.19}$$

Further, suppose that the use of two controllers is considered, so that the control vector has two components,

$$u' = \left[\Delta\delta_e \,|\, \Delta\delta_T\right] \tag{2.20}$$

where $\Delta\delta_e$ represents the elevator deflections and $\Delta\delta_T$ represents the throttle variation. Let the aircraft dynamics be described in first order form as

$$\begin{aligned} \dot{x} &= Fx + Gu + n(t) \\ Y &= Wx \end{aligned} \tag{2.21}$$

where $n(t)$ is an n dimensional vector which represents the noise input to the system (e.g., turbulence).

The operation $Y = WX$ can be thought of as selecting and/or combining those states which are either displayed or sensed by the pilot. As an example, consider single axis compensatory tracking task in which the controlled element is K/s^2 and there is a reference input R .

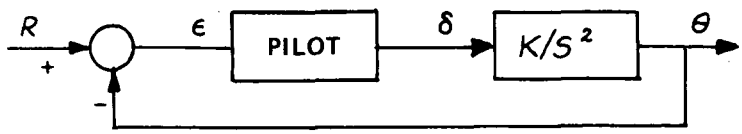

Figure 1.1 SCALAR TASK

Here the only physical entity displayed to the pilot is the error, the difference between the reference input and the output θ . This problem is easily reformulated in terms of Equation (2.21) by setting up the system

$$\begin{bmatrix} \dot{x} \\ \hline \dot{r} \end{bmatrix} = \left[\begin{array}{c|c} F_{11} & 0 \\ \hline 0 & F_{22} \end{array}\right] \begin{bmatrix} x \\ \hline r \end{bmatrix} + \begin{bmatrix} G \\ \hline 0 \end{bmatrix} U + \begin{bmatrix} n(t) \\ \\ 0 \end{bmatrix} \tag{2.22}$$

Here the $Y = WX$ operator would select only one component of the x vector and one component of the r vector to display to the pilot.

Returning to the ILS approach problem, the $Y = WX$ operator would be used to convert $\Delta\dot{x}$, Δx , $\Delta\dot{z}$ and Δz to a glideslope and localizer input for the pilot.

The entire pilot/aircraft combination can now be represented by the combination depicted in Figure 1.2 (in Figure 1.2, $N(s)$ is $[\alpha \quad n(t)]$, the disturbance input; $X(s)$ is the aircraft state vector, $U(s)$ is the control vector, $Y(s)$ is the pilot excitation vector).

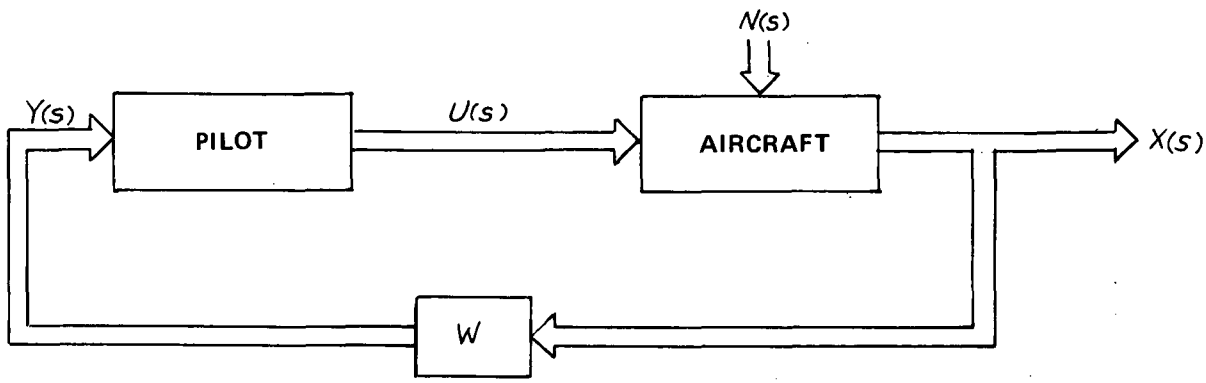

Figure 1.2 CLOSED-LOOP PILOT-AIRCRAFT COMBINATION

To employ the matrix model technique, replace the pilot in Figure 2 by a matrix of physically realizable transfer functions, $H(s)$, and an additive "remnant" vector $r(t)$; $r(t)$ must have the property that when it is added to the output of the matrix of transfer functions, the total output continues to be the same as the pilot output, namely, $u(t)$.

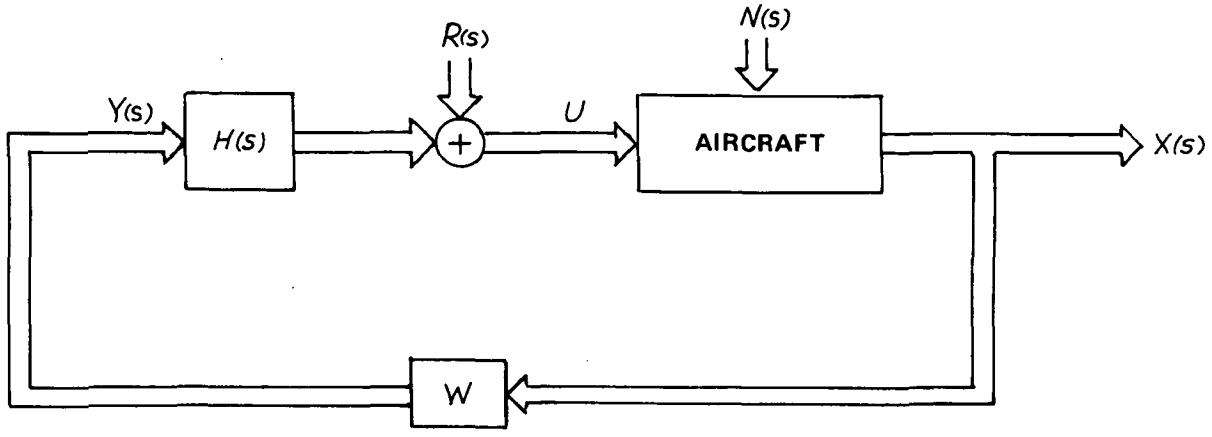

Figure 1.3 PILOT REPLACED BY MATRIX AND A "REMNANT"

It is now reasonable to ask that the matrix of transfer functions be selected in such a manner that the smallest remnant vector possible will have to be added in order that the output of the pilot model agrees with the pilot's true output. To be specific, it is required that the vector R be as small as possible in a mean square sense. The performance index is

$$J = \min_{h(t)} E\left\{r'(t)\, r(t)\right\} = \min_{H(s)} \frac{1}{2\pi j} \int_{-j\infty}^{j\infty} \Phi\, r'r \, ds \tag{2.23}$$

$$= \min_{H(s)} \frac{1}{2\pi j} \int_{-j\infty}^{j\infty} \lim_{T\to\infty} \frac{1}{2T} E\left\{R_* R\right\} ds \tag{2.24}$$

where

$$R(s) = \int_{-T}^{T} r(t)\, e^{-st}\, dt \tag{2.25}$$

and where $R = R(s)$ and $R_* = R'(-s)$. From Figure 1.3 it is clear that

$$R = U - HY$$

$$R_* = U_* - Y_* H_*$$

Assume, for simplicity of presentation, that $Y = X$ (i.e., all the states are displayed to the pilot). Then the integrand of the performance index, call it Φ, can be written as

$$\phi_{\bar{Y}Y'} W'(s) - \phi_{\bar{Y}U'} = \bar{Z} \qquad \text{where} \quad Y = WX$$

$$\Phi = \lim_{T\to\infty} \frac{1}{2T} E\left\{U_* U - U_* HX - X_* H_* U + X_* H_* HX\right\} \tag{2.26}$$

To find the matrix of transfer functions which minimizes the performance index, take the gradient of Φ with respect to H_*, take the expectation and set the result equal to the matrix $\bar{Z}(s)$. (Refer to the previous section for a summary of the technique).

$$\nabla_{H_*} \Phi = \bar{Z}(s) \tag{2.27}$$

$$\lim_{T\to\infty} \frac{1}{2\pi} \left[E\left\{X(-s)\, X'(s)\right\} H'(s) - E\left\{X(-s)\, U'(s)\right\}\right] = \bar{Z}(s) \tag{2.28}$$

$$\underset{n\times n}{\phi_{\bar{x}x'}} \underset{n\times p}{H'(s)} - \underset{n\times p}{\phi_{\bar{x}u'}} = \underset{n\times p}{\bar{Z}(s)} \tag{2.29}$$

The meaning of $\bar{Z}(s)$ is the same as in other Wiener-Hopf minimization problems -- it is a matrix such that $\mathcal{L}^{-1}\left[\bar{Z}(s)\right] = 0$ for $t \geq 0$. The solution to Equation (2.29) is standard, if we set $\phi_{\bar{x}x'} = \theta_* \theta$

$$H'(s) = \theta^{-1}\left[\theta_*^{-1}\, \phi_{\bar{x}u'}\right]_+ \tag{2.30}$$

At this point an illustrative example will be used to emphasize the fact that several options are available in setting up equations such as (2.29) (i.e., depending on which states and which control outputs are measureable). For example, suppose that two control outputs (u_1, u_2) are measurable, but that only one signal is to be displayed to the pilot. Let X be of dimension 3 and let

$$Y = \begin{bmatrix} W_{11} & o & W_{13} \end{bmatrix} \begin{bmatrix} X_1 & X_2 & X_3 \end{bmatrix}' \tag{2.31}$$

That is, the variable displayed to the pilot is a linear combination of X_1 and X_3, the X_2 variable being excluded. In this event

$$R^* R = U^* U - U^* H Y - Y^* H^* U + Y^* H^* H Y \tag{2.32}$$

so that $\nabla_{H^*} \Phi$ gives

$$\phi_{YY} H' - \begin{bmatrix} \phi_{YU_1} & \phi_{YU_2} \end{bmatrix} = \begin{bmatrix} Z_1 & Z_2 \end{bmatrix} \tag{2.33}$$

This problem reduces to the solution of two scalar W-H equations, namely

$$\left.\begin{aligned} \phi_{YY} H_1 - \phi_{YU_1} &= Z_1 \\ \phi_{YY} H_2 - \phi_{YU_2} &= Z_2 \end{aligned}\right\} \tag{2.34}$$

Here, the transfer function H_1 is indicative of the pilot's activity with controller #1 when Y is displayed to him while H_2 is indicative of his control activity with controller #2.

In contrast, if all three states were displayed, as in the previous analysis (with W being the identity matrix), then Equation (2.29) is applicable and takes the form

$$\begin{bmatrix} \phi_{x_1x_1} & \phi_{x_1x_2} & \phi_{x_1x_3} \\ \phi_{x_2x_1} & \phi_{x_2x_2} & \phi_{x_2x_3} \\ \phi_{x_3x_1} & \phi_{x_3x_2} & \phi_{x_3x_3} \end{bmatrix} \begin{bmatrix} H_{11} & H_{12} \\ H_{21} & H_{22} \\ H_{31} & H_{32} \end{bmatrix} - \begin{bmatrix} \phi_{x_1u_1} & \phi_{x_1u_2} \\ \phi_{x_2u_1} & \phi_{x_2u_2} \\ \phi_{x_3u_1} & \phi_{x_3u_2} \end{bmatrix} = \begin{bmatrix} Z_{11} & Z_{12} \\ Z_{21} & Z_{22} \\ Z_{31} & Z_{32} \end{bmatrix} \tag{2.35}$$

The transfer functions now represent more complex entities; the equations are coupled by the cross spectra terms and must be solved using factorization techniques. H_{z_1} , for example, represents the pilots number one control activity in response to the second input signal, given that he must also watch the first and third input signals.

In conclusion, we state the general result when $Y = WX$ is the vector displayed to the pilot. It is

$$\Phi[W_*' X_*' X' W'] H' - \Phi(W_*' X_*' U') = Z \tag{2.36}$$

where the dimensions of H' (and Z) are commensurate with the dimensions of $W_*' X_*' U'$.

2.4 One Method for Solving Wiener-Hopf Equations

In this section a particular method for solving vector W-H equations will be discussed. The details of the analysis will make it clear that one, in practice, is forced into making assumptions concerning the form and/or order of the model.

In order to demonstrate the method, a particular (analytic) example of a W-H equation will be given. The reader will be asked to pretend the entries of the spectral matrix and the cross-spectral vector are available only as raw data (either as Bode plots or a readout of computer data). Specifically, the intent is to demonstrate that a vector W-H equation can be solved.

(1) without factorizing the spectral matrix

(2) without explicitly knowing <u>all</u> of the entries in the spectral matrix

(3) the known entries need only be identified by experimental data. That is, <u>analytic equations</u> of the entries of the spectral matrix are not required.

To begin, suppose that a problem of interest (for example, consider a roll mode tracking task where $x_1 = \phi$, $x_2 = \dot{\phi}$, $U = \delta_A$) leads to the system configuration of Figure 1.4.

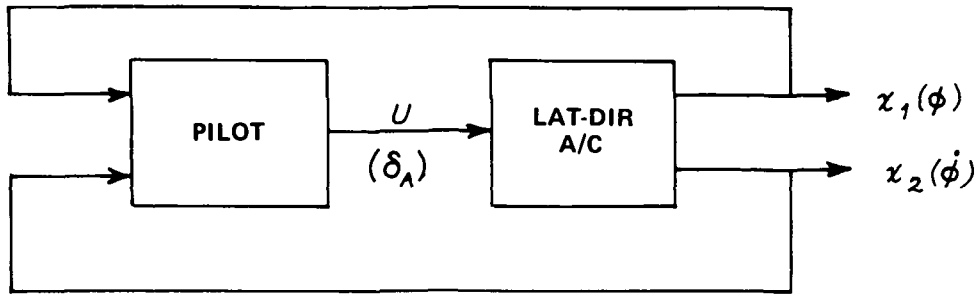

Figure 1.4 TWO-OUTPUT EXAMPLE

Since this particular illustrative problem involves two states $(\phi, \dot{\phi})$ and one controller (δ_A), the vector approach suggests that Figure 1.4 be replaced with Figure 1.5.

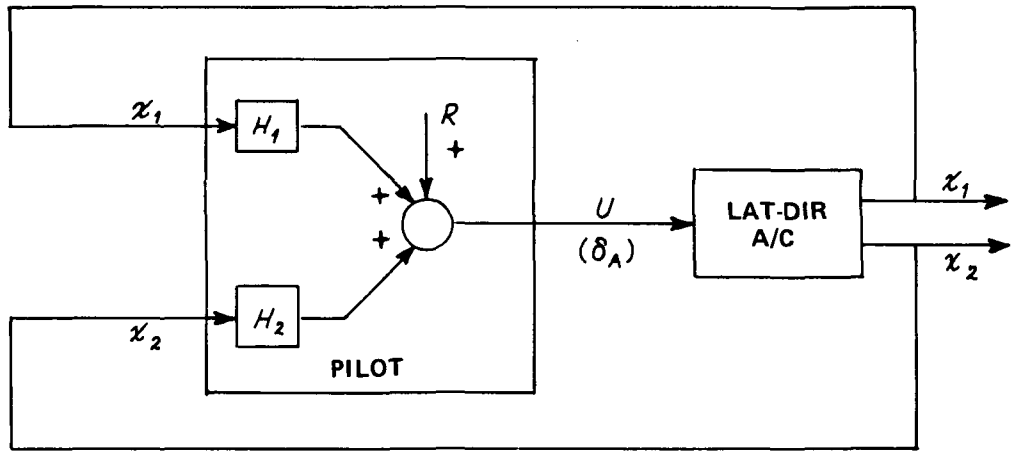

Figure 1.5 TWO-OUTPUT EXAMPLE WITH PILOT MODEL

That is, we wish to find the $H_1(s)$ and $H_2(s)$ which will, in a mean square sense, make the remnant (R) a minimum.

Suppose that an experiment has been run for which the signals x_1 , x_2 , and U were recorded. Suppose further that the various auto and cross-spectral densities have been computed, giving the W-H equation of Equation (2.36).

$$\begin{bmatrix} \frac{1}{7}(s^4-5s^2+144) & -10s \\ \hline s^4-5s^2+4 & s^4-5s^2+4 \\ \\ \frac{10s}{s^4-5s^2+4} & \frac{\frac{1}{4}(s^4-25s^2+4)}{s^4-5s^2+4} \end{bmatrix} \begin{bmatrix} H_1 \\ H_2 \end{bmatrix} - \begin{bmatrix} \frac{10s-2}{s^4-5s^2+4} \\ \\ \frac{5s^2-s}{s^4-5s^2+4} \end{bmatrix} = \begin{bmatrix} Z_1(s) \\ \\ Z_2(s) \end{bmatrix} \tag{2.36}$$

The essense of the technique is to realize that, in the linear case, determinant of the spectral matrix is a rational polynominal in $-s^2$ and that there are particular (finite) values of s for which the spectral matrix is either identically equal to zero or equal to infinity. For this particular example, the values of s which force an infinite determinant are -1, -2, 1, 2 while the zero determinant values are -3, -4, 3, 4. However, suppose these values were not known and that only experimental frequency response data, which describe $\phi_{x_1 x_1}$, $\phi_{x_1 x_2}$, etc. is given. A reasonable procedure would be to guess at the order of the rational polynominal and then generate, using the experimental data, $n+1$ equations in terms of $n+1$ unknown coefficients. If the initial guess is too low, then results which are inconsistent with the next higher order guess will be obtained. If the guess is too high, then precise pole-zero cancellation will occur, reducing the order to the correct level. This procedure is, of course, valid only if the true underlying spectra are describable by rational polynomials in s. A discussion of the difficulties that can be expected when there is error in measuring the experimental data and/or nonlinear pilot behavior is reflected in the spectra, will be deferred until section 5, where two controller experimental data is analyzed.

To illustrate this procedure, the determinant of the spectral matrix in Equation 2.36 is

$$det = \frac{1}{28}\left[\frac{s^4-25s^2+144}{s^4-5s^2+4}\right] = \frac{\frac{s^4}{112} - \frac{25}{112}s^2 + \frac{9}{7}}{\frac{s^4}{4} - \frac{5}{4}s^2 + 1} \tag{2.37}$$

Let $$det\,\phi = \frac{a_0 s^4 + a_1 s^2 + a_2}{b_0 s^4 + b_1 s^2 + 1} \tag{2.38}$$

or $$(a_0 - b_0\,det\,\phi)s^4 + (a_1 - b_1\,det\,\phi)s^2 + a_2 = det\,\phi \tag{2.39}$$

Using the experimental data, let S take on five values and generate five equations in five unknowns. For example, let

$$\left.\begin{array}{lll}
\omega = 0 & \det\phi = \frac{9}{7}, & a_2 = \frac{9}{7} \\
\omega = 1 & \det\phi = \frac{17}{28}, & a_0 - \frac{17}{28} b_0 - a_1 + \frac{17}{28} b_1 + a_2 = \frac{17}{28} \\
\omega = 2 & \det\phi = \frac{13}{56}, & 16 a_0 - \frac{16(13)}{56} b_0 - 4 a_1 + \frac{4(13)}{56} b_1 + a_2 = \frac{13}{56} \\
\omega = 3 & \det\phi = \frac{45}{13(28)}, & 81 a_0 - \frac{45(81)}{13(28)} b_0 - 9 a_1 + \frac{9(45)}{13(28)} b_1 + a_2 = \frac{45}{13(28)} \\
\omega = 4 & \det\phi = \frac{10}{119}, & 256 a_0 - \frac{256(10)}{119} b_0 - 16 a_1 + \frac{16(10)}{119} b_1 + a_2 = \frac{10}{119}
\end{array}\right\} \quad (2.40)$$

The solution to the set 2.40 gives Equation 2.37. A higher order initial guess would result in some pole-zero cancelation whereas a lower order initial polynominal would, of course, give a totally different result.

Once the poles and zeroes of the spectral determinant are known, one may proceed to solve for $H_1(s)$ and $H_2(s)$ by <u>avoiding</u> these values of S . To demonstrate this, consider in the example the second row of Equation 2.36.

$$\underbrace{\left[\frac{10S}{S^4 - 5S^2 + 4}\right]}_{\phi_{x_2 x_1}} H_1 + \underbrace{\left[\frac{\frac{1}{4}(S^4 - 25S^2 + 4)}{S^4 - 5S^2 + 4}\right]}_{\phi_{x_2 x_2}} H_2 - \underbrace{\frac{(5s^2 - s)}{S^4 - 5S^2 + 4}}_{\phi_{x_2 U}} = Z_2 \quad (2.41)$$

Recall now that the procedure is to assume that $\phi_{x_2 x_1}$, $\phi_{x_2 x_1}$ and $\phi_{x_2 U}$ are only available in the form of experimental Bode plots. For example, if one were to consider the frequency $\omega = 1$ $(S = 0 + j\,1)$, from the experimental Bode plot, we could read

$$\phi_{x_2 x_1}\Big|_{\omega=1} = 1 \angle 90^\circ = 0 + j$$

$$\phi_{x_2 x_2}\Big|_{\omega=1} = .75 \angle 0^\circ = .75 + j0$$

$$\phi_{x_2 U}\Big|_{\omega=1} = \sqrt{.26} \angle 180^\circ + \tan^{-1}\left(\frac{1}{5}\right) = -\frac{1}{2} - \frac{1}{10} j$$

The task is now to solve for $H_1(s)$ and $H_2(s)$ using only the experimental results. Knowing that the poles and zeroes of the spectral determinant are = -1, -2, 1, 2, -3, -4, 3, 4, it is possible to specify the form of H_1, H_2, Z_1 and Z_2. Equation (2.36) becomes

$$\left.\begin{aligned} \phi_{x_1 x_1}\frac{a_0 S + a_1}{(S+3)(S+4)} + \phi_{x_1 x_2}\frac{(b_0 S + b_1)}{(S+3)(S+4)} - \phi_{x_1 U} &= \frac{c_0 S + c_1}{(-S+1)(-S+2)} \\ \phi_{x_2 x_1}\frac{a_0 S + a_1}{(S+3)(S+4)} + \phi_{x_2 x_2}\frac{b_0 S + b_1}{(S+3)(S+4)} - \phi_{x_2 U} &= \frac{d_0 S + d_1}{(S+1)(-S+2)} \end{aligned}\right\} \quad (2.42)$$

That is, the physical fact that H_1 and H_2 must have left half plane poles while Z_1 and Z_2 must have all right half plane poles lead to the formulation given in Equation (2.42). H_1, H_2, Z_1, and Z_2 are characterized by numerators which are at least one order less than their denominators (if this were not so, the performance index would "blow up"). The poles of H_1 and H_2 are the left half plane zeroes of the spectral determinant while the poles of Z_1 (and Z_2) are the right half plane poles of the spectral determinant.

One may now pick two values of frequency (for example, $S = j$, $2j$ which is equivalent to $\omega = 1, 2$) and obtain eight equations in the eight unknown coefficients. Recall that each value of S will give two equations in terms of the eight unknowns when real is equated to real and imaginary is equated to imaginary. For example, let $S = j$ in the first of the equations of the set 2.42 and equate real to real, imaginary to imaginary:

$$-a_0 + \frac{3}{4}b_1 + c_1 + 4c_0 = -4.8 \quad (2.43)$$

$$a_1 + \frac{3}{4}b_0 + c_0 - 4c_1 = -4.6 \quad (2.44)$$

Solving eight equations in eight unknowns, one finds

$$H_1 = \frac{.7S - 2.8}{(S+3)(S+4)} \tag{2.45}$$

$$H_2 = \frac{-2.2S - 2.4}{(S+3)(S+4)} \tag{2.46}$$

$$Z_1 = \frac{.1S - 1.4}{(-S+1)(-S+2)} \tag{2.47}$$

$$Z_2 = \frac{-.55S - .1}{(-S+1)(-S+2)} \tag{2.48}$$

To summarize, by means of an illustrative example, it has been demonstrated that a vector W-H equation can be solved without recourse to factorizing the spectral matrix and in addition, requires only experimentally derived data for the entries of the spectral matrix. Thus it is not necessary to fit analytical expressions to the entries of the spectral matrix. However, it is also clear that the determinant of the spectral matrices must be a rational polynominal in $-S^2$ for this technique to work and therefore the form of model has, in some sense, been preordained. The deviations from this linear model due to the use of experimental data, obtained with a pilot in the loop, are largely unknown entities for the multi controller case. This facet of the problem will be explored in section 5, where the factorization algorithm will be applied to two controller roll tracking data.

3. ESTIMATION OF POWER SPECTRA USING FINITE RECORD LENGTHS

3.1 Introduction

The theory of the previous section was based on ideal conditions in that record lengths were assumed to be of infinite length and, moreover, it was assumed that an infinite number were available to ensemble across. In this section, the realities of having only a finite number of runs, each of finite length, is reviewed.

3.2 Constraints of Finite Data

The first obvious constraint when working with finite lengths of data is that the lowest Fourier Component which can be computed, given a record of length 2T seconds, is π/T rad/sec. The high frequency limit is generally accepted as being the "folding frequency", which is one half of the frequency associated with the sampling rate ($\omega_s = 2\pi$ sampling rate, e.g., if one samples at 125 S/S, the folding frequency is on the order of 390 rad/sec while the sampling frequency is $\approx$ 780 rad/sec).

Generally speaking, with the human pilot data, frequency information from about 0.1 rad/sec to approximately 100 rad/sec is desirable. The spectral densities themselves can be expected to have a dynamic range on the order of 60 to 70 dB (power basis) for scalar tracking experiments.

The useful frequency range will, in practice, be further restricted by anomalies associated with the sharpness of the spectral filter used, how fast the power spectra is dropping along the frequency axis, and the basic length of the data available. A discussion concerning the nature of these anomalies will be deferred until Section 4 where the results of the first two experiments will be discussed. At that point, tangible examples of the anomalies we have termed "roll up", "break up" and "roll down" will be presented. In this section, the underlying theory, which can be used to explain the phenomena, will be set down.

3.3 Direct Computation of Power Spectra Using the Fast Fourier Transform

First it is important to realize that several approaches are possible for the computation of power spectra. One may first use the time signals in the computation of the auto-correlation function, followed by a Fourier transform to arrive at an estimate of the power spectra. This is an attractive way to proceed in those cases where an estimate of the power spectra is desired at only a few discrete frequencies. An alternate approach, which is preferable when the power is being estimated at a very large number of frequencies, is to estimate the auto or cross spectra directly from the time signals themselves, using, for example, the equation

$$\hat{\Phi}_{XY}(\omega) = \frac{1}{2T}\frac{1}{N}\sum_{i=1}^{N} X_i(-j\omega)\, Y(j\omega) \tag{3.1}$$

That is, compute the truncated transform of $x(t)$ and $y(t)$ using the equations

$$X_T(j\omega) = \int_{-T}^{T} x(t)\, e^{-j\omega t}\, dt \tag{3.2}$$

$$Y_T(j\omega) = \int_{-T}^{T} y(t)\, e^{-j\omega t}\, dt \tag{3.3}$$

Theoretically, one does this for a very large number of realizations of the random variables x and y and ensemble averages (across frequency) to arrive at a smooth estimate. In the limit, the true cross power spectrum

$$\phi_{xy} = \lim_{T\to\infty} \frac{1}{2T} E\left\{X(-j\omega)\, Y(j\omega)\right\} \tag{3.4}$$

is attained as the number ensembled across and the length of each record approaches infinity. The advantage (a considerable one) in using Equation (3.1) to approximate Equation (3.4) is that the Fast Fourier Transform can be used to compute the (truncated) Fourier Transforms. That is, one proceeds directly from the time to the frequency domain without the intermediate stop in the correlation (τ) domain.

3.4 Time Windows and Their Relationship to Lag and Spectral Windows

Since the literature which discusses the "Lag" and "Spectral" windows is concerned with the relationships which exist between the correlation and frequency domains, and since our interest is with relationships which exist between time and frequency, it will next be necessary to present a slight clarification of the relationships which exist between all three of these domains (i.e., t , τ and ω).

Basically, the process of working with finite lengths of data can be visualized as multiplying the infinite record length by a signal such as

$$f(t) = \begin{cases} 1 & -T < t < T \\ 0 & |t| \geq T \end{cases} \tag{3.5}$$

This $f(t)$ is called a time window, and has a corresponding spectral window of the form $\left(\frac{\sin \omega T}{\omega T}\right)^2$. The basic relationships associated with the square time window are given in Equation (3.6)

$$\hat{\phi}_{xy} = \frac{1}{2T} E\left\{X(-s)\ Y(s)\right\}\Big|_{s=j\omega}$$

$$= \int_{-2T}^{2T} \left(1 - \frac{|\tau|}{2T}\right) R(\tau)\, e^{-j\omega\tau}\, d\tau = \frac{T}{\pi} \int_{-\infty}^{\infty} \phi(\omega_1) \left[\frac{\sin(\omega-\omega_1)T}{(\omega-\omega_1)T}\right]^2 d\omega_1 \qquad (3.6)$$

In Equation (3.6), $\hat{\phi}_{xy}$ is the estimate of the power spectra while R_{xy} is the true underlying correlation function and $\phi(\omega)$ is the true underlying power spectra. From Equation (3.6) it can be seen that the estimate of the power spectra obtained from many records, each of length 2T, is equivalent to the convolution of the true power spectra with a spectral window of the form $\left(\frac{\sin x}{x}\right)^2$. This window has an envelope that falls off at -20 dB/decade on a power basis. We hypothesize that the spectral estimate, ϕ_{xy}, will be distorted at those frequencies for which the true power spectrum is falling off at a rate exceeding that of the spectral window. However, just what form this distortion will take is not clear and one must therefore resort to analytical examples and experimental setups typical of pilot/aircraft estimation problems in order to gain insight into the implications of Equation (3.6). This will be done in Section 4 with the experimental data and in Appendix B with the analytical examples.

Equation (3.6) will now be extended to a more general case, which will permit the use of temporal windows other than the usually used square one. This is most important, because the use of the Fast Fourier Transform (FFT) requires direct computation of the Fourier Transform of the signals. Thus we are not at liberty to work with the correlation function and filter the data in the τ domain -- we must know what the temporal windows look like in order to filter directly in the time domain.

Let

$$f(t) = \begin{cases} \text{even} & -T < t < T \\ 0 & |t| \geq T \end{cases}, \qquad (3.7)$$

then Equation (3.6) becomes

$$\hat{\phi}_{xy} = \frac{1}{2T} E\left\{X_T(-s)\, Y_T(s)\right\} = \frac{1}{2T} \int_{-\infty}^{\infty} R(\tau) \left[\int_{-\infty}^{\infty} f(t)\, f(\tau - t)\, dt\right] e^{-j\omega\tau}\, d\tau$$

$$= \frac{1}{4\pi T} \int_{-\infty}^{\infty} \phi(\omega_1)\, F^2(\omega - \omega_1)\, d\omega_1, \quad \text{where } F(\omega) = \mathcal{F}\left\{f(t)\right\} \qquad (3.8)^*$$

*Refer to Appendix C for a derivation.

Using Equation (3.8), one may look at the problems encountered in estimating transfer functions using a variety of temporal windows. The windows considered in this report are tabulated, along with their more important characteristics, in Table I.

This list is obviously not all inclusive, however the three time windows presented do represent a good cross section of typical filter characteristics. In particular, the reader will recognize, from an inspection of Table I, that placing a triangular window on the data in time leads to a relationship between the lag window and spectral window which is known as a Parzen window. The square window in time leads to a triangular window in the τ domain and a $\left(\frac{\sin x}{x}\right)^2$ window in the frequency domain. This window is called a "Bartlett" window. The three windows shown are relatively simple ones in that the relationship between the t , τ and ω domains are easy to set down. Other "classical" filters (or windows), defined in the τ domain are more difficult to describe in time. For example, the time domain window that corresponds to the Tuckey window is the inverse Fourier transform of

$$\left[m \left(\frac{\sin 2\pi f m}{2\pi f m}\right) \left(\frac{1}{1-(2fm)^2}\right)\right]^{1/2} \tag{3.9}$$

In general, as one proceeds from the $\left(\frac{\sin x}{x}\right)^2$ window to the $\left(\frac{\sin x/4}{x/4}\right)^8$ window, a tradeoff is made between the sharpness of the main lobe and suppression of the side lobes. The side lobes in the $\left(\frac{\sin x/4}{x/4}\right)^8$ filter are of no practical concern while the main lobe is broader than, for example, the main lobe of the $\left(\frac{\sin x}{x}\right)^2$ spectral window. These filters will be applied to the data of the first two experiments. The results are discussed in the next section. Before proceeding to Section 4, the conditions under which Equation (3.8) is valid are emphasized:

1. The records are of finite length (for our work, typically on the order of 2T = 2 minutes).
2. A sufficient number of records of length 2T are available so that the ensemble average of an infinite number is approximately true.
3. A noise free environment.
4. The sampling frequency is high enough so that folded power is of no concern.

In the next section (and in Appendix B) it will be shown that even under these relatively ideal conditions, the finite length of record, coupled with the "sharpness" of the spectral filter, lead to anomalies in the power estimates that one must learn to recognize in order to avoid false conclusions.

Table I

CHARACTERISTICS OF SPECTRAL WINDOWS

TIME WINDOW	LAG (τ) WINDOW	SPECTRAL WINDOW	$\hat{\phi}_{XY}$
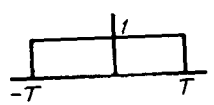	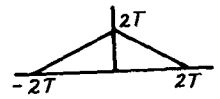	$\left(\frac{\sin \omega T}{\omega T}\right)^2$	$\frac{T}{\pi}\int_{-\infty}^{\infty}\phi(\omega_1)\left[\frac{\sin(\omega-\omega_1)T}{(\omega-\omega_1)T}\right]^2 d\omega_1$
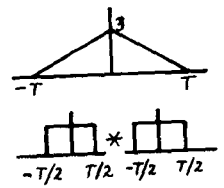	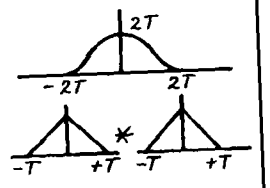	$\left(\frac{\sin\left(\frac{\omega T}{2}\right)}{\frac{\omega T}{2}}\right)^4$	$\frac{T}{4\pi}\int_{-\infty}^{\infty}\phi(\omega_1)\left[\frac{\sin\frac{(\omega-\omega_1)T}{2}}{\left(\frac{\omega-\omega_1}{2}\right)T}\right]^4 d\omega_1$
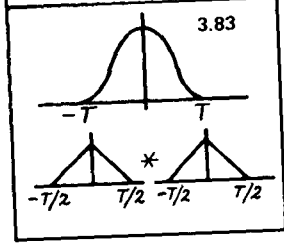	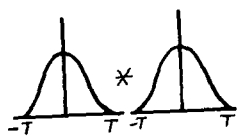	$\left(\frac{\sin\left(\frac{\omega T}{4}\right)}{\frac{\omega T}{4}}\right)^8$	$\approx\int_{-\infty}^{\infty}\phi(\omega_1)\left[\frac{\sin\frac{(\omega-\omega_1)T}{4}}{\left(\frac{\omega-\omega_1}{4}\right)T}\right]^8 d\omega_1$

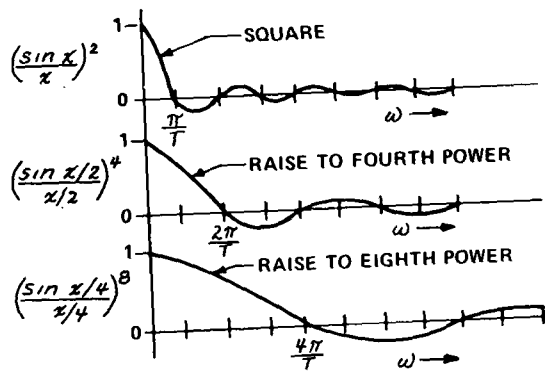

$$\hat{\phi}_{XY} = \frac{1}{2T} E\left\{X(-s)\,Y(s)\right\} = \frac{1}{4\pi T}\int_{-\infty}^{\infty}\phi(\omega_1)\,F^2(\omega-\omega_1)\,d\omega_1$$

$$= \frac{1}{2T}\int_{-\infty}^{\infty} R(\tau)\left[\int_{-\infty}^{\infty} f(t)\,f(\tau-t)\,dt\right] e^{-j\omega\tau}\,d\tau$$

WHERE $f(t) = \begin{cases} \text{EVEN} & -T < t < T \\ 0 & |t| \geq T \end{cases}$

$$\mathcal{F}\left\{f(t)\right\} = F(\omega)$$

4. EXPERIMENTAL RESULTS AND CONCLUSIONS FOR THE TWO SCALAR EXPERIMENTS

4.1 Introduction

The first experiment, a scalar, pilot-in-the-loop roll tracking task was set up in order to

1. check on the accuracy of spectral estimation techniques in identifying the fixed dynamics of the system.
2. help finalize the data taking requirements.

The experimental setup is depicted in Figure 4.1

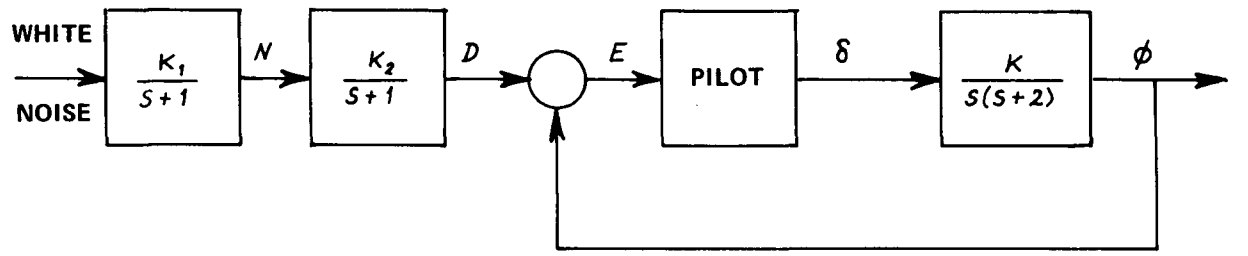

Figure 4.1 EXPERIMENT #1

Analog data was recorded and, simultaneously converted to digital form through the use of analog to digital recording equipment. The various power spectras were then computed on the CAL IBM 370 Model 165 computer (refer to Appendix D for a more detailed analysis).

The final sampling rate used was 125 S/S, given a sampling frequency of approximately 785 rad/sec and a folding frequency of about 392 rad/sec. In that experiment, the CAL fixed base simulator was flown by an instrument rated pilot. The disturbance source was derived from a gaussian white noise source passed through two cascaded first order filters.

The second scalar roll tracking task is described in Figure 4.2.

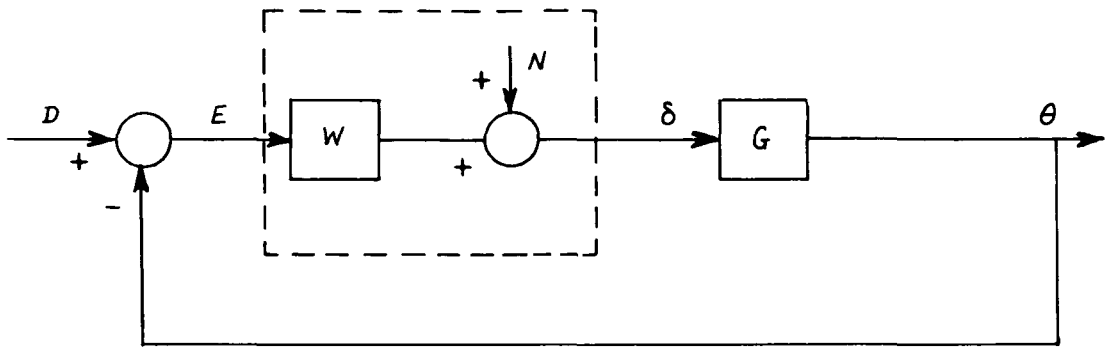

Figure 4.2 EXPERIMENT #2

This experiment is an analog simulation of the "Subject M" run described in Table III of Reference 1, the case where Disturbance (Volts^2) = 5.61.

The disturbance input in Figure 4.2 is obtained by feeding white noise through the transfer function $K/(S+1)^2$ while the noise (remnant) is obtained by feeding white noise through the transfer function $K/(S+10)^2$. For the mean square value given in Reference 1, the following spectral densities were calculated:

$$\phi_{NN} = \frac{1.424}{(\frac{S}{10}+1)^2(-\frac{S}{10}+1)^2} \tag{4.1}$$

$$\phi_{DD} = \frac{22.4}{(S+1)^2(-S+1)^2} \tag{4.2}$$

The given transfer functions are

$$H = \frac{24S + 52}{(S+13)^2} \tag{4.3}$$

$$G = \frac{10}{S^2} \tag{4.4}$$

In the analog simulation, the signals D, E, N, δ and θ were recorded.

The main task in this experiment is to estimate the given W of Figure 4.2, given that the noise source N cannot be measured (i.e., N is internal pilot noise). In addition, it was felt that estimates of $K/S2$ should also be made since the dynamic range of the input power spectra, was quite large (on the order of 60 dB).

4.2 Overview of Computational Efforts

At this point, it is reasonable to review the computational efforts on these two experiments in order to make it quite clear that the spectral estimates presented in this report represent the net effort of following several alternate options. First, the matter of data rate was explored. In each experiment we observed a "roll up" and "breakup" phenomenon (to be defined shortly) which was first attributed to folded power (the sampling rate was initially 20 S/S). However, increasing the sampling rate to 125 S/S did not improve matters.

Next, averaging "around" a frequency point was tried. That is, the hypothesis that frequency estimates in the immediate neighborhood of a given frequency were (in some sense) "close" estimates of what was occurring at the given frequency, gave impetus to the idea of averaging adjacent points in the frequency domain. This procedure was also unsuccessful in improving the estimates.

Next, the correlation (lag) method was tried, even though the computations were considerably more costly to carry out. The results were essentially identical with the estimates obtained directly in the frequency domain.

Increasing record length from 20 sec. to 60 sec. to two minutes did enlarge the range of frequencies over which the estimates were better, however, it did not eliminate the basic phenomenon observed ("roll up" and "breakup") at the end points of the estimates.

Next, the number of estimates ensembled across was carried to a very high number ($\approx$ 134) but even this did not eliminate the "roll up" in the spectral estimates.

To investigate the possibility that the problem was noise generated by the analog-to-digital recording process, the experiment was run in an all digital manner (using a state space approach) on the IBM 370 digital computer. However, the problem still persisted.

These long series of experiments convinced us that the experimental anomalies were not due to noise, that ensemble averaging did not eliminate them and neither did filtering alone seem to have a great effect.

Finally a combination of ensemble averaging (in the frequency domain) and filtering (in the time domain) was hit upon that produced a significant improvement in the estimates of the power spectra. Moreover, even with this significant improvement, the deviation from the true values of the system dynamics at high and low frequencies was significant. This finally led to the conclusion that the observed anomalies were truly the result of the computational algorithm that worked with finite pieces of data. With this hypothesis, it was possible, by applying Equation 3.8 of Section 3 to several illustrative examples (Appendix B), to conclusively demonstrate the presence of three anomalies in the spectral estimates. We identify these as:

(1) "Roll Up" at high frequency

(2) "Breakup" at high frequency

(3) "Roll Down" at low frequency

4.3 Roll Up, Break Up and Roll Down

These terms are best understood with the aid of Figure 4.3 (from Experiment #2). "Roll Up" is defined to be an increase in the power magnitude for $\omega > 50$ rad/sec, "Break Up" is the term we ascribe to the large divergence (oscillations) in both the phase and magnitude plots for $\omega > 50$ rad/sec, while "Roll Down" is the term used to describe a magnitude plot which has decreased to about - 2 dB at $\omega = .048$ rad/sec when it should read around +22 dB.

The theoretical analysis given in Appendix B demonstrates that all three of these phenomena are fundamentally tied to the finite length of the data available. That is, even when the signals are well above the digital noise level, the sampling rate is extremely high, and an infinite number of the fixed length records are available, we can still observe roll up, break up and roll down!

4.4 Results of Experiment #1

The spectral estimate of the dynamics $\frac{K}{s(s+2)}$ is given in Figure 4.4. The sampling rate was 125 S/S giving a folding frequency of approximately 360 rad/sec (only data out to 100 rad/sec was plotted). The case shown is for ensemble average across 28 estimates of the various auto and cross spectral densities. The time window used was the "square" window of Table I. Observe that "break up" (and roll up) occur in Figure 4.4 at about 20 rad/sec, more than a decade away from the folding frequency. It was this plot which first convinced us that the break up was truly built into the algorithm used for computing the estimates and further, that some combination of direct filtering on the temporal data, as well as ensemble averaging, were required to reduce the bias in the high frequency region. It should be noted that in previous runs of this experiment (and Experiment #2), filtering appeared to be ineffective in reducing the variances in the spectral estimates. Thus our idea was to employ the triangular data window of Table 1 in the hope of decreasing the bias while at the same time depending on ensemble averaging to keep the variance at in acceptance level. The results of this approach are shown in Figure 4.5, where it is seen that a dramatic improvement has been achieved. Specifically, the frequency at which break up starts has been moved out on the order of two octaves and, more importantly, the dynamic range has been extended by approximately 10 dB (in power).

These results show that the filter is extremely effective in reducing the bias. However, it must not be presumed that filtering is the entire story. In order to demonstrate that ensemble averaging is also required, a plot of the $\frac{K}{s(s+2)}$ dynamics, without ensemble averaging, is shown in Figure 4.6.

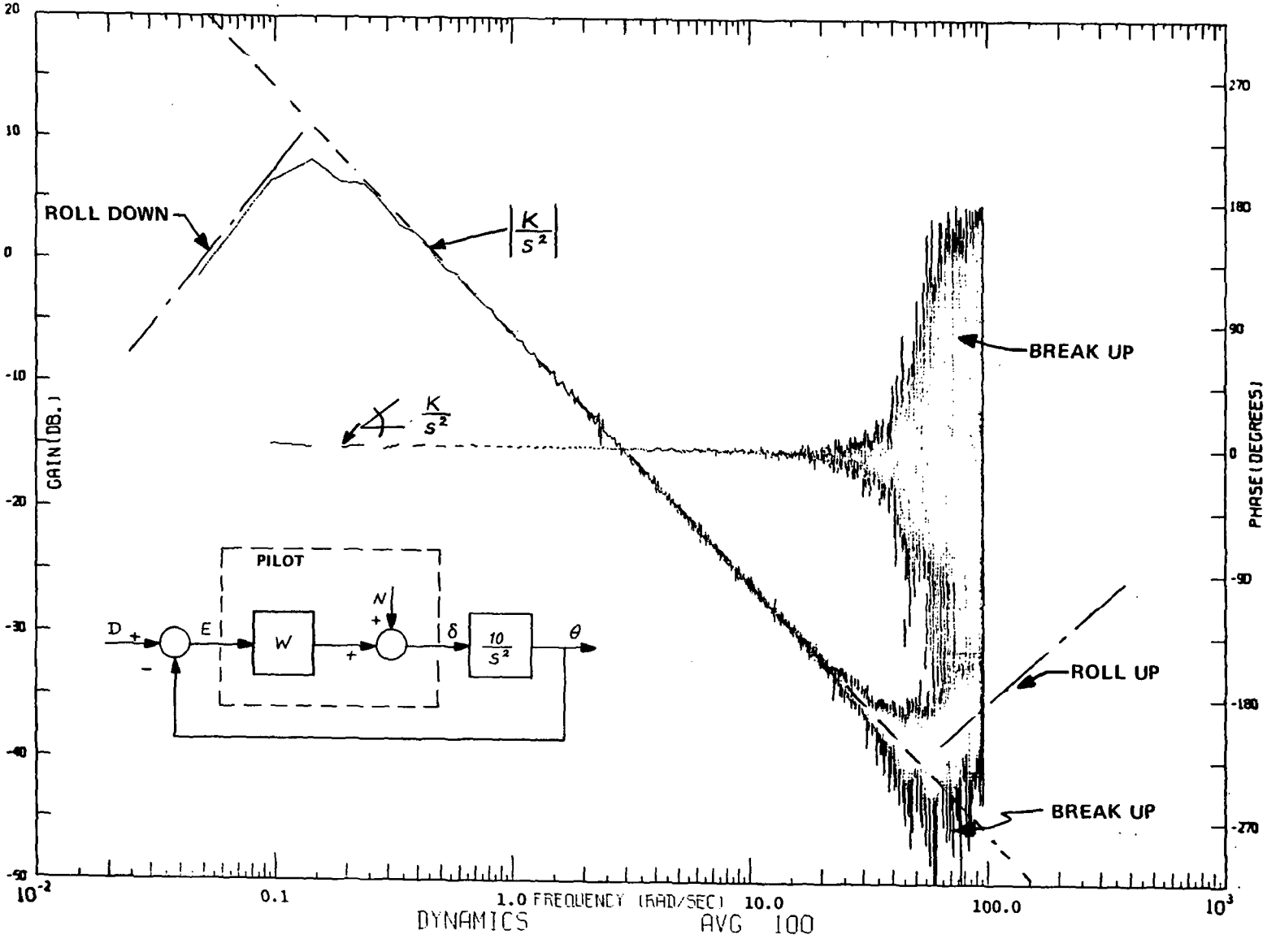

Figure 4.3 SUBJECT M , K/s^2 , AVERAGE 100

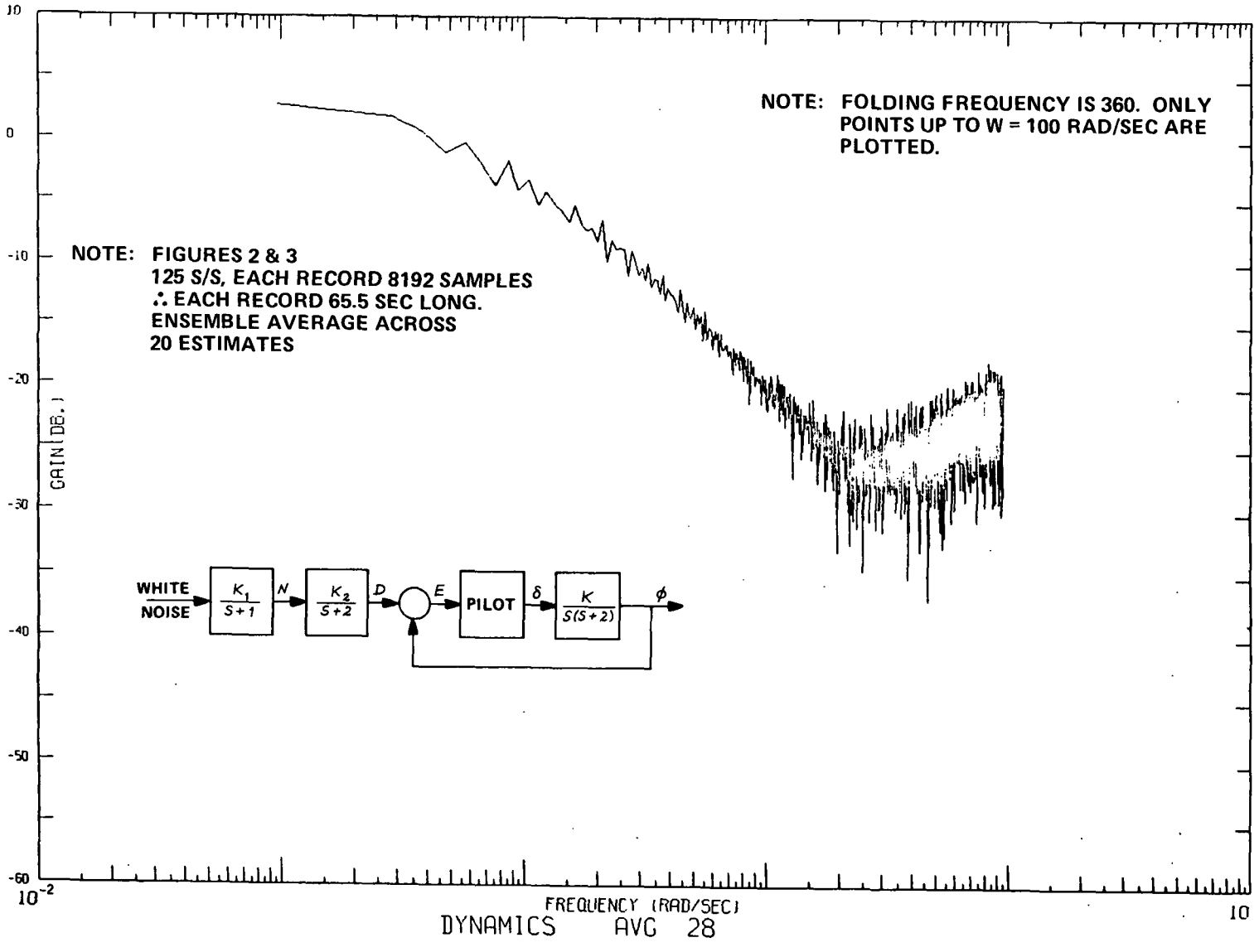

Figure 4.4 SINGLE CONTROLLER ROLL TRACKING EXPERIMENT, ONLY ENSEMBLE AVERAGE

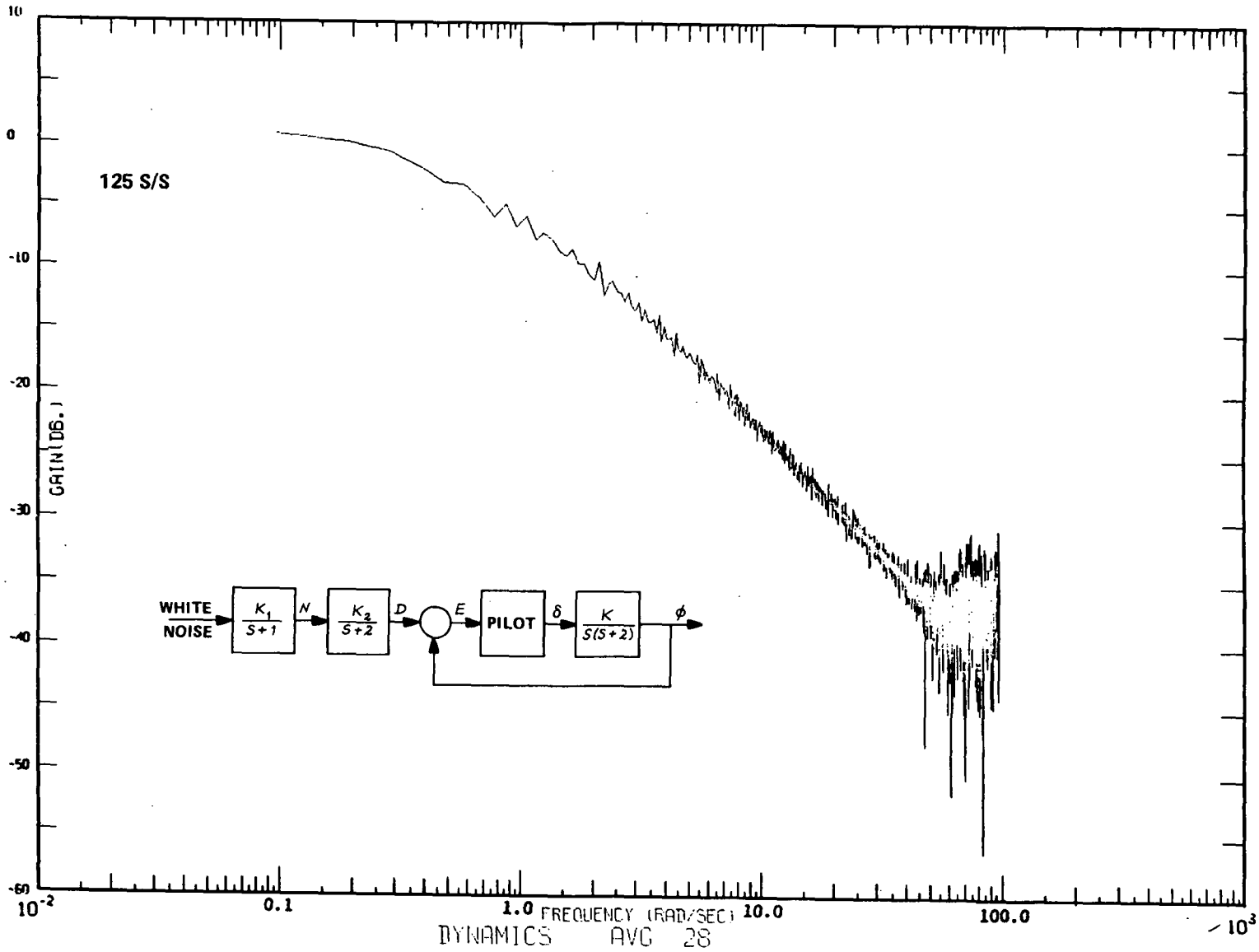

Figure 4.5 SINGLE CONTROLLER ROLL TRACKING EXPERIMENT, FILTER AND ENSEMBLE AVERAGE

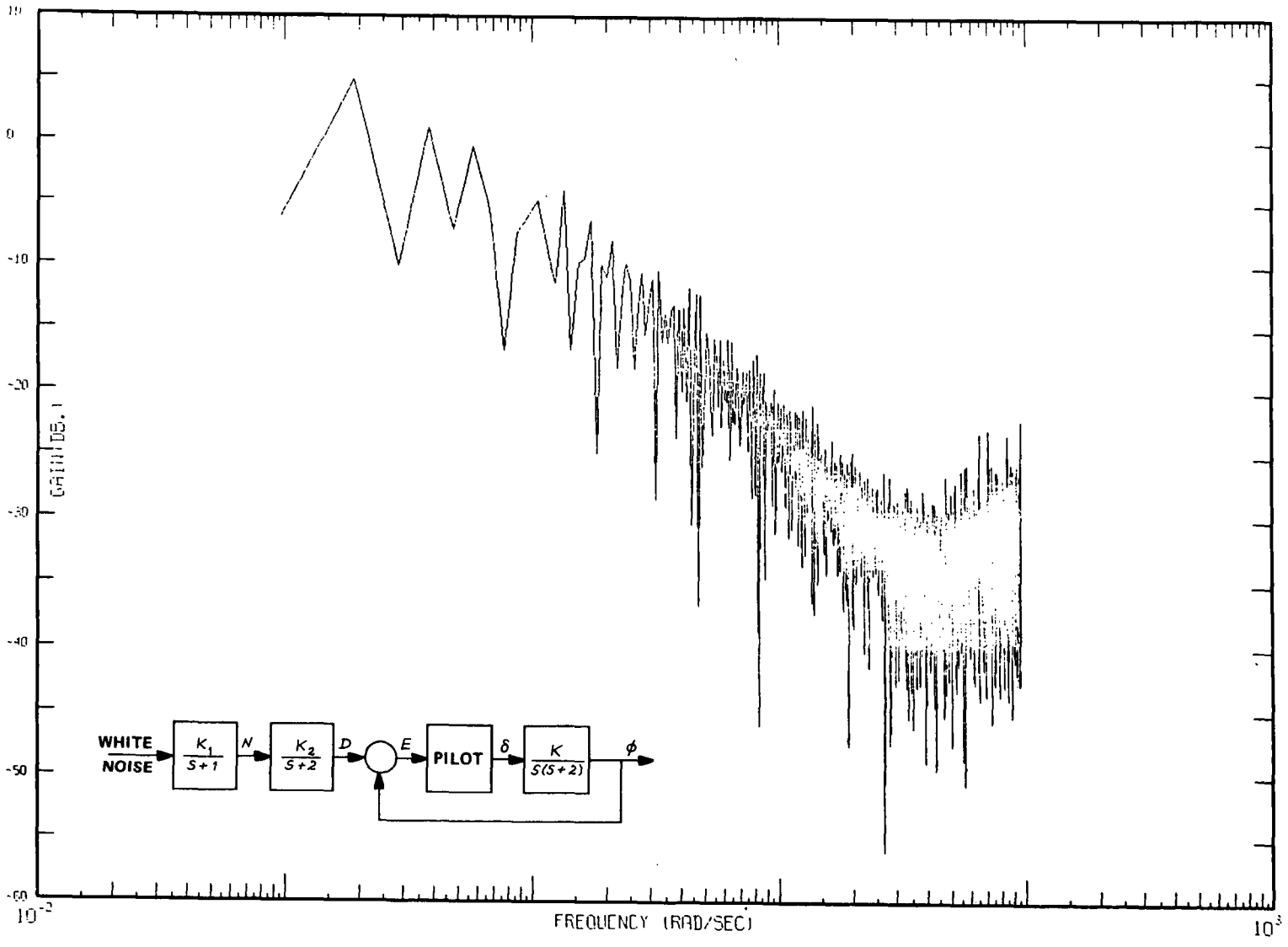

Figure 4.6 SINGLE CONTROLLER ROLL TRACKING EXPERIMENT, FILTER ALONE (NO ENSEMBLE AVERAGING)

In Figure 4.5, the estimate of $\frac{K}{S(S+2)}$ is quite good for the frequency range of $0.1 < \omega < 60$ rad/sec.

4.5 Cross Power Between Two Independent Signals

Before enumerating the results for the second experiment an important result, associated with the finite length of data (one not too well appreciated by the manual control community) must be clarified. The intent of the subject "M" experiment is to identify the W transfer function of Figure 4.2 in the presence of the unmeasurable noise N. It is hypothesized that the remnant (N) is uncorrelated with the disturbance input D. This says, for the ideal situation of infinite record length that the exact equation for estimating W,

$$W = \frac{\phi_{DS} - \phi_{DN}}{\phi_{DE}} \tag{4.5}$$

can be reduced to

$$W = \frac{\phi_{DS}}{\phi_{DE}} \tag{4.6}$$

because $\phi_{DN} \equiv 0$.

While this is true for infinite record lengths, it is a fact of life that the estimate of ϕ_{DN} will have, for finite data length, appreciable power. In Appendix C, it is shown that the magnitude of the estimate of cross power between two independent signals (call them X and Y) is, when no ensemble averaging is employed, is

$$|\phi_{XY}| = \gamma \sqrt{|\phi_{XX}| \cdot |\phi_{YY}|} \tag{4.7}$$

Furthermore, the employment of ensemble averaging diminishes this estimate of the cross power only by $1/\sqrt{n}$, n being the number of estimates ensembled across.

In addition to the theoretical analysis of Appendix C, experimental verification is given in the subject "M" results that follow (see Figures 4.9 and 4.13).

4.6 Results of Experiment #2

In the running of the Subject "M" experiment (Experiment #2), two time windows were used. They are the triangular window of Table 1 (the $\left(\frac{\sin \chi/2}{\chi/2}\right)^4$ spectral window) and a time window arrived at by convolving a triangular window with a triangular window (a $\left(\frac{\sin \chi/4}{\chi/4}\right)^8$ spectral window). The majority of the results presented are for the triangular window with supplementary results to show

what sort of improvements can be expected with the higher order window. The results are presented in Figures 4.7 through 4.28. A detailed description of the information contained in these plots follows. Figures 4.7 through 4.25 were computed using the triangular time window while Figures 4.26 through 4.28 were computed using the $\left(\frac{\sin \pi/4}{\pi/4}\right)^8$ spectral window.

Figures 4.7, 4.8, 4.9: Plots of ϕ_{NN} , ϕ_{DD} and ϕ_{DN} with filtering but no ensemble averaging. Note that the power in ϕ_{NN} is appreciable compared to ϕ_{DD} and, more importantly, the power in ϕ_{DN} is high.

Figure 4.10: Figure 4.10 is the same as Figure 4.9 except that the phase plot of ϕ_{DN} has been included. Notice the violent "break up" in the phase plot.

Figures 4.11, 4.12, 4.13 ϕ_{NN} , ϕ_{DD} , ϕ_{DN} with filtering and ensemble averaging across one hundred estimates. Note the smoothness of ϕ_{NN} and ϕ_{DD} while ϕ_{DN} is still quite rough. Also note that ϕ_{DN} averaged across 100 has dropped by approximately 10 dB (power basis) indicating that D and N are independent. That is, if D and N are independent then their cross power would go down as $1/\sqrt{n}$ of the number n of estimates averaged across. Since this truly does occur, then we must conclude that D and N are independent, thus satisfying the postulates of the subject M experiment. Also note that ϕ_{DN} is unequal to zero, for finite data lengths, even though D and N are independent.

Figure 4.14: Same as Figure 4.13 except that the phase information has been included. The breakup in the phase is quite severe.

Figures 4.15-4.19: $K/S2$ dynamics are shown for ensemble averages of 1, 5, 10, 50, 100. The phase plots are also included. The estimate of $K/S2$ is quite acceptable at 10, very good at 50 and excellent for 100. Note that the phase is read off as zero degrees, since the analog set up really gave $-K/S2$ rather than $K/S2$.*

Figure 4.20: $K/S2$ dynamics from a previous run of the subject "M" experiment are shown. These runs were made with ensemble averaging but without filtering. It can be seen that the estimate of $K/S2$ is unacceptable even when 134 averages are used. Compare this figure with Figures 4.15-4.19.

Figure 4.21: Estimate of the pilot using the equation

$$W = \frac{\phi_{D\delta}}{\phi_{DE}}^*$$

*The $K/S2$ plots are 15 dB low because of a miscalculation in the scale factors of the various cross spectra. This does not effect the estimates for W since only ratios of cross spectra are involved.

This estimate is based on the hypothesis that D and N are uncorrelated and therefore $\phi_{DN} \equiv 0$. Of course, the power in the estimate of ϕ_{DN} is finite even when D and N are independent. Thus the use of $\phi_{D\delta}/\phi_{D\varepsilon}$ must give a biased estimate which will approach W only when the number of estimates averaged over is large and/or the power in ϕ_{NN} is small compared to the power in ϕ_{DD} (i.e., a "large" signal-to-noise ratio).

Figure 4.22: Same as Figure 4.21 except that the phase plot has been included.

Figure 4.23: Since the power in ϕ_{DN} is finite even when D and N are independent, this plot gives the estimate of the pilot when N is assumed to be measurable. As can be seen from the figure, the estimate of W is extremely good. Compare Figure 4.23 with Figure 4.21.

Figure 4.24: Same as Figure 4.23, except the phase plot is included.

Figure 4.25: The estimate of the pilot from an early running of the subject M experiment which employed no filtering (only ensemble averaging). As can be seen, the ensemble average alone estimates, even across 134 estimates, are poor. Compare with Figure 4.23.

Figures 4.26-4.28: Estimates of $K/_S 2$ using $\left(\frac{\sin x/4}{x/4}\right)^8$ window. Observe that there is no further increase in the frequency at which roll up and break up occur. However, the ensemble across 5 is not noticeably superior to the ensemble across 10 with the triangular window. (Compare with Figure 4.17). Thus a point of diminishing returns appears to have been arrived at somewhere between the fourth and eighth order filter.

These runs of the subject "M" experiment utilized basic record lengths which were 131 seconds long. Thus the lowest frequency which can be estimated is approximately .048 rad/sec, which means that there are only two or three data points in the immediate vicinity of W = .1 rad/sec.

4.7 Summary of Theoretical Conclusions and Experimental Observations

In closing, it is convenient to summarize the theoretical analysis as well as the experimental observations:

(1) When working with finite lengths of data, the roll up, break up and roll down phenomena are to be expected.

(2) Knowing that they exist, Equation (3.8) can theoretically be used to predict the frequency band for which relatively undistorted estimates can be anticipated.

(3) In general, one may anticipate distortion at a given frequency when the spectral window, which corresponds to a time domain filtering algorithm, is falling off more slowly than the true underlying spectral density.

(4) Previously we used ensemble averaging with no overt filtering (i.e., the square time window). The estimate obtained by ensemble averaging over as many as 134 estimates was considered unsatisfactory. For example, had we not known the underlying dynamics were K/S^2, it is doubtful that we would approximate it as K/S^2.

(5) The triangular filtering algorithm in time, which corresponds to a $\left(\frac{\sin x/2}{x/2}\right)^4$ spectral window, produced results which were an order of magnitude better when used in conjunction with ensemble averaging.

(6) Filtering alone, without ensemble averaging, also produced unsatisfactory results. However, with filtering, the number of ensembles necessary to produce acceptable results, is reduced.

(7) Break up occurs if any of the cross and auto power spectra being estimated contain lightly damped modes.

(8) In general, the experimental variability in the estimation of cross spectral densities is greater than the variability observed in the estimation of auto spectra. For example, a typical observation is that ensemble averages across 5 or 10 on auto spectra have less variability than cross spectral averages across 100. Thus the estimation of dynamics and pilots via ratios of cross/cross, as opposed to ratios of cross/auto, are very likely to display more distortion (see Appendix B).

(9) Regardless of what time domain filtering algorithm is invoked, the estimate of the cross power between two independent random variables goes down only as $1/\sqrt{n}$, n being the number ensembled across.

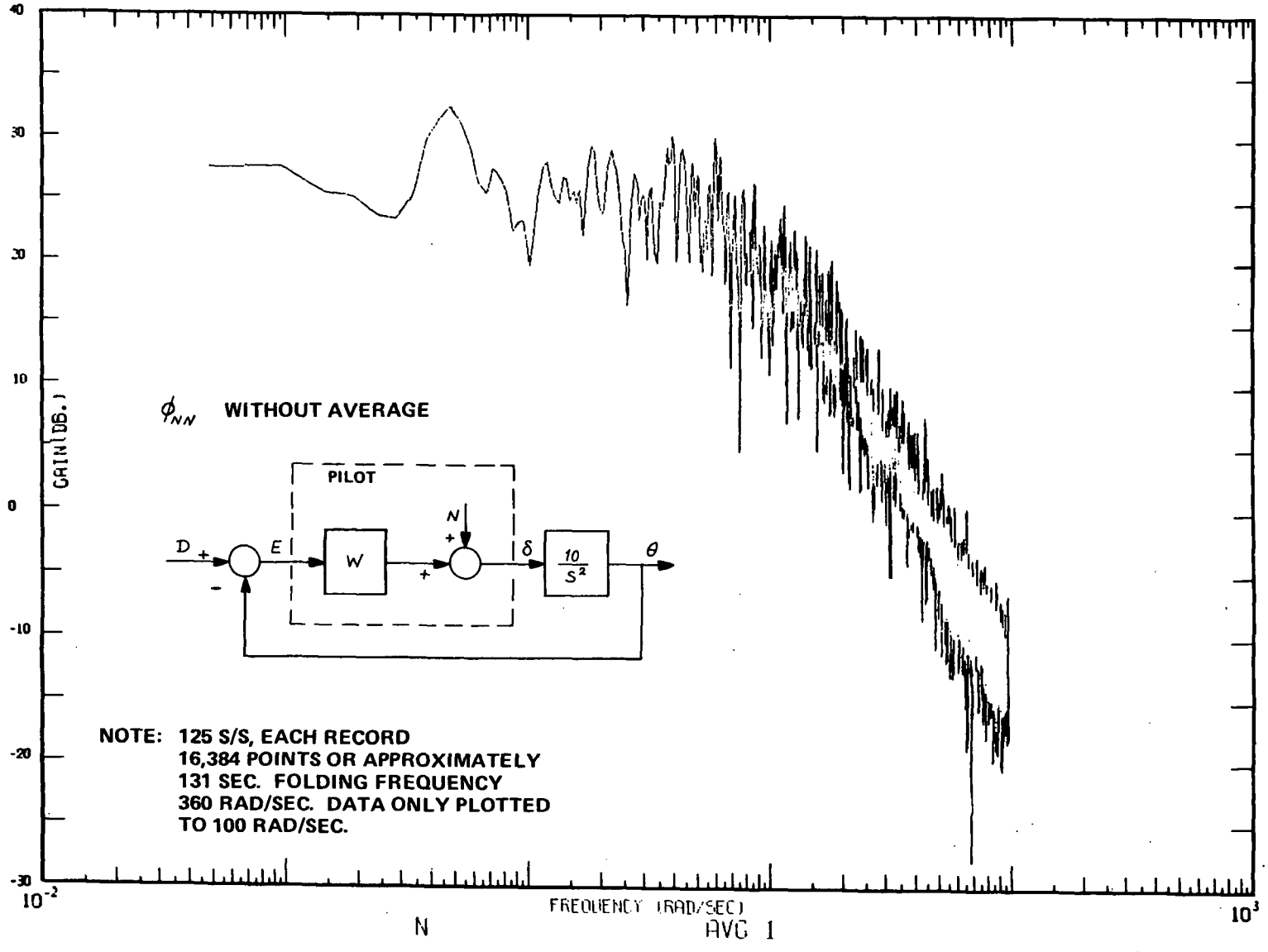

Figure 4.7 SUBJECT M EXPERIMENT, ϕ_{NN} (FILTERING AND ENSEMBLE) AVERAGE 1

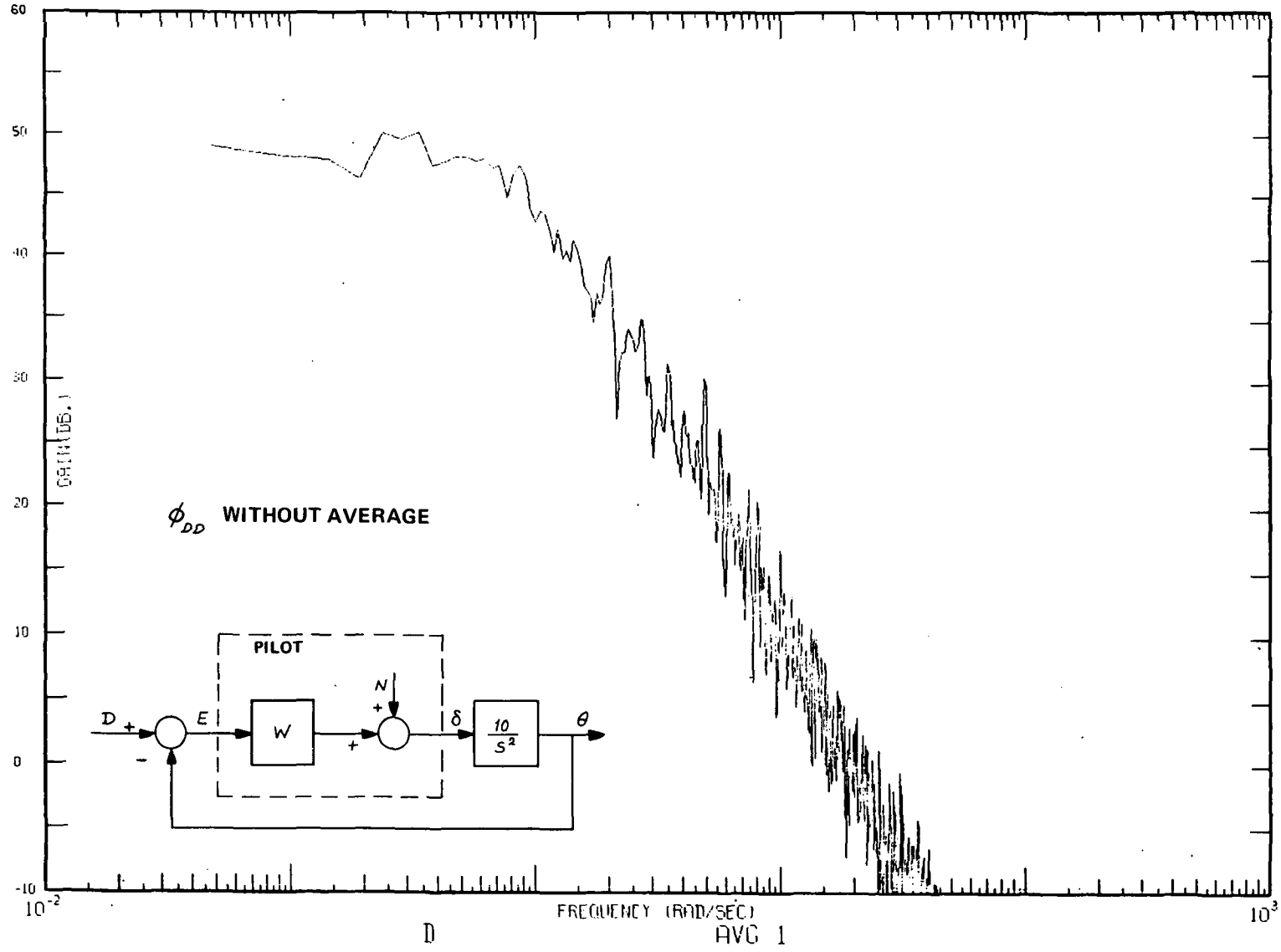

Figure 4.8 SUBJECT M, ϕ_{DD}, AVERAGE 1

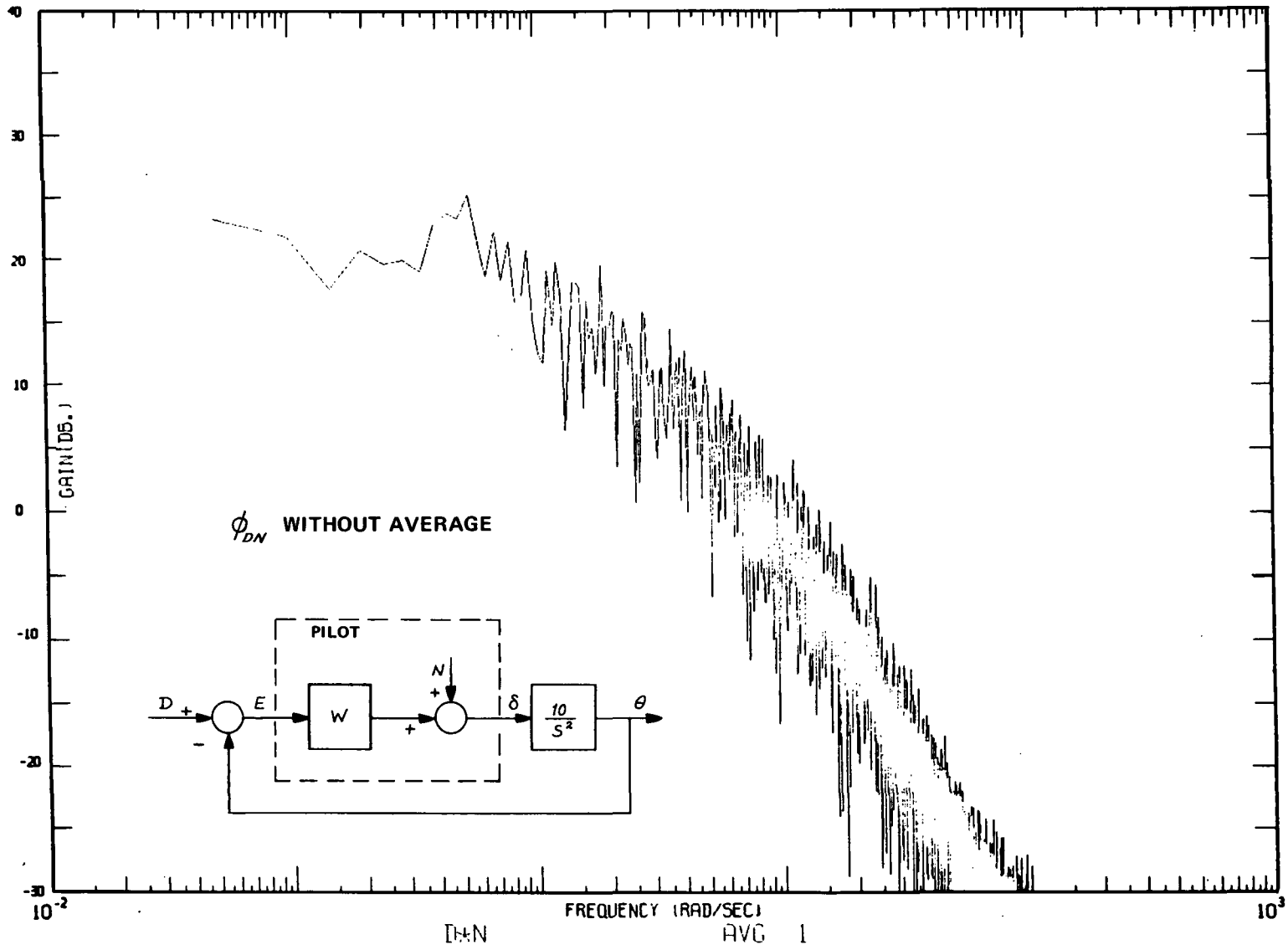

Figure 4.9 SUBJECT *M*, ϕ_{DN}, AVERAGE 1

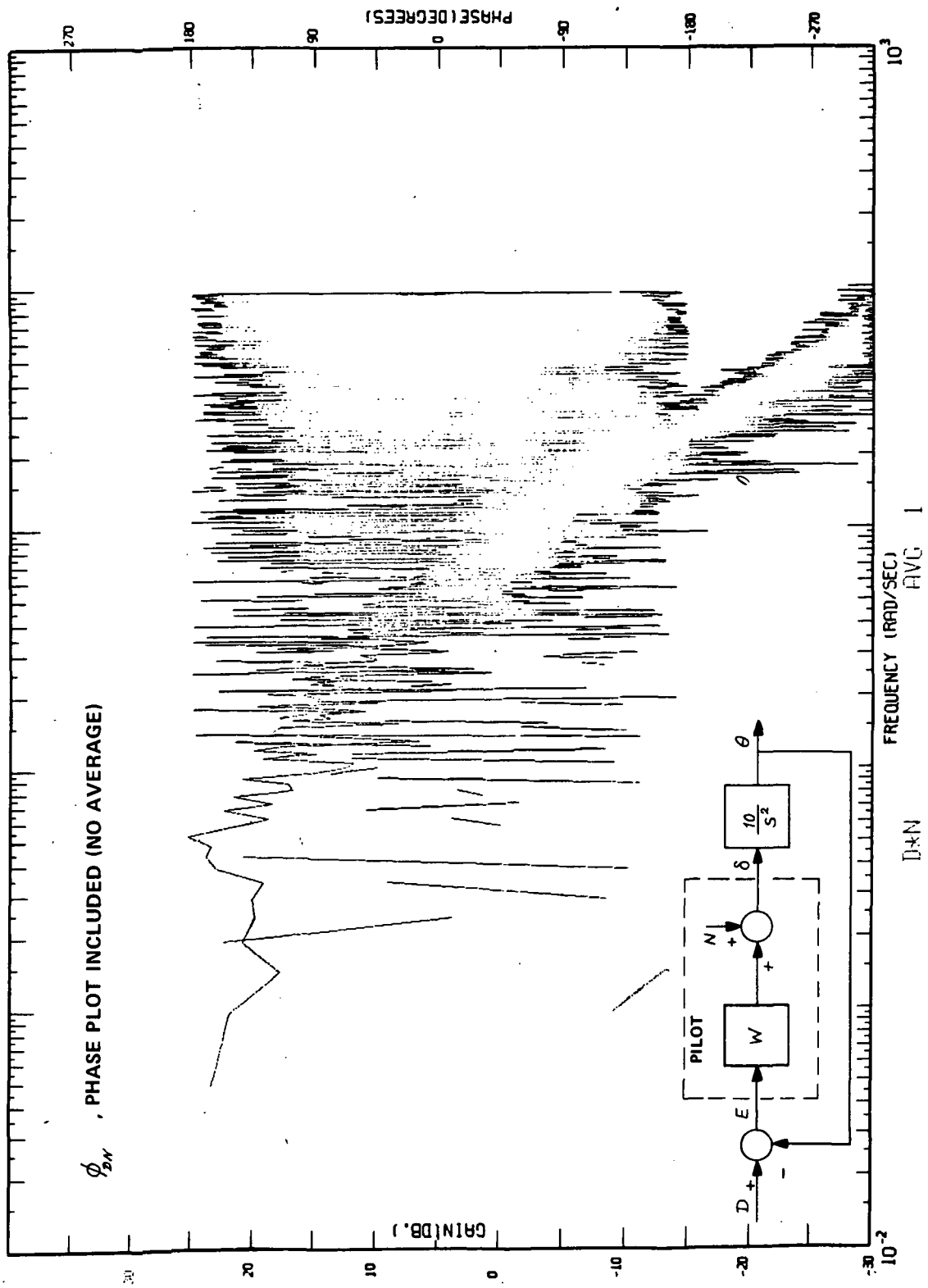

Figure 4.10 SUBJECT M1, ϕ_{z_N}, AVERAGE 1, PHASE INCLUDED

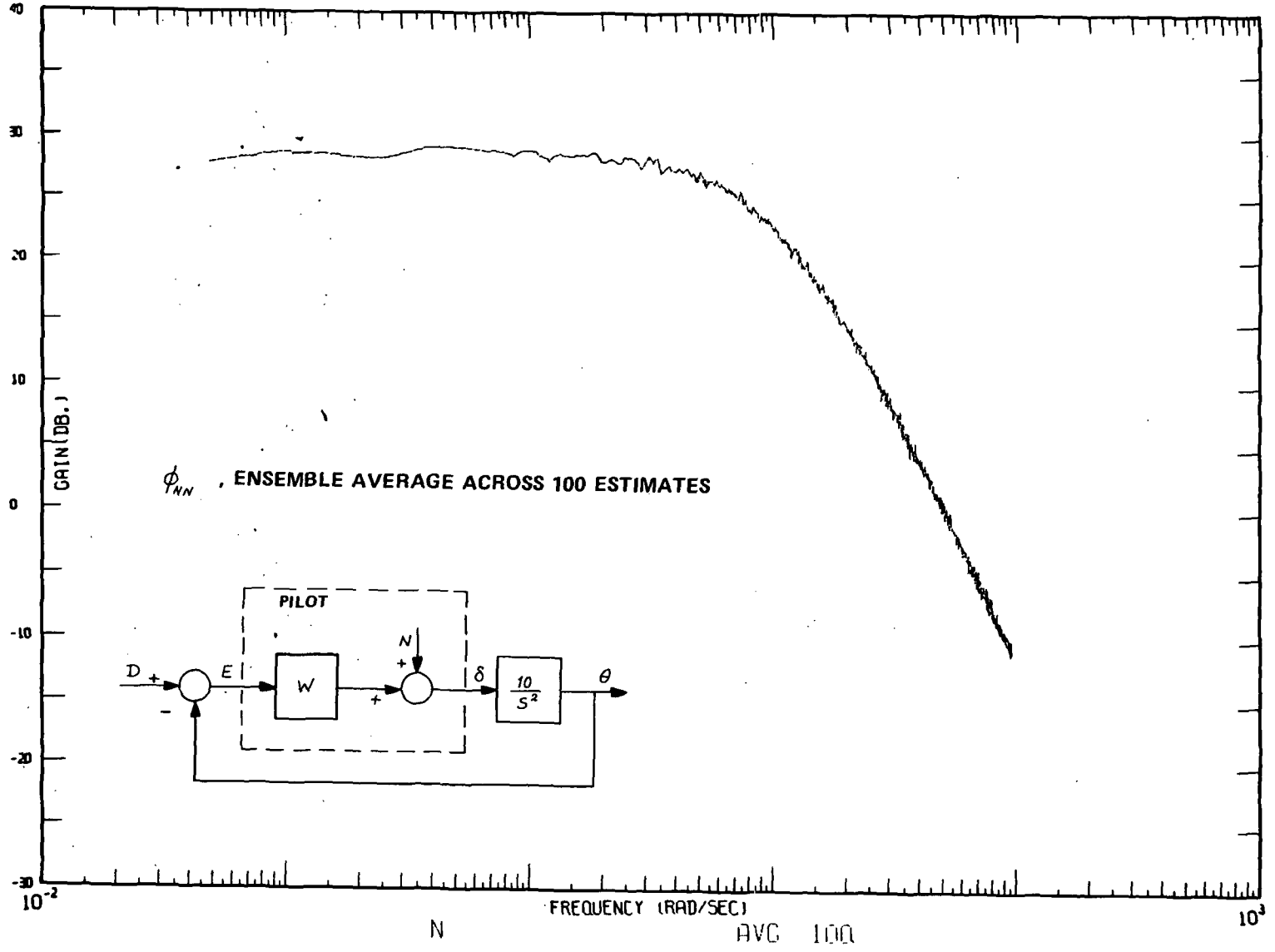

Figure 4.11 SUBJECT *M* , ϕ_{NN} , AVERAGE 100

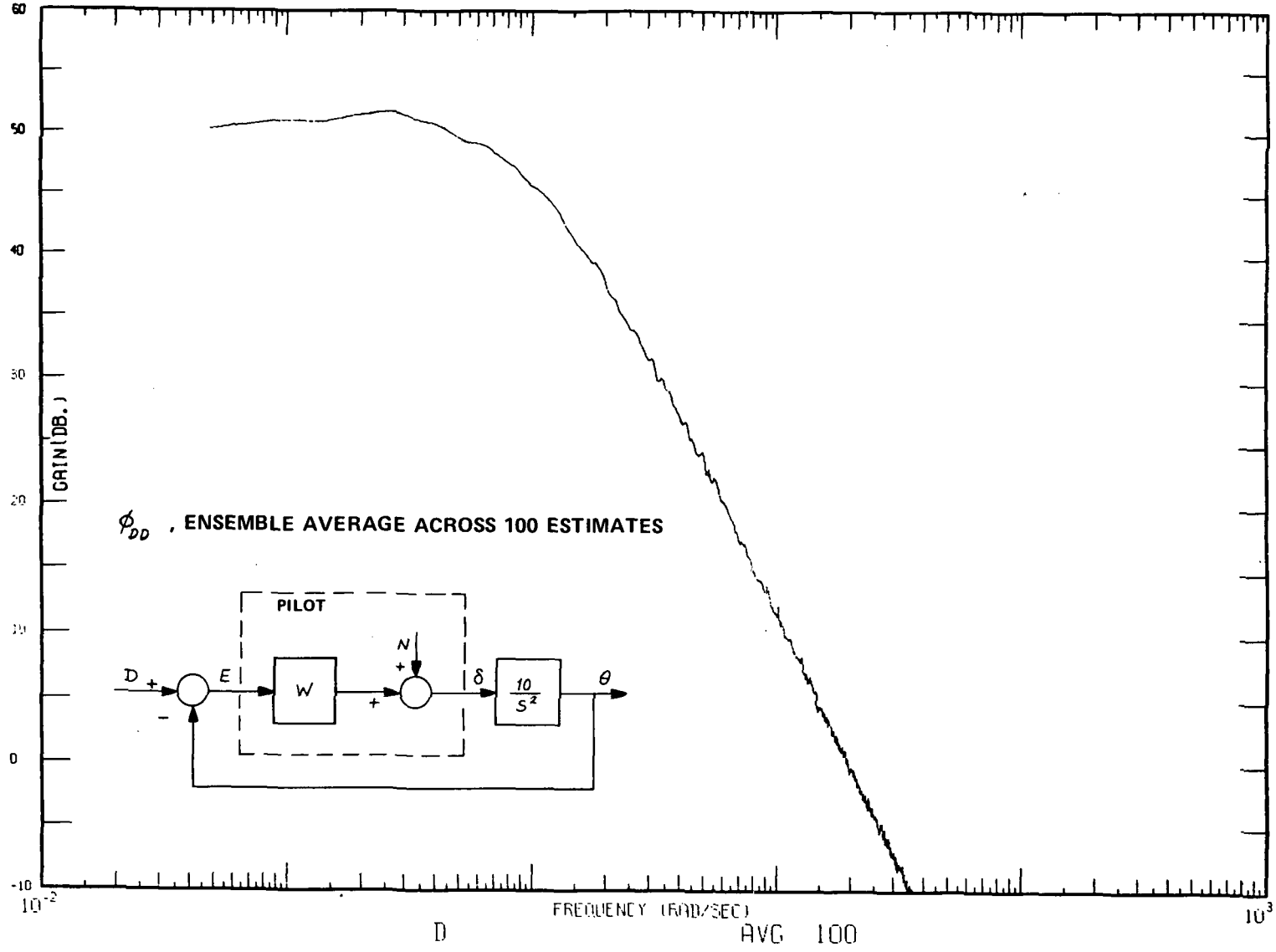

Figure 4.12 SUBJECT M , ϕ_{DD} , AVERAGE 100

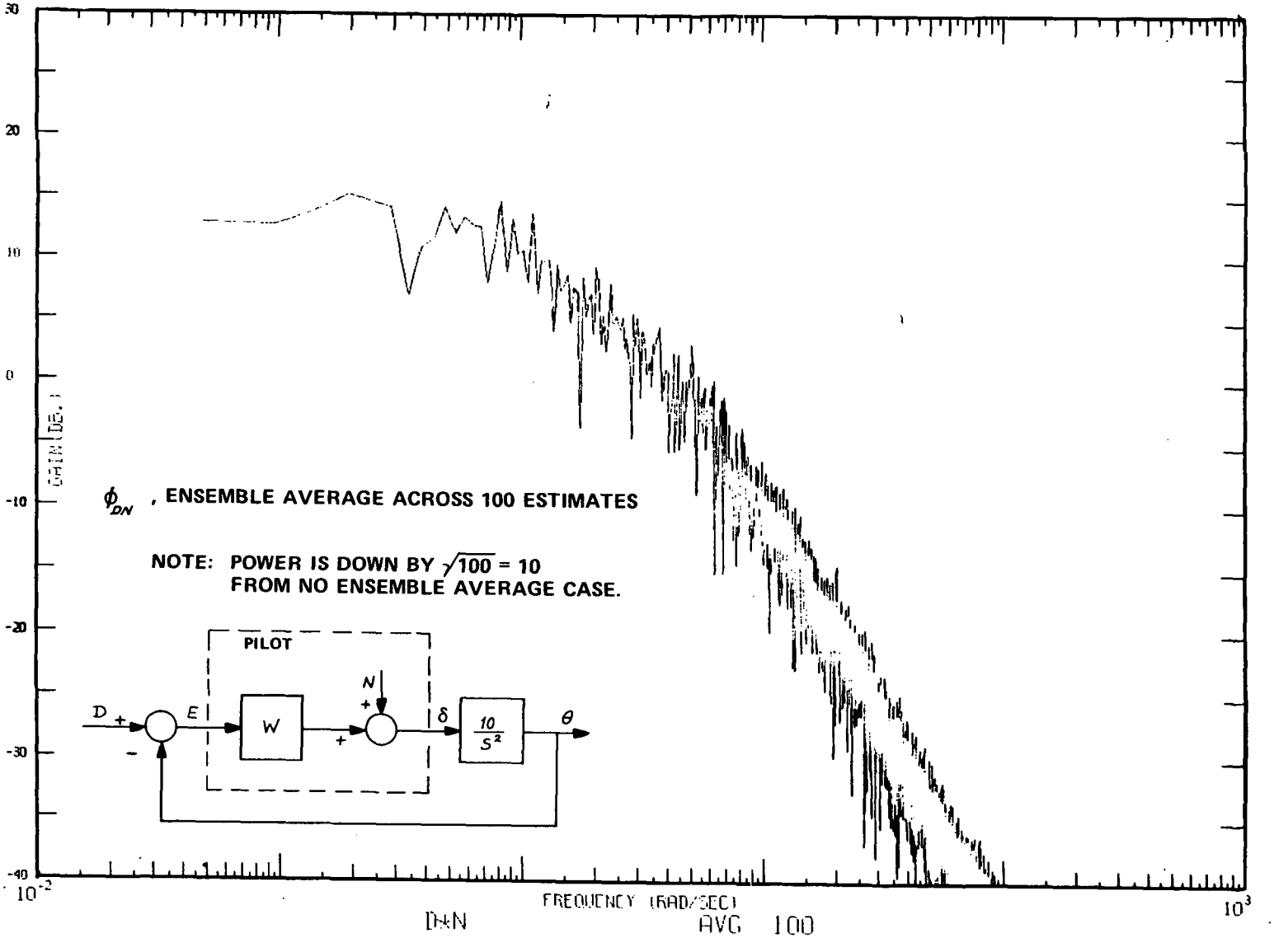

Figure 4.13 SUBJECT *M* , ϕ_{DN} , AVERAGE 100

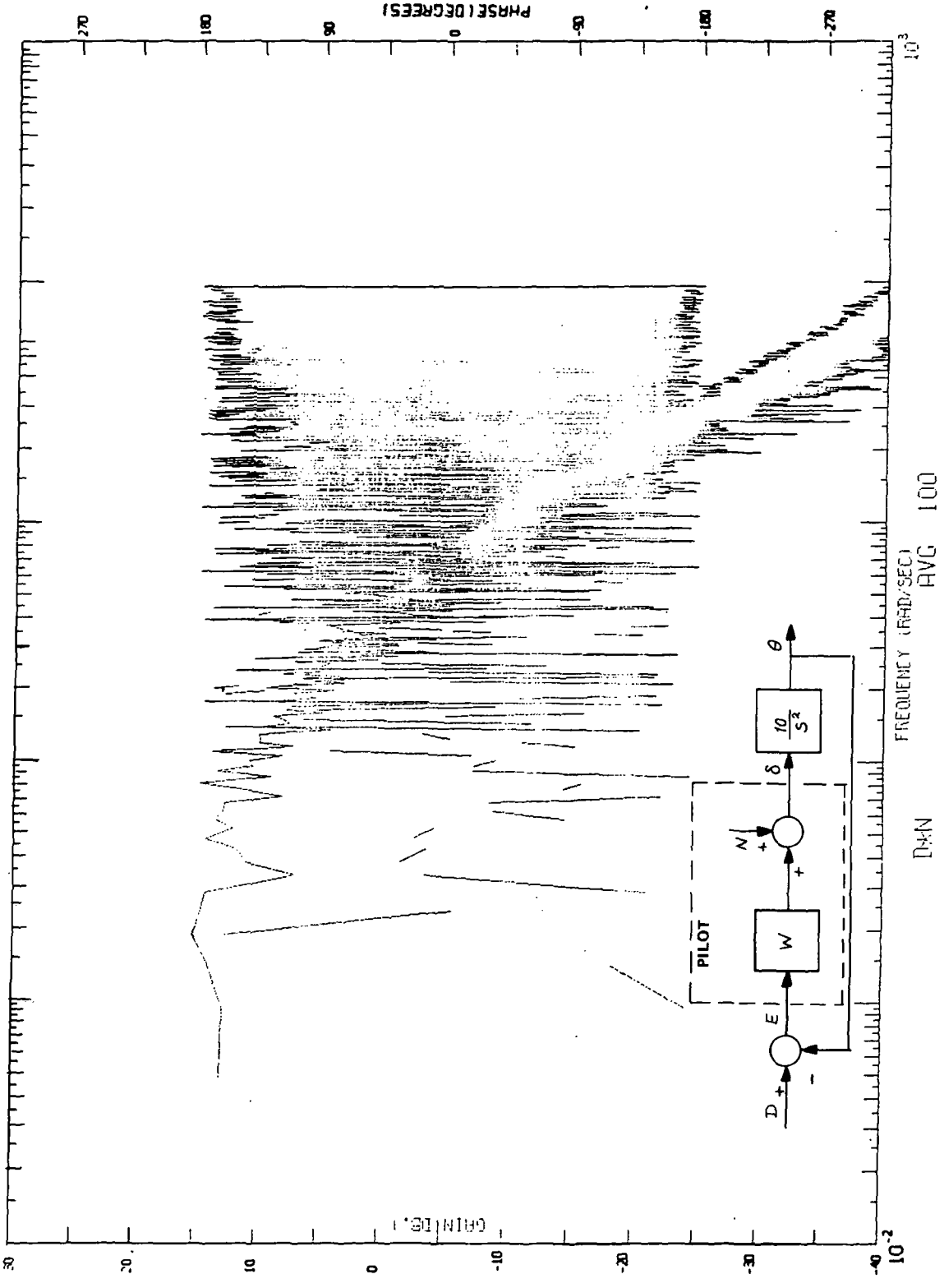

Figure 4.14 SUBJECT M , ϕ_{DN} , AVERAGE 100, PHASE INCLUDED

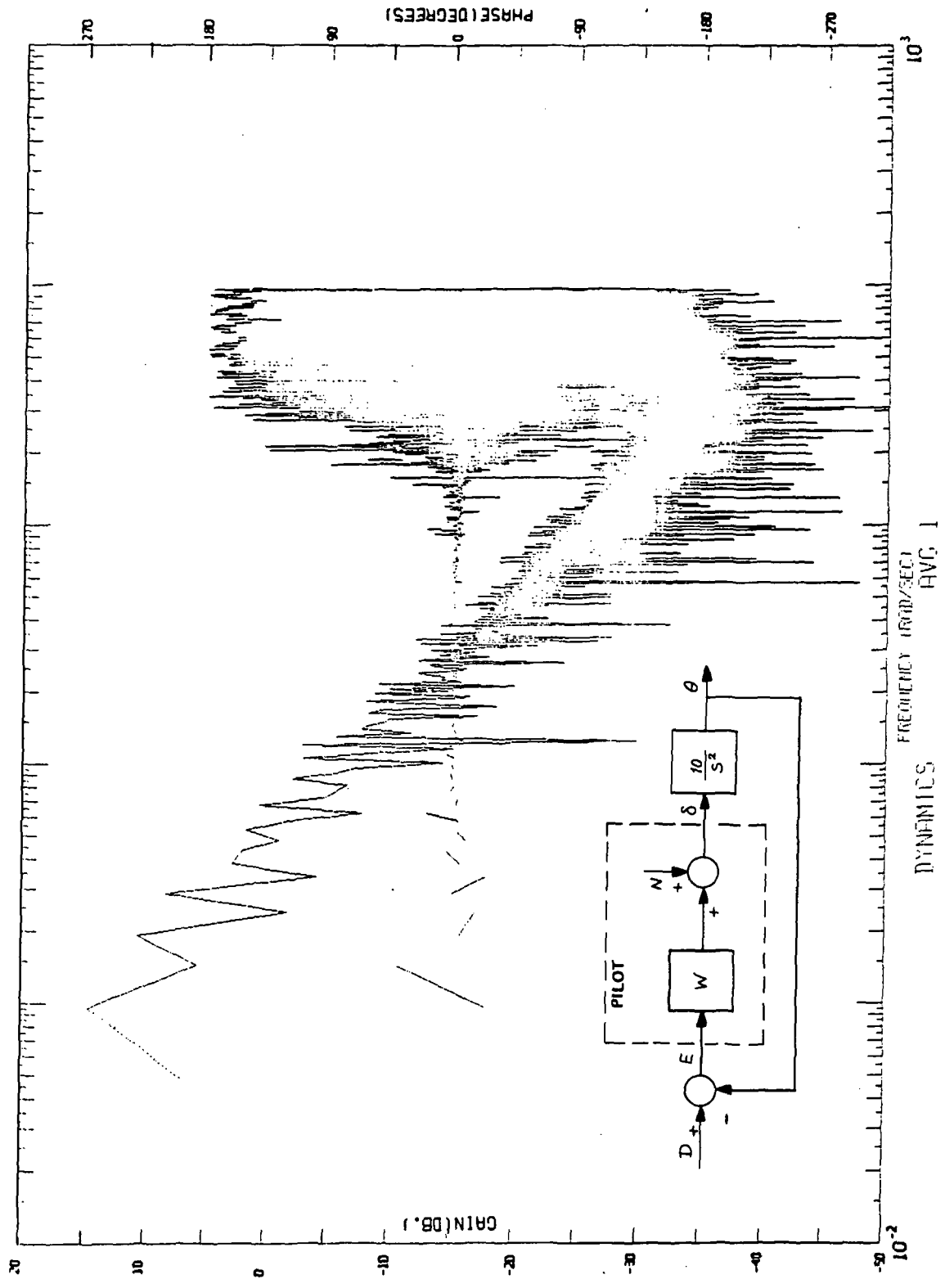

Figure 4.15 SUBJECT *M*, K/S^2, AVERAGE 1

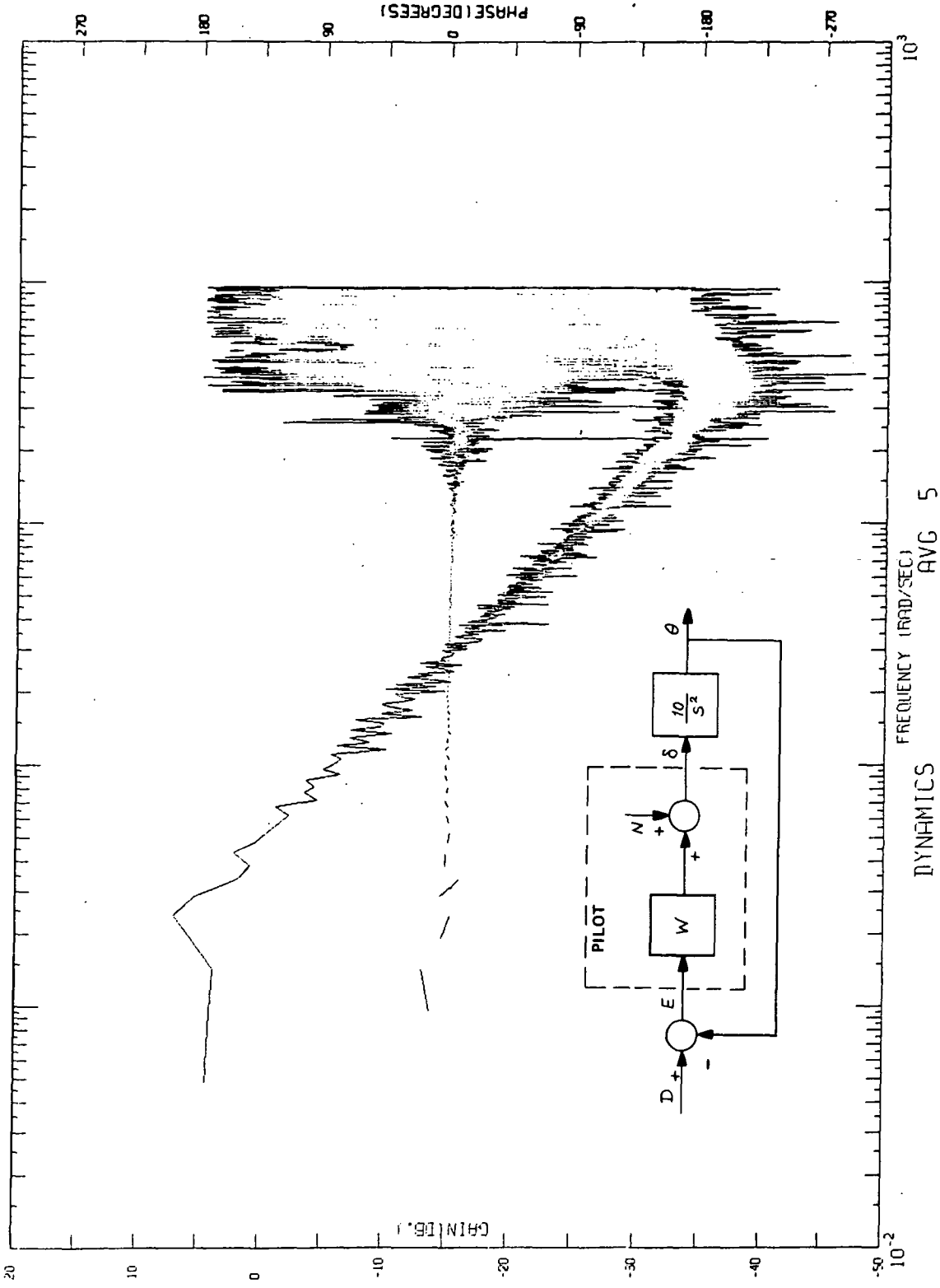

Figure 4.16 SUBJECT M, K/s^2, AVERAGE 5

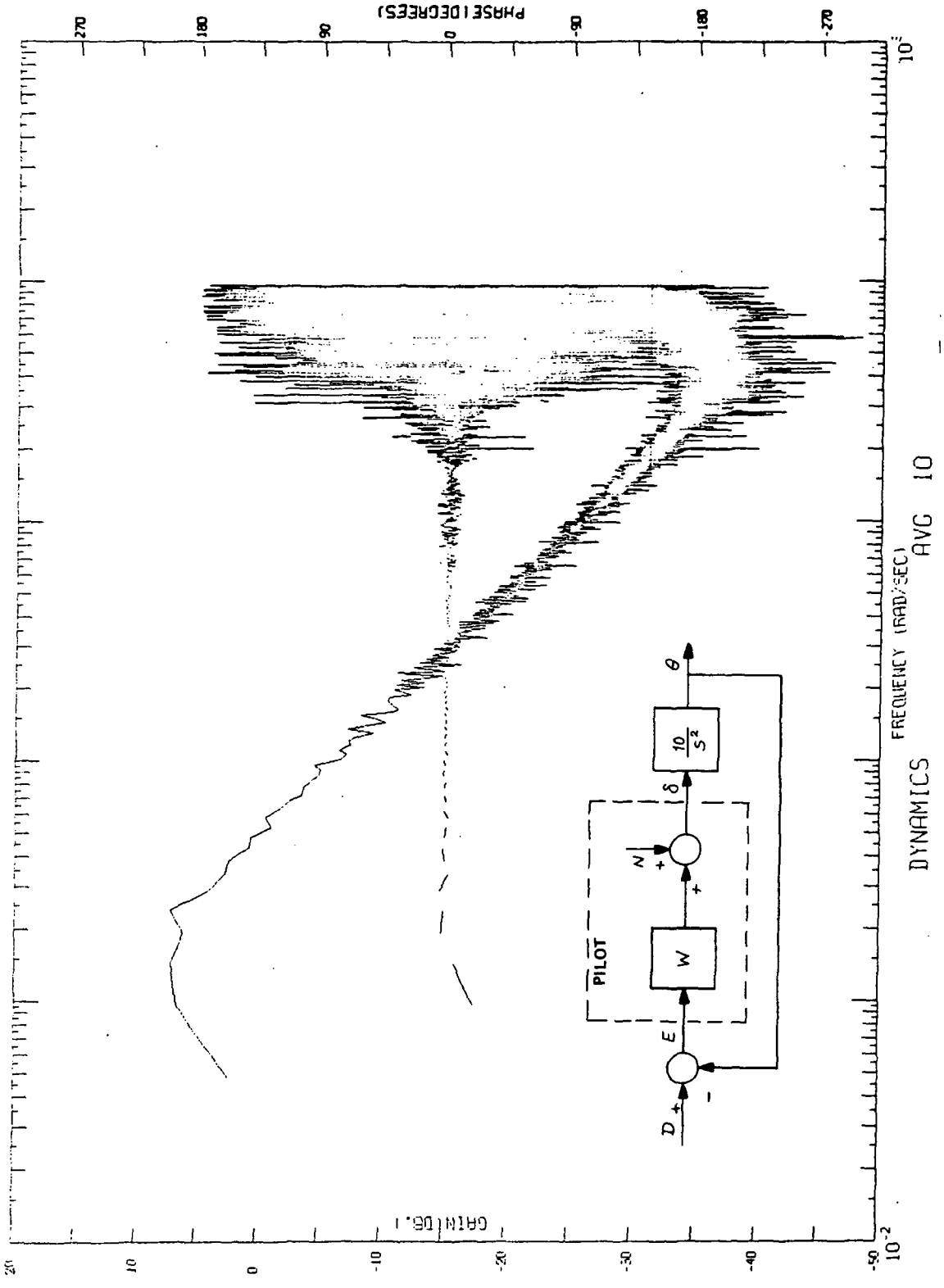

Figure 4.17 SUBJECT M, K/s^2, AVERAGE 10

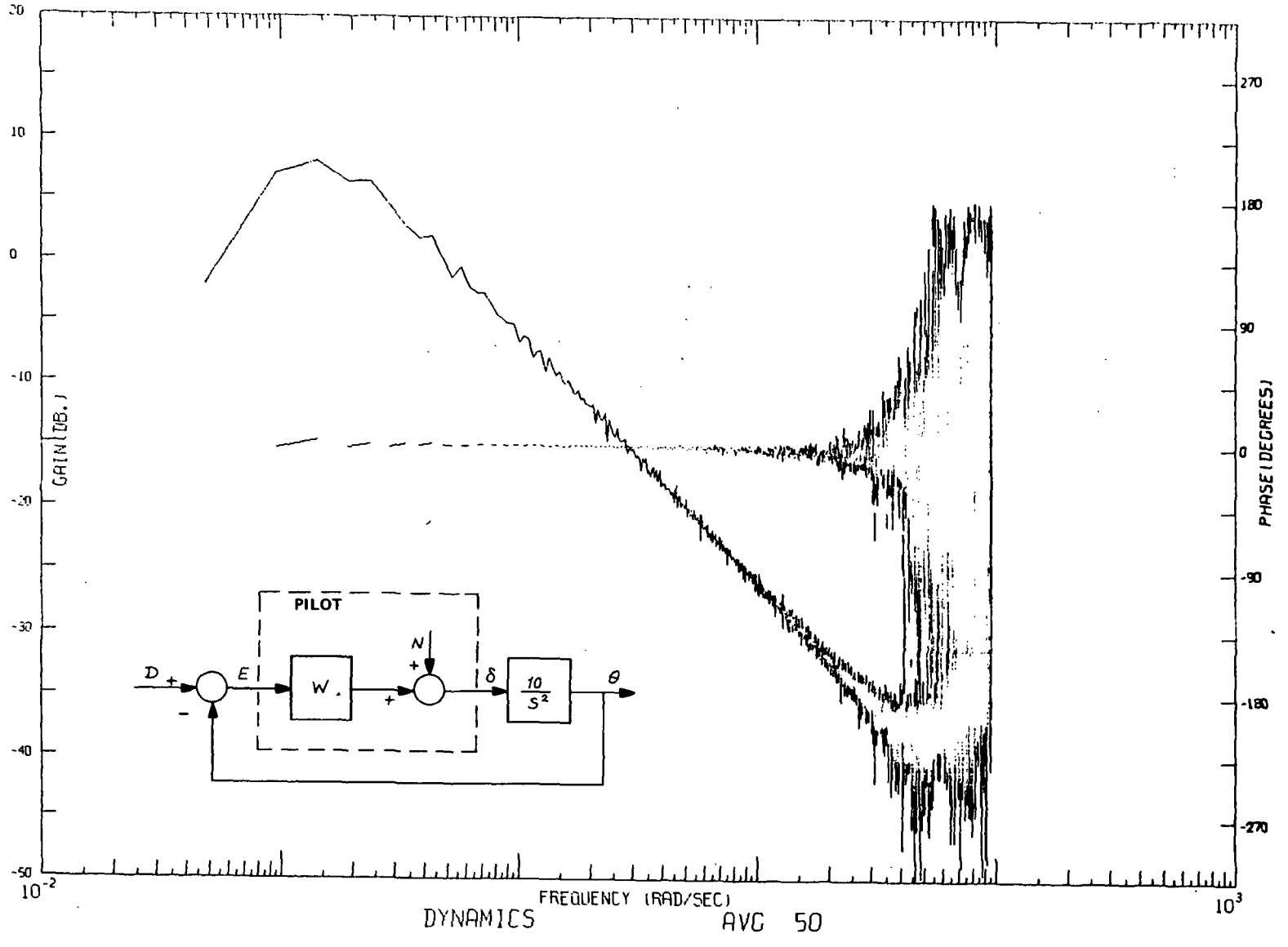

Figure 4.18 SUBJECT M, K/s^2, AVERAGE 50

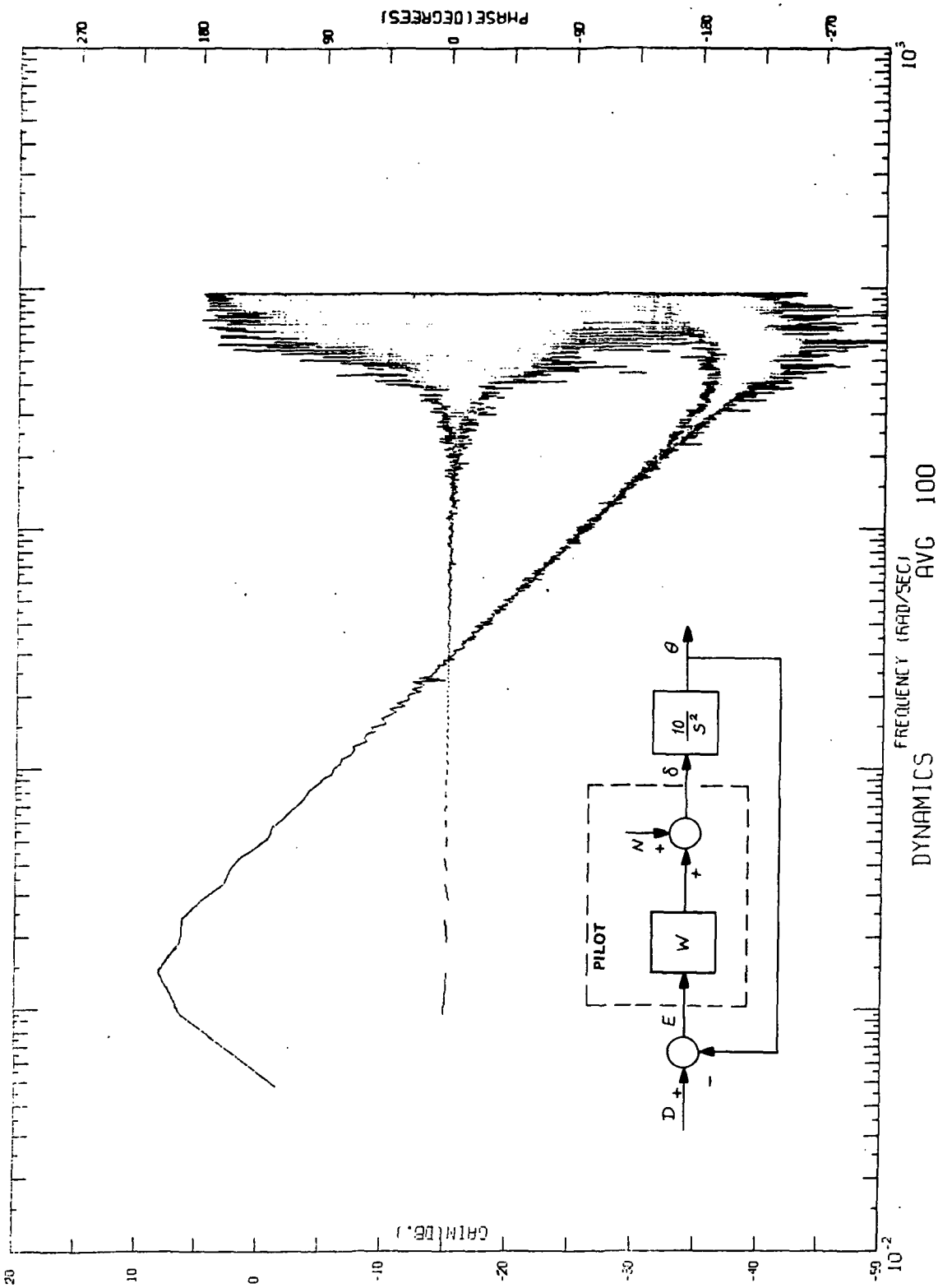

Figure 4.19 SUBJECT *M*, K/s^2, AVERAGE 100

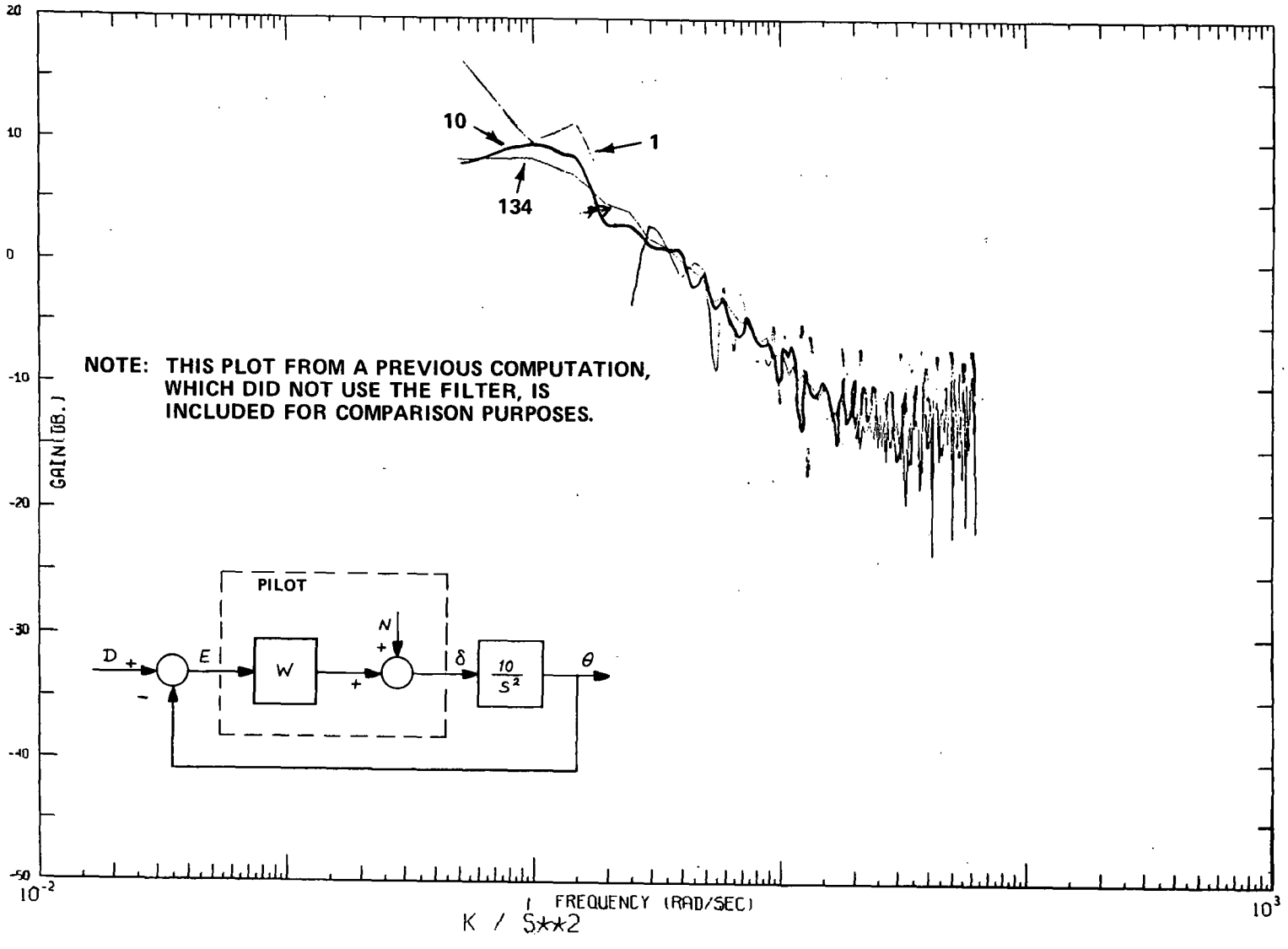

Figure 4.20 SUBJECT M, K/s^2 WITHOUT FILTERING (ONLY ENSEMBLE AVERAGE) FOR AVERAGE 1, 10, 134

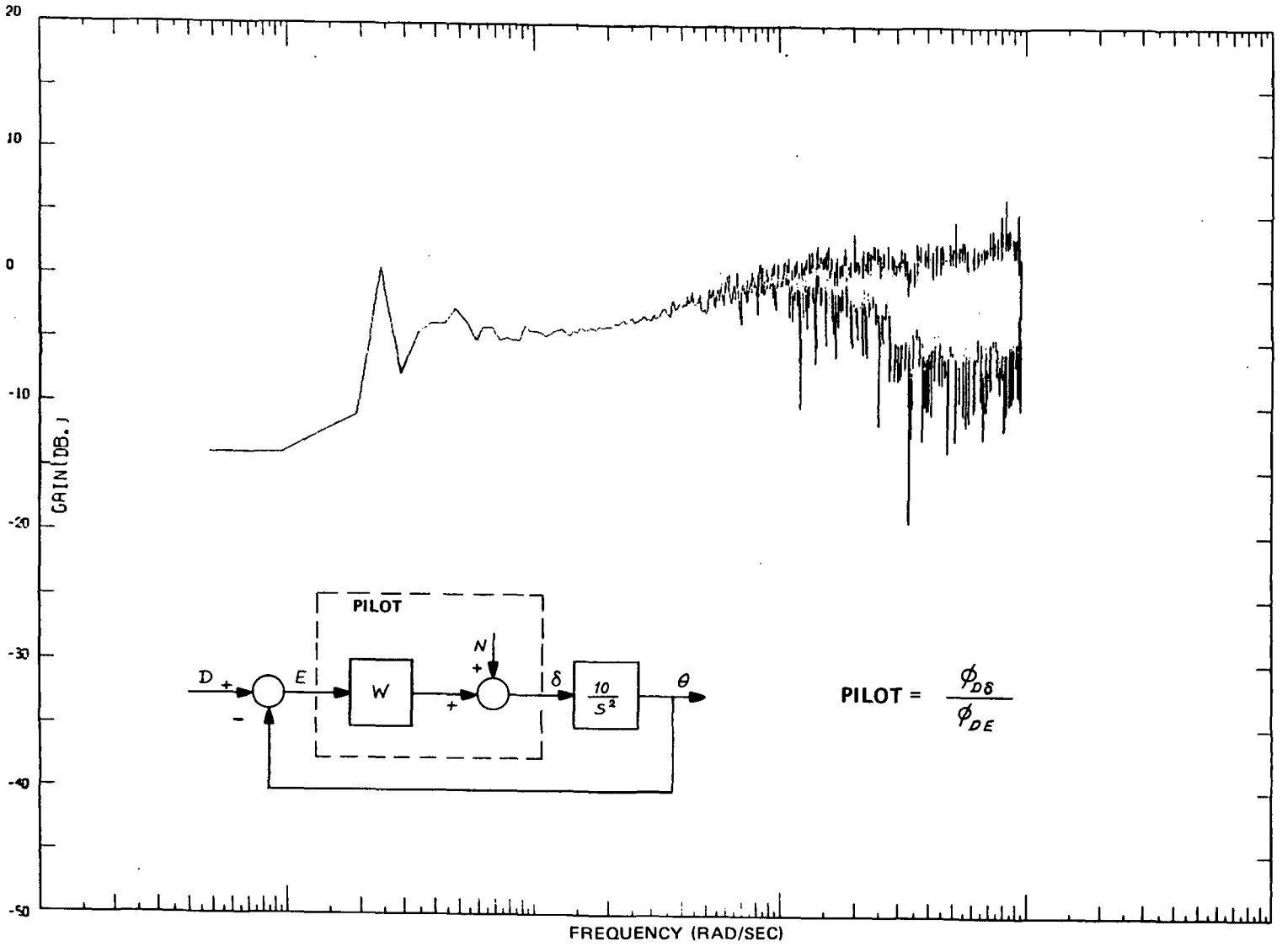

Figure 4.21 SUBJECT *M* , PILOT, AVERAGE 100 (ASSUME *N* IS NOT MEASURABLE)

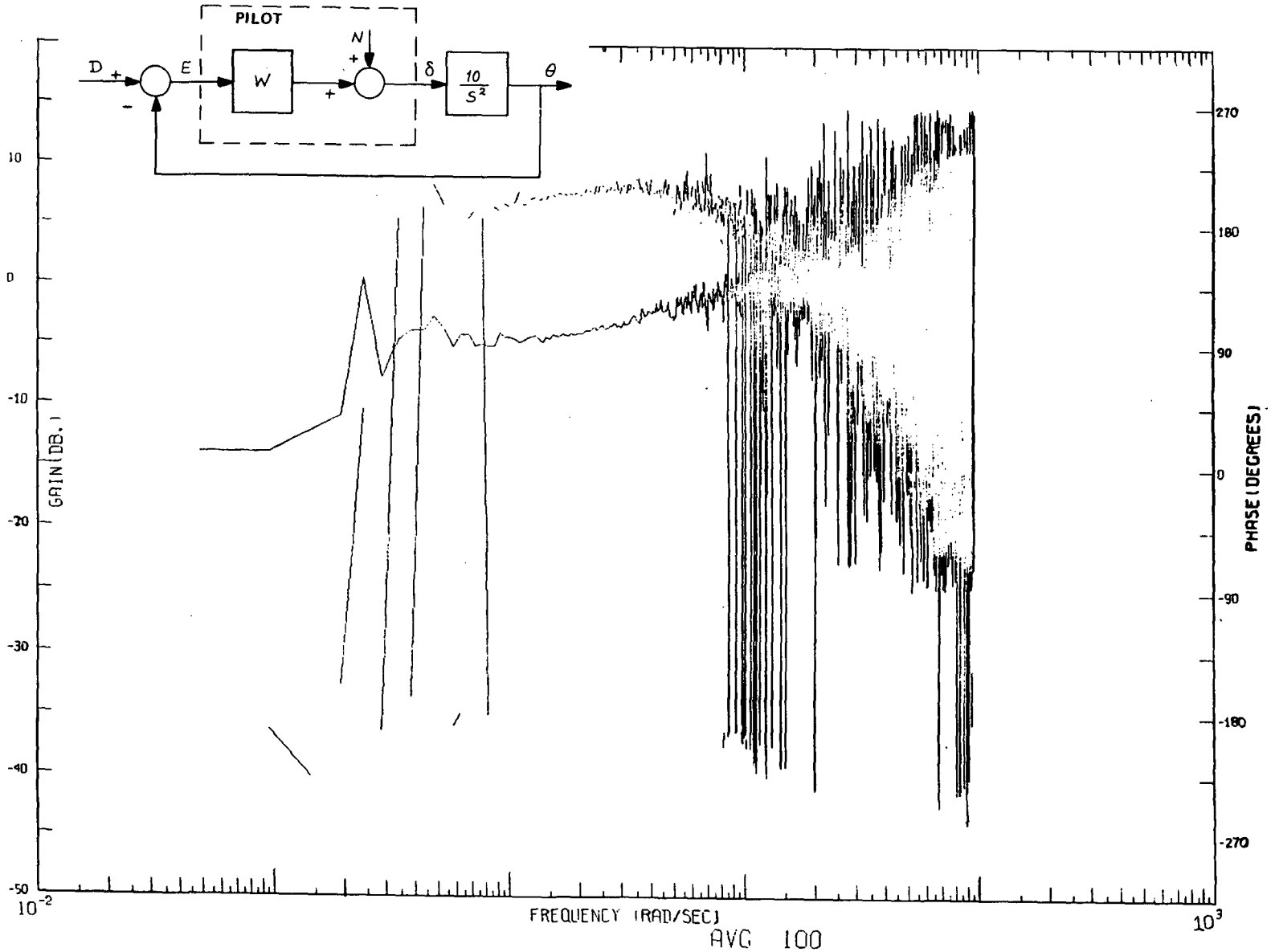

Figure 4.22 SUBJECT *M* , PILOT, AVERAGE (100), PHASE INCLUDED (*N* NOT MEASURABLE)

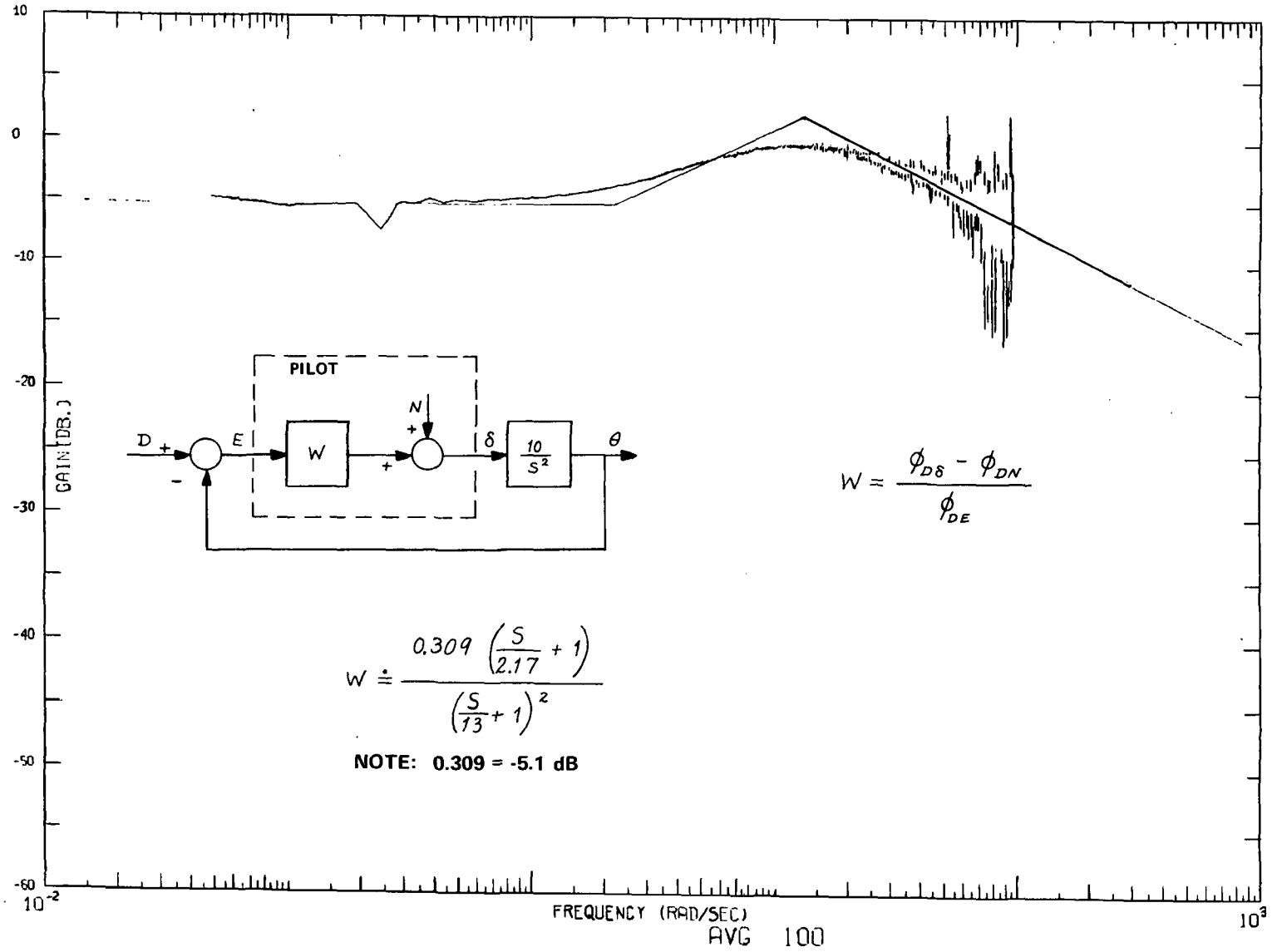

Figure 4.23 SUBJECT *M*, PILOT, AVERAGE 100 (*N* IS MEASURABLE)

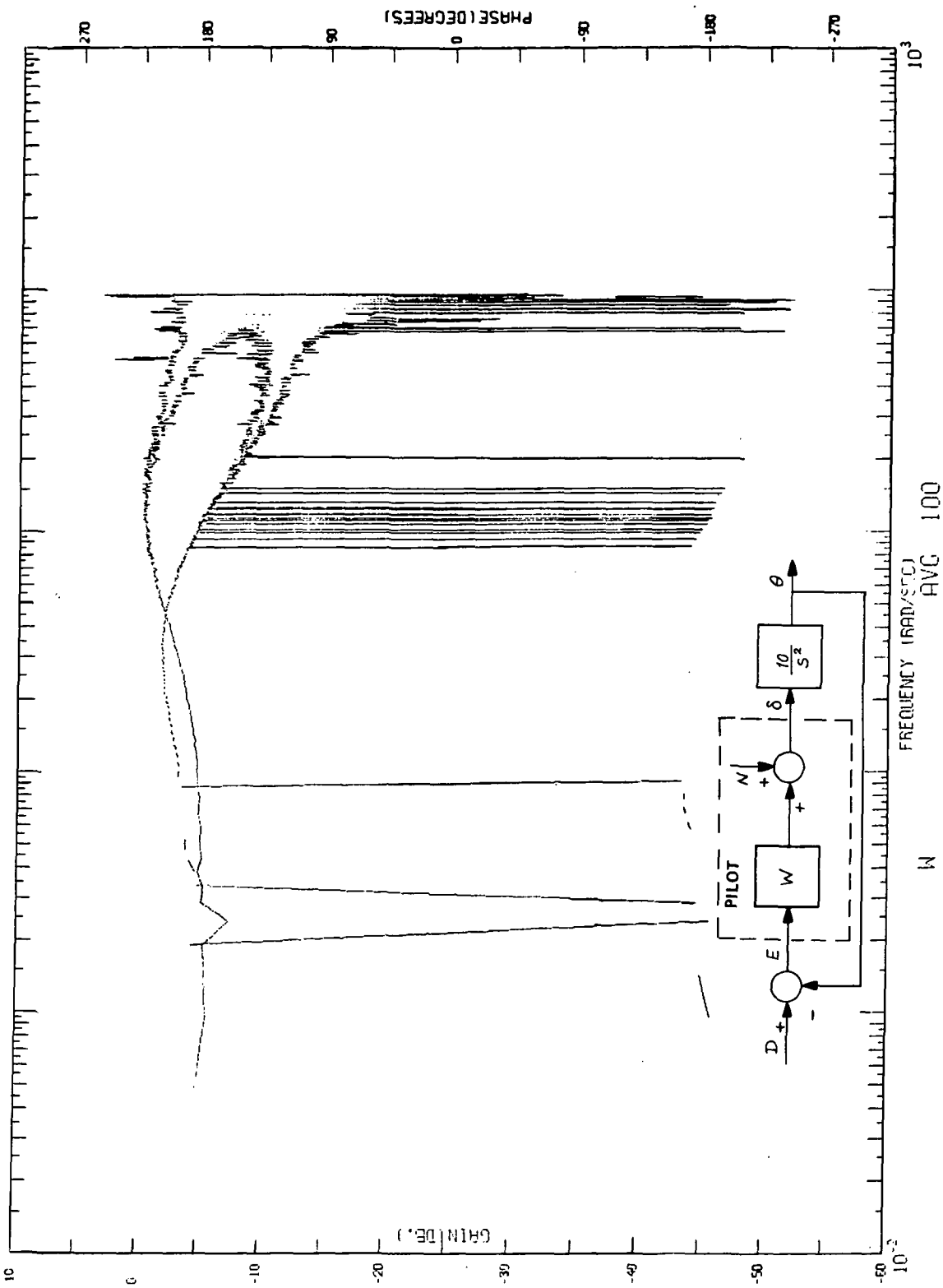

Figure 4.24 SUBJECT *M*, PILOT, AVERAGE 100, PHASE INCLUDED (*N* IS MEASURABLE)

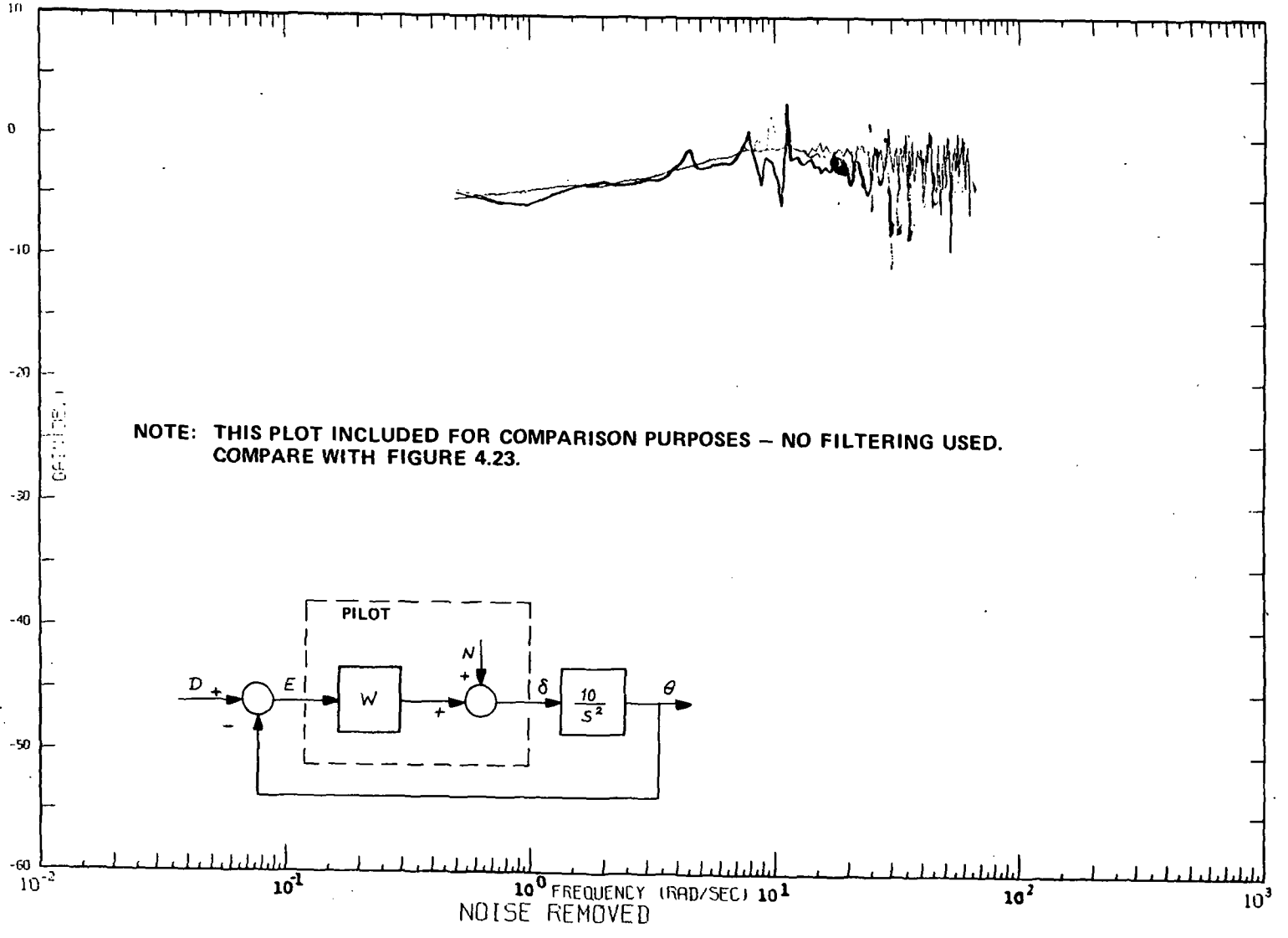

Figure 4.25 SUBJECT *M* , PILOT, AVERAGE 1, 10, 134, NOT FILTERED (*N* IS MEASURABLE)

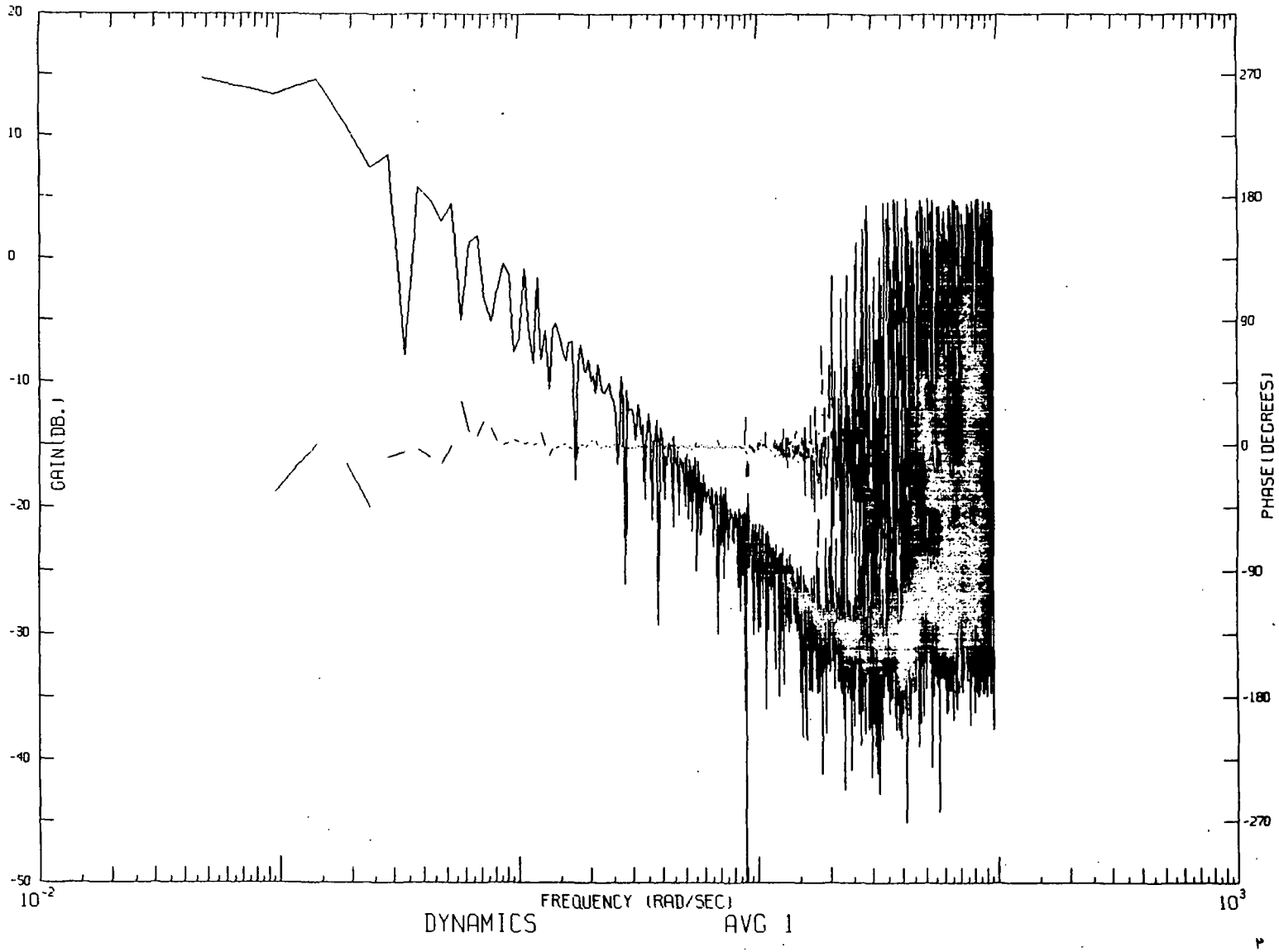

Figure 4.26 K/s^2 **DYNAMICS,** $\left(\frac{\sin x/4}{x/4}\right)^8$ **SPECTRAL FILTER, AVERAGE 1**

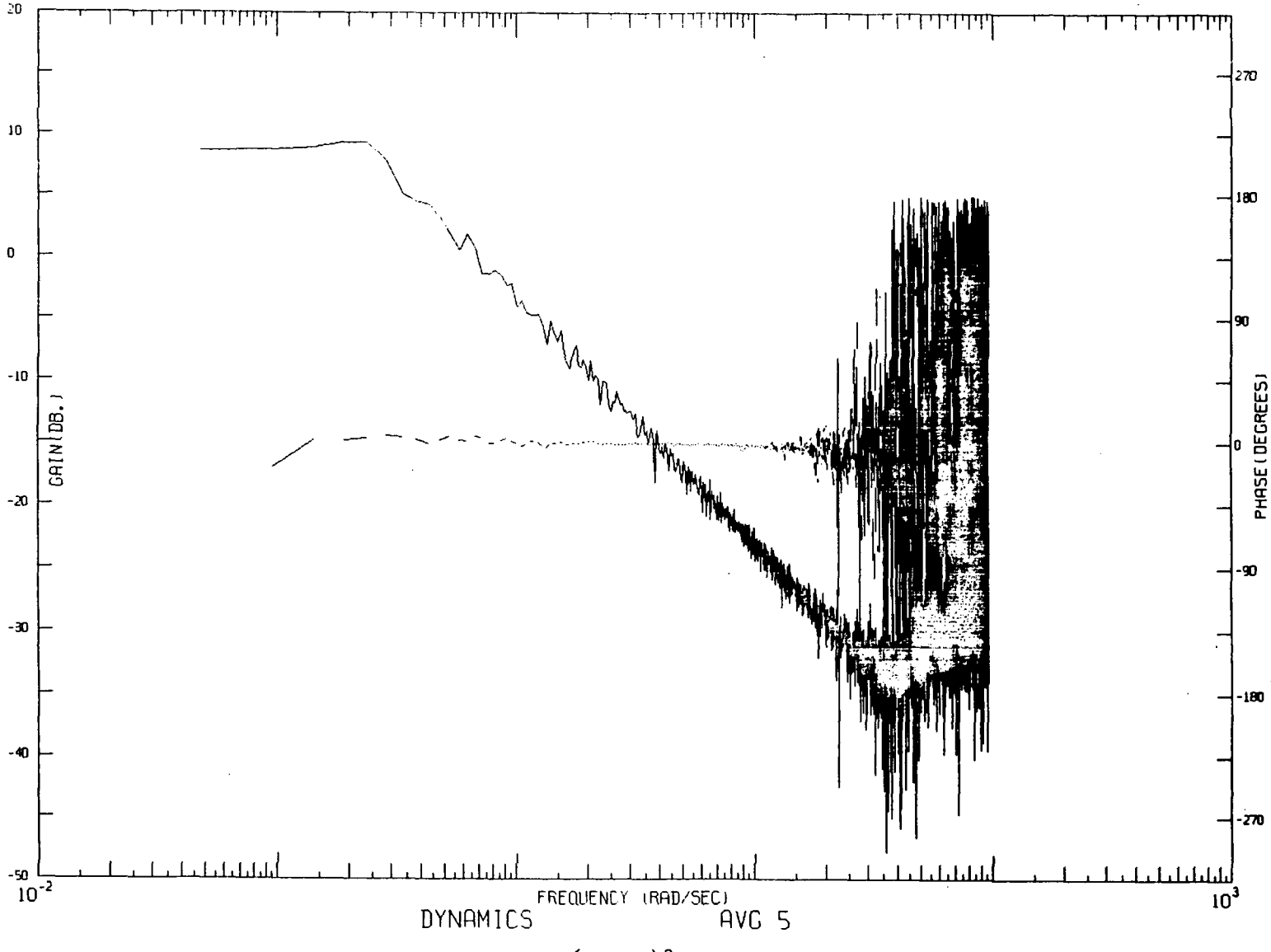

Figure 4.27 K/S^2 **DYNAMICS,** $\left(\frac{\sin x/4}{x/4}\right)^8$ **SPECTRAL FILTER, AVERAGE 5**

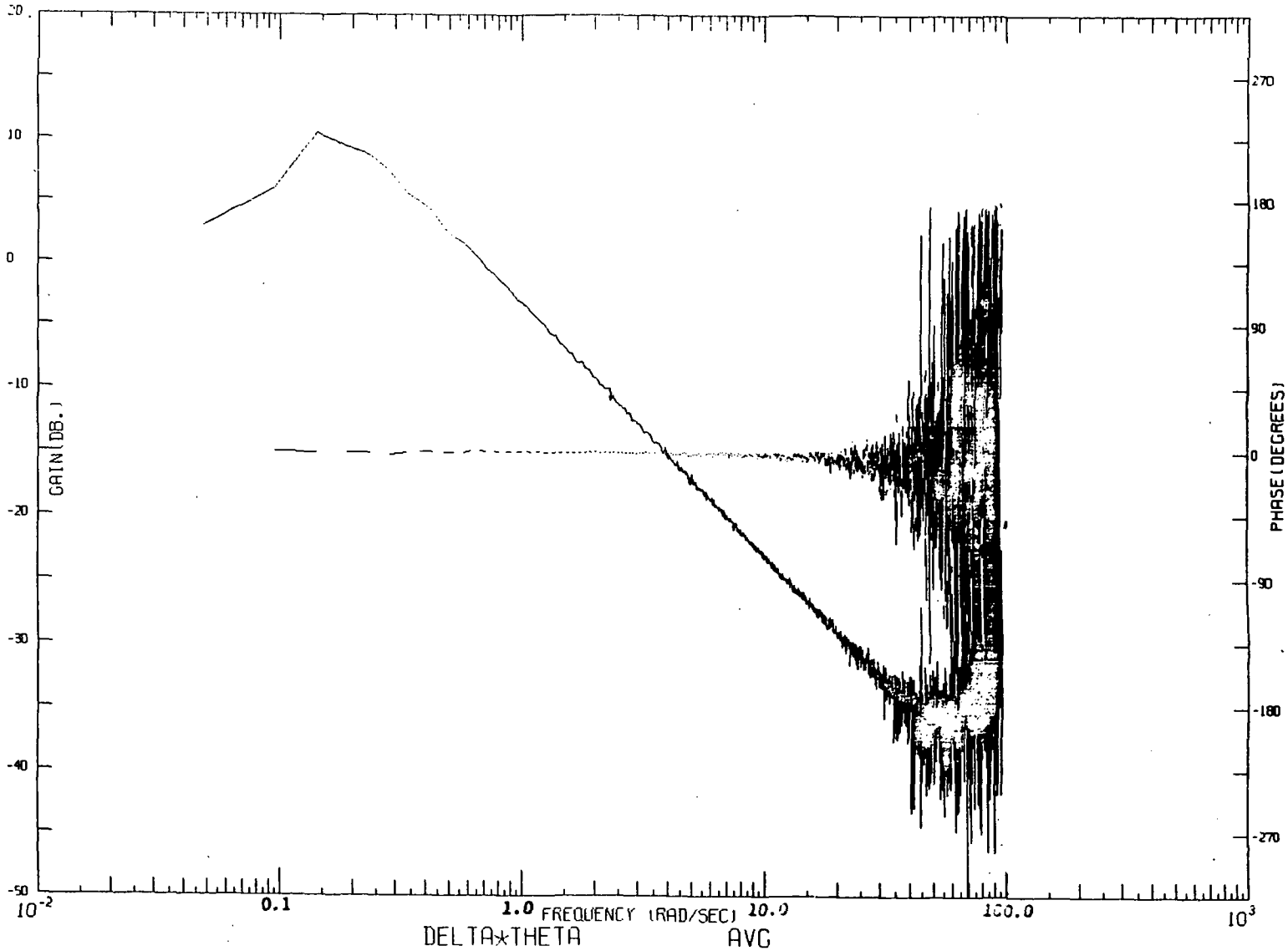

Figure 4.28 K/s^2 **DYNAMICS,** $\left(\frac{\sin x/4}{x/4}\right)^8$ **SPECTRAL FILTER, AVERAGE 102**

5. TWO CONTROLLER ROLL TRACKING EXPERIMENT

5.1 Introduction

This section discusses the application of the matrix modeling approach to the analysis of the data collected on a two controller roll tracking experiment. The experiment, which was carried out on the CAL fixed base flight simulator, was carefully designed to force an instrument rated pilot to use rudder (in a continuous fashion) to overcome the adverse yaw introduced by his roll tracking efforts with the aileron.

The experimental setup is described in the first section (Section 5.2). This is followed by a theoretical discussion of the difficulties encountered in multi-controller modeling (Section 5.3). In particular, it is shown that the determinant of the spectral matrix is always identically equal to zero if no ensemble averaging is used. Furthermore, it is shown that care must be exercised in the experiment formulation in order to insure the uniqueness of the matrix model. That is, for a particular experimental setup, there may well be more than one way of realizing the transfer functions which make up the entries of the matrix model - yet each realization gives the same mean square error between the outputs of the model and the pilots' recorded outputs.

In Section 5.4, an analysis made on the spectral matrices associated with the roll tracking experiment demonstrates that it is reasonable to expect that the experimental data will yield unique models.

In Section 5.5 the W-H conditions are given for the roll tracking while the experimental results are presented in Section 5.6, together with a discussion of the results. The reader is reminded that these efforts represent a preliminary excursion into defining the data requirements for a more detailed pilot model and therefore the preliminary nature of the pilot model estimates given in Section 5.6 should be kept clearly in mind.

5.2 Description of Experiment

The equations used in the simulation are limited six degree-of-freedom equations. They are limited in magnitude of permissible velocity and altitude variations. The present set of coefficients represent a T-33 at 250 KIAS at 23,000 feet. There is adverse aileron yaw.

The task requires the pilot to track in a situation in which adverse aileron yaw is sufficient to force the use of rudder in order to coordinate and reduce the effects of the aileron yaw.

The information available for display was:

(1) bank angle (roll tracking error)
(2) roll rate
(3) pitch angle
(4) sideslip angle
(5) yaw rate
(6) altitude
(7) indicated airspeed
(8) pitch rate
(9) heading
(10) rate of climb

For the experiment, the configuration AB and BA of the Meeker, Hall report (Reference 7) was used as a guide to initially determine the amount of adverse aileron yaw.* Because the cited configurations represent actual in-flight situations in which side acceleration is naturally felt, and whereas side acceleration is not felt in the ground based simulator, then some differences in pilot reactions may occur. However, since the main purpose of the experiment is to determine the requirements for the data analysis of a multi-controller task, it is necessary that both aileron and rudder be actively used by the pilot. Some "tailoring", on a trial and error basis, of the simulator configuration was done before the data runs were recorded, to ensure that this requirement was satisfied.

The development of a model which precisely takes into account the information displays on which the pilot views the various signals (e.g., an attitude indicator) is beyond the scope of the present study. In this exploratory effort, we will restrict ourselves to two hypothetical situations. In the first, it will be assumed that only two input signals can be measured (the error and yaw angle) but that both the aileron and rudder signals can be measured. The error is defined to be the difference between a noise input and the roll angle.

In the second case, it will be assumed that the measurable states are error and roll angle. The error is again defined as the difference between a noise input and roll angle.

The block diagram of the experimental configuration is given in Figure 5-1.

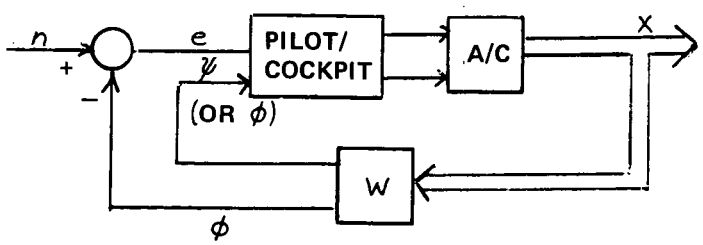

Figure 5.1 TWO CONTROLLER CONFIGURATION

*Refer to page 152 of Reference 7 for the aircraft equations of motion.

It was deemed wise to initially restrict the problem to one in which the spectral matrix was a 2x2 (the number of signals displayed to the pilot are restricted to two) since this experiment represents an exploratory effort in the two controller modeling area. In the next section, it will be shown that there is another good reason to restrict the spectral matrix to a 2x2. That is, it is desirable that the solution be unique.

5.3 The Spectral Matrix

The limited experience gained to date in the multi-controller modeling effort has identified two fundamental points that are critical to the vector approach (points which are of no particular concern in scalar modeling efforts). These points are:

(1) With no ensemble averaging, the determinant of the spectral matrix is identically equal to zero. This result is not affected by the type of time domain window placed on the data.

(2) Even with perfect estimates of the auto and cross spectra that make up the spectral matrix, it is possible to formulate a multi-controller experiment in a manner which theoretically gives a spectral matrix with a zero determinant.

The proof of (1) above is quite simple and can better be demonstrated with an example rather than a proof. Suppose the underlying (true) spectral matrix has the form

$$\phi = \begin{bmatrix} \phi_{x_1x_1} & \phi_{x_1x_2} \\ \phi_{x_2x_1} & \phi_{x_2x_2} \end{bmatrix} \tag{5.1}$$

so that an ensemble of 1 would give

$$\hat{\phi} = \frac{1}{2T} \begin{bmatrix} X_1(-s)X_1(s) & X_1(-s)X_2(s) \\ X_2(-s)X_2(s) & X_2(-s)X_2(s) \end{bmatrix} \tag{5.2}$$

The determinant of $\hat{\phi}$ is therefore

$$\det \hat{\phi} = \frac{1}{4T^2}\left[X_1(-s)X_1(s)X_2(-s)X_2(s) - X_1(-s)X_2(s)X_2(-s)X_2(s)\right] \equiv 0 \tag{5.3}$$

Thus, when there is ensemble averaging, the Fourier coefficients computed for the truncated transforms will always yield a zero determinant, indicating that ensemble averaging is a necessity in the vector approach.

We turn now to the more difficult topic associated with (2) above - namely, under what conditions will the determinant of the spectral matrix be identically equal to zero? At this point in time, we are unable to furnish a general answer to that question. However, a limited result, one which is applicable to the pilot modeling task, is in hand. This result can best be demonstrated by means of an example. The approach used will then be applied, in the next section, to the roll tracking experiment.

Suppost that the aircraft equations of motion are given in the first order form

$$\dot{x} = F x + G u + n(t) \tag{5.4}$$

In equation (5.4), x is the state vector, u is the control vector and n is the noise and/or disturbance vector. Taking the LaPlace transform of Equation (5.4) gives

$$X_{(s)} = \left[I S - F \right]^{-1} \left[G U + N \right] \tag{5.5}$$

Therefore

$$X' = X'_{(s)} = \left[U' G' + N' \right] \left[I S - F' \right]^{-1} \tag{5.6}$$

Suppose now that all of the states are displayed to the pilot. That is

$$W'_* X'_* X' W' = X_{(-s)} X'_{(s)} \tag{5.7}$$

so that

$$\phi_{xx'} = \lim_{T \to \infty} \frac{1}{2T} E\left\{ X_{(-s)} X'_{(s)} \right\} = \left[-IS - F \right]^{-1} \left[G \phi_{uu'} G' + G \phi_{un'} + \phi_{nu'} G' + \phi_{nn'} \right] \left[IS - F' \right]^{-1} \tag{5.8}$$

$$= \left[-IS - F \right]^{-1} \left[\text{---} \right] \left[IS - F' \right]^{-1} \tag{5.9}$$

The determinant of the spectral matrix is identically equal to zero if $\det \multimap\!\!\circ\!\!\multimap = 0$ since the determinant of $[I\,S - F']^{-1} \neq 0$ for all values of ω .

The matrix of transfer functions which represent the linear portion of the pilot's output will be unique if

$$\det \left[G \phi_{uu'} G' + G \phi_{un'} + \phi_{nu'} G' + \phi_{nn'} \right] \neq 0 \tag{5.10}$$

example: two output, single controller

$$\begin{bmatrix} \dot{x}_1 \\ \dot{x}_2 \end{bmatrix} = \begin{bmatrix} 0 & 1 \\ -a & -b \end{bmatrix} \begin{bmatrix} x_1 \\ x_2 \end{bmatrix} + \begin{bmatrix} 0 \\ 1 \end{bmatrix} u + \begin{bmatrix} n_1 \\ n_2 \end{bmatrix} \tag{5.11}$$

$$G \phi_{uu'} G^{-1} = \begin{bmatrix} 0 \\ \\ 1 \end{bmatrix} \phi_{uu} \begin{bmatrix} 0 & 1 \end{bmatrix} = \begin{bmatrix} 0 & 1 \\ \\ 0 & \phi_{uu} \end{bmatrix} \tag{5.12}$$

$$G \phi_{un'} = \begin{bmatrix} 0 \\ \\ 1 \end{bmatrix} \begin{bmatrix} \phi_{un_1} & \phi_{un_2} \end{bmatrix} = \begin{bmatrix} 0 & 0 \\ \\ \phi_{un_1} & \phi_{un_2} \end{bmatrix} \tag{5.13}$$

$$\phi_{nu'} G' = \begin{bmatrix} \phi_{n_1 u} \\ \\ \phi_{n_2 u} \end{bmatrix} \begin{bmatrix} 0 & 1 \end{bmatrix} = \begin{bmatrix} 0 & \phi_{n_1 u} \\ \\ 0 & \phi_{n_2 u} \end{bmatrix} \tag{5.14}$$

$$\phi_{nn'} = \begin{bmatrix} \phi_{n_1 n_1} & \phi_{n_1 n_2} \\ \\ \phi_{n_2 n_1} & \phi_{n_2 n_2} \end{bmatrix} \tag{5.15}$$

$$\therefore \quad \multimap\!\!\circ\!\!\multimap = \left[\begin{array}{c|c} \phi_{n_1 n_1} & \phi_{n_1 n_2} + \phi_{n_1 u} \\ \hline \phi_{n_2 n_1} + \phi_{u n_1} & \phi_{n_2 n_2} + \phi_{uu} + \phi_{u n_2} + \phi_{n_2 u} \end{array}\right] \tag{5.16}$$

The det $\leftrightarrow\!\ominus\!\leftrightarrow$ would equal zero if the noise signal n_1 were equal to zero -- no matter what kind of noise was introduced on the x_2 component of the state vector! That is, if we had let

$$U = \begin{bmatrix} H_{11} & H_{12} \end{bmatrix} \begin{bmatrix} x_1 \\ x_2 \end{bmatrix} + R \quad , \tag{5.17}$$

there would be an infinity of combinations of H_{11}'s and H_{12}'s that would satisfy the vector Wiener-Hopf equations if the noise on the x_1 component were omitted.

The example cited above is apparently typical of what can occur in the matrix model when it is assumed that all of the states are available for display to the pilots and when there is not a sufficient number of inputs to perturb the situation. That is, in a poorly designed experiment, the matrix of transfer functions might be much larger than is really necessary to account for the power in a limited number of disturbances and hence there are many ways in which the power can be split up within the model and still satisfy the mean square error criteria. In the two controller roll tracking experiment, for reasons of both economy and prudence, only one disturbance noise source was introduced.

5.4 The Spectral Matrix for the Roll Tracking Task

Even though the input spectral matrix has been restricted to a 2x2 (only one noise source is being used), it is still prudent to check, as much as possible, on the characteristics of the spectral matrix. Two cases will be considered. First, the signals displayed to the pilot will be error and yaw, where the error is defined to be the difference between the noise input and bank angle. That is,

$$e = n - \phi \tag{5.18}$$

The spectral matrix is

$$\Phi = \begin{bmatrix} \phi_{ee} & \phi_{e\psi} \\ \phi_{\psi e} & \phi_{\psi\psi} \end{bmatrix} \tag{5.19}$$

In terms of n , ϕ and ψ , the determinant of Equation (5.19) is

$$\det \Phi = \Phi_{nn}\,\Phi_{\psi\psi} - \Phi_{n\phi}\,\Phi_{\psi\psi} - \Phi_{\phi n}\,\Phi_{\psi\psi} + \Phi_{\phi\phi}\,\Phi_{\psi\phi}$$

$$- \Phi_{n\psi}\,\Phi_{\psi n} + \Phi_{n\psi}\,\Phi_{\psi\phi} + \Phi_{\phi\psi}\,\Phi_{\psi n} - \Phi_{\phi\psi}\,\Phi_{\psi\phi} \qquad (5.20)$$

There is no reason in particular to suspect that Equation (5.20) is identically zero for all values of ω , hence the experimental formulation seems sound enough.

In the second case studied, error and bank angles were used as inputs so that the spectral matrix becomes

$$\Phi = \begin{bmatrix} \Phi_{ee} & \Phi_{e\phi} \\ \Phi_{\phi e} & \Phi_{\phi\phi} \end{bmatrix} \qquad (5.21)$$

In terms of n and ϕ , the spectral matrix is

$$\Phi = \left[\begin{array}{c|c} \Phi_{nn} - \Phi_{n\phi} - \Phi_{\phi n} + \Phi_{\phi\phi} & \Phi_{n\phi} - \Phi_{\phi\phi} \\ \hline \Phi_{\phi n} - \Phi_{\phi\phi} & \Phi_{\phi\phi} \end{array}\right] \qquad (5.22)$$

For this case, there is cancellation of terms in the determinant, giving

$$\det \Phi = \left[\Phi_{nn}\,\Phi_{\phi\phi} - \Phi_{n\phi}\,\Phi_{\phi n}\right] \qquad (5.23)$$

Equation (5.23) could be identically zero if bank angle were related to the noise input by means of a linear transfer function. That is, if

$$\phi = G(s)\, n \qquad (5.24)$$

then

$$\det \phi = \left[\phi_{nn} \cdot G(-s)\, G(s)\, \phi_{nn} - G(-s)\, \phi_{nn} \cdot G(s)\, \phi_{nn} \right] = 0 \tag{5.25}$$

This seems unlikely and therefore we feel that this case is also a reasonable one to pursue.

5.5 Wiener-Hopf Equation for the Two Controller Roll Task

The two cases are defined by the following Wiener Hops equations:

$$\left[\begin{array}{c|c} \phi_{ee} & \phi_{e\gamma} \\ \hline \phi_{\psi e} & \phi_{\psi\gamma} \end{array}\right] \left[\begin{array}{c|c} H_{11} & H_{12} \\ \hline H_{21} & H_{22} \end{array}\right] - \left[\begin{array}{c|c} \phi_{e\delta_a} & \phi_{e\delta_r} \\ \hline \phi_{\psi\delta_a} & \phi_{\psi\delta_r} \end{array}\right] = \left[\begin{array}{c|c} Z_{11} & Z_{12} \\ \hline Z_{21} & Z_{22} \end{array}\right] \tag{5.26}$$

$$\left[\begin{array}{cc} \phi_{ee} & \phi_{e\phi} \\ \phi_{\phi e} & \phi_{\phi\phi} \end{array}\right] \left[\begin{array}{cc} H_{11} & H_{12} \\ H_{21} & H_{22} \end{array}\right] - \left[\begin{array}{cc} \phi_{e\delta_a} & \phi_{e\delta_r} \\ \phi_{\phi\delta_a} & \phi_{\phi\delta_r} \end{array}\right] = \left[\begin{array}{c|c} Z_{11} & Z_{12} \\ \hline Z_{21} & Z_{22} \end{array}\right] \tag{5.27}$$

The matrix H which models the pilot will have four entries, since two inputs are assumed and there are two active controllers available.

For comparative purposes, it is desirable to present results using three different approaches. In the first two approaches, solutions "without regard to physical realizibility" are found (i.e., the Z matrix in Equations (5.26) and (5.27) are set equal to zero). In order to produce a reference set of transfer functions, the first approach will set the off-diagonal terms in the spectral matrix equal to zero. That is, produce a decoupled result suitable for comparison purposes. The second approach will retain the off diagonal terms in the spectral matrix and therefore will give a "coupled" result. The third, more desirable approach is to implement the technique illustrated in Section 2.4 in which the factorization was carried through using experimental data.

The factorization algorithm described in Section 2.4 was programmed for the digital computer and checked out on relatively low order, precise analytical examples. By low order, we mean that the root finding algorithms and standard matrix inversions routines required at various points in the program were able to handle reasonable polynomials (on the order of s^{16}) when the "nice" numbers associated with the analytical examples were used. However,

the extreme dynamic range of the signals encountered in the two controller experiment (on the order of 120 dB) results in ill conditioned data that lead to poor checks on inversion routines and root finding algorithms. That is when roots of a polynomial are multiplied together they do not yield the original polynomial and multiplying the calculated inverse of a matrix by the matrix itself does not give a very good approximation to the identity matrix. For these reasons, the estimates of the matrix model presented in this section should be regarded only as preliminary and perhaps as indicative of some underlying trend. That is, there is a noticeable difference between the factorized results and the results obtained when physical realizability is ignored.

At any rate, it appears that the theoretical approach to obtaining the factorized model is a sound one and that the quality of the estimates is basically limited by factors which are associated with the wide dynamic range data obtained when the six degree of freedom aircraft equations are used.

5.6 Two Controller Roll Tracking Task Experimental Results

As discussed in the previous section, the following solutions will be presented.

Approach 1: $\not\equiv$ matrix $\equiv 0$, $\phi_{e\psi} \equiv 0$ (decoupled solution)

Case 1:

$$H_{11} = \frac{\phi_{e\delta_a}}{\phi_{ee}} , \quad H_{12} = \frac{\phi_{e\delta_r}}{\phi_{ee}} \tag{5.28}$$

$$H_{21} = \frac{\phi_{\psi\delta_a}}{\phi_{\psi\psi}} , \quad H_{22} = \frac{\phi_{\psi\delta_r}}{\phi_{\psi\psi}} \tag{5.29}$$

Case 2: $\not\equiv$ matrix $\equiv 0$, $\phi_e \equiv 0$ (decoupled solution)

H_{11} (same as Case 1) H_{12} (same as Case 1)

$$H_{21} = \frac{\phi_{\phi\delta_a}}{\phi_{\phi\phi}} , \quad H_{22} = \frac{\phi_{\phi\delta_r}}{\phi_{\phi\phi}} \tag{5.30}$$

Approach 2: $\not\equiv$ matrix $\equiv 0$; $\phi_{e\psi}$, $\phi_{e\phi} \neq 0$

Case 1:

$$\begin{bmatrix} H_{11} & H_{12} \\ H_{21} & H_{22} \end{bmatrix} = \begin{bmatrix} \phi_{ee} & \phi_{e\psi} \\ \phi_{\psi e} & \phi_{\psi\psi} \end{bmatrix}^{-1} \begin{bmatrix} \phi_{e\delta_a} & \phi_{e\delta_r} \\ \phi_{\psi\delta_a} & \phi_{\psi\delta_r} \end{bmatrix} \tag{5.31}$$

Case 2:
$$\begin{bmatrix} H_{11} & H_{12} \\ H_{21} & H_{22} \end{bmatrix} = \begin{bmatrix} \phi_{ee} & \phi_{e\phi} \\ \phi_{\phi e} & \phi_{\phi\phi} \end{bmatrix}^{-1} \begin{bmatrix} \phi_{e\delta_a} & \phi_{e\delta_r} \\ \phi_{\phi\delta_a} & \phi_{\phi\delta_r} \end{bmatrix} \tag{5.32}$$

Approach 3: Factorized results are given which employ a digital computational algorithm patterned after the illustrative example of Section 2.4.

The experimental results are presented in Figures 5.2 through 5.28. Figures 5.2 through 5.4 are representative of the auto and cross spectra used in the computation of the transfer functions. The remainder of the figures present the transfer function computed according to either Equation (5.31) (e , ψ input data) or Equation (5.32) (e , ϕ input data, refer to Table 2).

Figures	Input Signals	Coupling	Phase Information Included
5.5 - 5.8	e, ψ	coupled and decoupled	No
5.9 - 5.12	e, ϕ	coupled and decoupled	No
5.13-5.16	e, ψ	decoupled	Yes
5.17-5.20	e, ϕ	decoupled	Yes
5.21-5-24	e, ψ	coupled	Yes
5.25-5.28	e, ϕ	coupled	Yes

TABLE 2. INFORMATION CONTENT OF FIGURES 5.5 THROUGH 5.28

Figure 5.2 shows the error signal autospectra for ensemble averaging across 1, 5, 10 and 20 estimates using the $\left(\frac{\sin \pi/4}{\pi/4}\right)^8$ spectral window. It is seen that the convergence is quite rapid and there is no reason to expect that the average 20 results will be noticeably superior to, say, the average 10 results. The estimates of transfer function presented later will all use the ensemble 20 data. The data for an average of one was checked and it was verified that the determinant of the spectral matrix was identically equal to zero. It was non zero for all the other averages (5, 10, 20).

The cross spectra between roll and aileron as well as roll and rudder are given in Figure 5.3. It is seen that cross power are approximately of equal order of magnitude, with slightly more power in the roll, aileron cross spectra. Notice also how stable the $\hat{\phi}_{\phi\delta_a}$ phase plot is compared to the phase plot for $\hat{\phi}_{\phi\delta_r}$.

Basic data is presented in Figure 5.4 which can be checked against Figure 5.3 to compare the pilots' aileron effort against both roll and yaw.

In addition the break up in phase occurs much lower in frequency indicating that signals related to ψ are dropping off at a much faster rate than are those connected with ϕ . The $\hat{\phi}_{\psi\psi}$ spectral plots verify this, giving evidence of a true dynamic range on the order of 90 to 120 dB ($\hat{\phi}_{\psi\psi}$ not shown).

Figures 5.5 through 5.12 show the transfer functions for both the coupled and decoupled case. Recall that the decoupled case was set up as a reference and is computed by setting the off diagonal terms in the spectral matrix identically equal to zero. In each of these plots, a smooth line has been faired in on the "decoupled" transfer function. This smooth line is then superimposed on the coupled transfer function in order that the reader may more readily evaluate the differences in spectral content. It is emphasized that this line was merely "eyeballed" in and therefore does not represent a smoothed, rational polynomial model of the transfer function.

Figures 5.13 through 5.28 present the transfer functions for the various cases along with the associated phase information. In general, the break up in phase seems to be the most serious source of error. The factorized results, using only the e , ψ data are presented in Figures 5.29 through 5.32. From an inspection of these figures, the following conclusions are drawn:

(1) Using the $\left(\frac{\sin x/4}{x/4}\right)^8$ window, a useful frequency range of $.2 < \omega < 20$ rad/sec. was achieved in the vector roll tracking task when the input variables were error and roll angles. This was reduced to $.2 < \omega < 7$ when the input variables were error and yaw. That is, the dynamic range of ψ seems to be far greater than that of roll.

(2) In general, the coupled models displayed more power at lower frequency than did the decoupled models. The decoupled models are computed by setting the off-diagonal terms in the spectral matrix equal to zero, resulting in a set of scalar definitions.

(3) In general, the coupled models which were generated using error and bank angle to specify the spectral matrix displayed far less power at low frequency that did the coupled models generated using error and yaw angle.

(4) The power in the transfer functions, making up the pilot model, are comparable in magnitude. In the case of the coupled models whose spectral matrix depends on error and yaw angle, the diagonal term (H_{11}, H_{22}) are slightly higher in power (5-10 dB) than are the off-diagonal terms (H_{12}, H_{21}).

(5) Along the lines of (4) above, there is less that can be said about the models which use error and bank angle as the input signals for the differences appear to be smaller. In fact, H_{21} produces a higher peak than any observed in the other three transfer functions.

(6) The differences between the various models appear to be quite significant. That is, it does make a difference whether one sets up decoupled or coupled models or whether the model was generated using e , $\not{v}$ as opposed to e , $\not{\phi}$. The factorized results exhibit marked differences when compared with the non-factorized answers. However, the preliminary nature of these estimates, due to the ill-conditional inputs (120 dB dynamic range) and the poor checks obtained on the root finding and matrix inversion routine must be kept in mind.

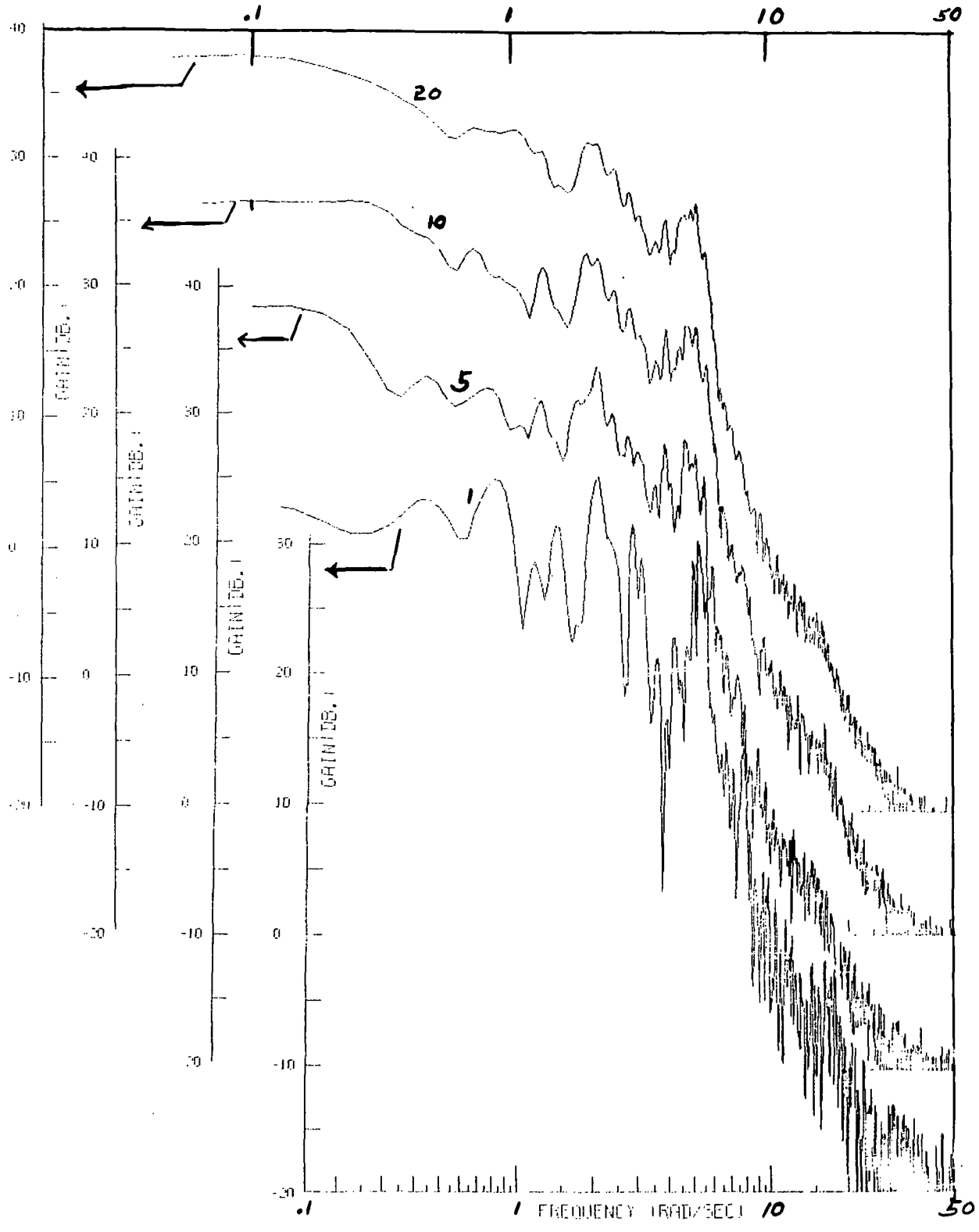

FIGURE 5.2. ϕ_{ee} FOR ENSEMBLES OF 1, 5, 10 and 20

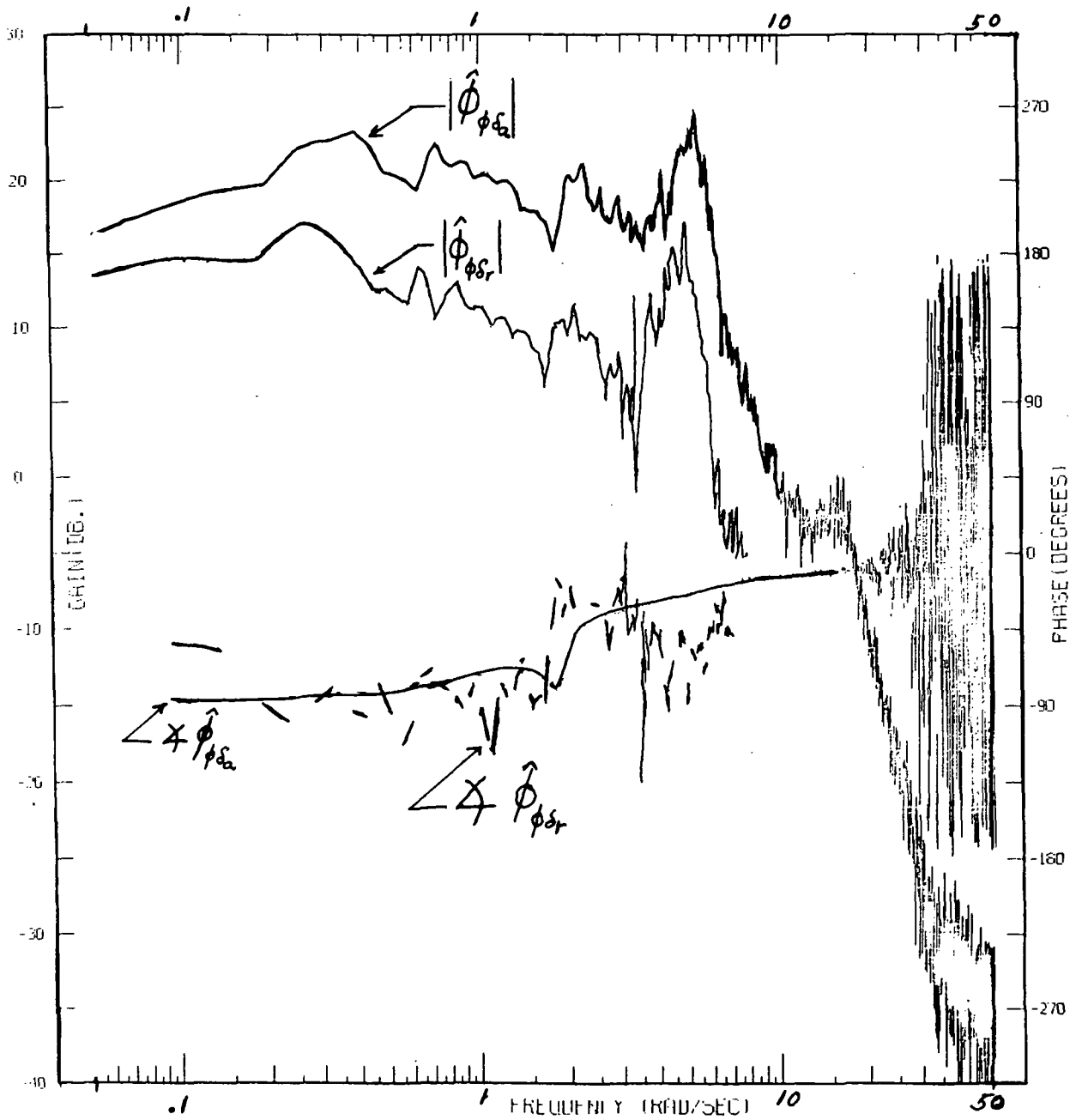

FIGURE 5.3. $\hat{\phi}_{\phi\delta_a}$, $\hat{\phi}_{\phi\delta_r}$ vs ω

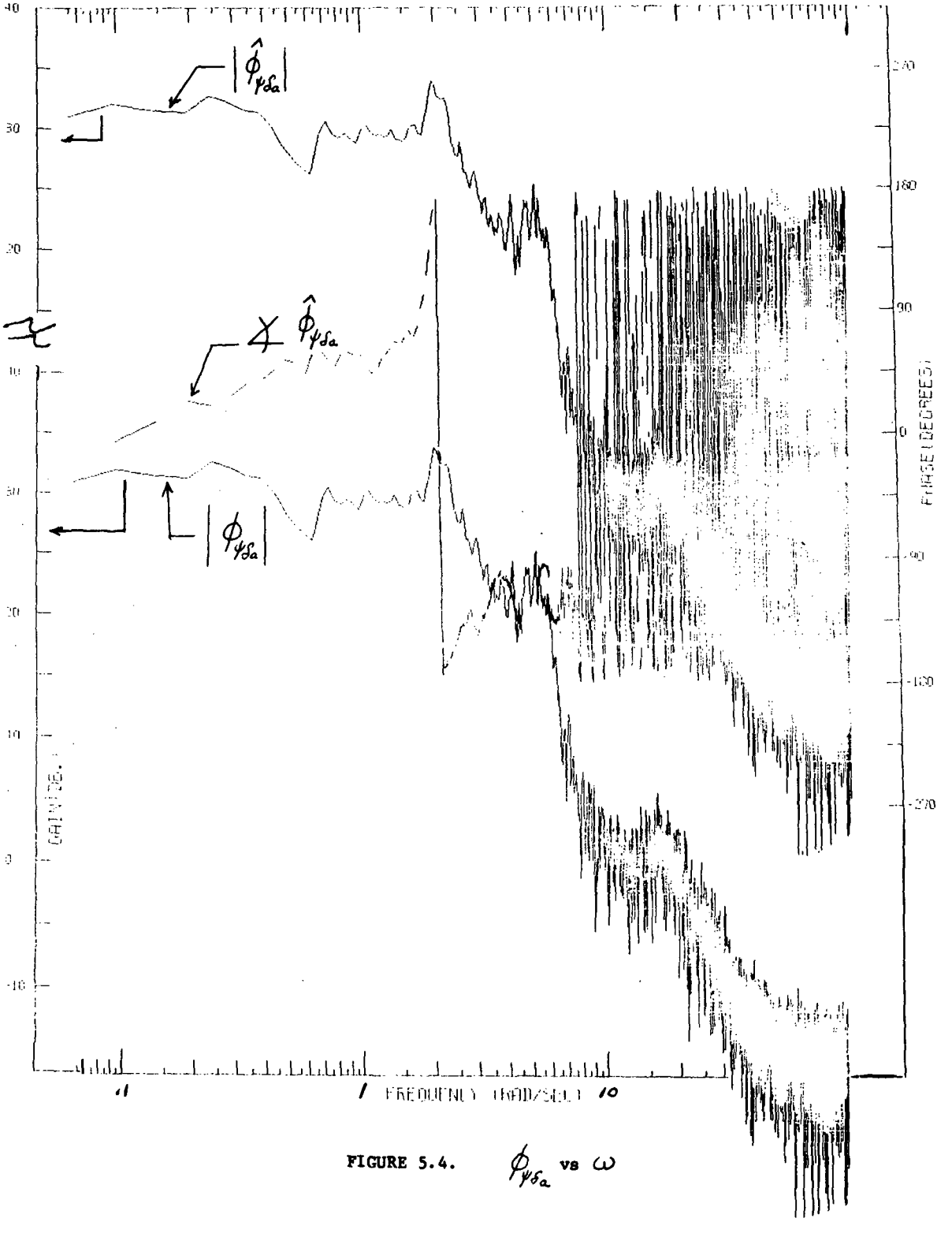

FIGURE 5.4. $\phi_{\psi\delta a}$ vs ω

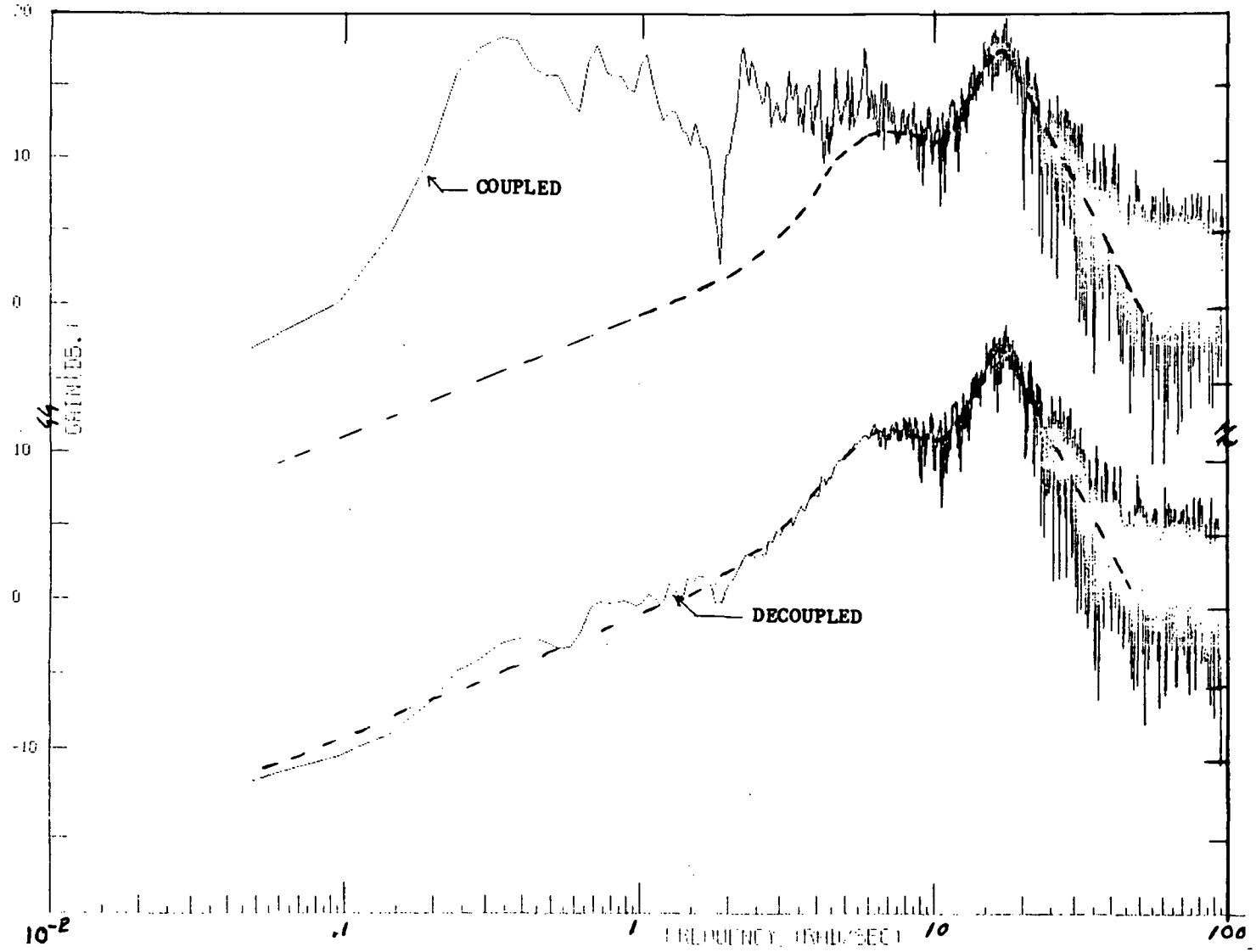

FIGURE 5.5. $H_{//}$; COUPLED AND DECOUPLED; e, ψ

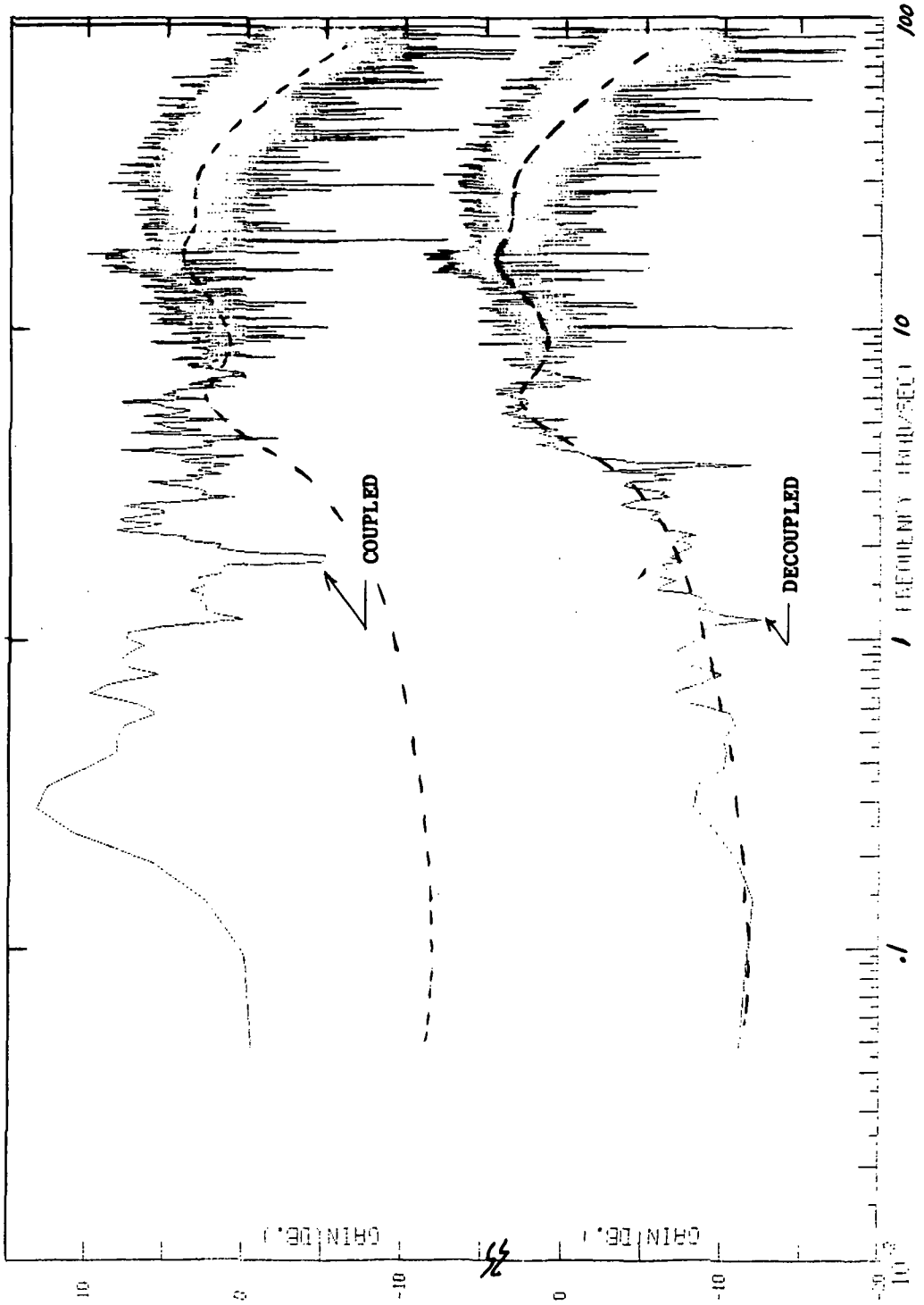

FIGURE 5.6. H_{12}; COUPLED AND DECOUPLED; e, ψ

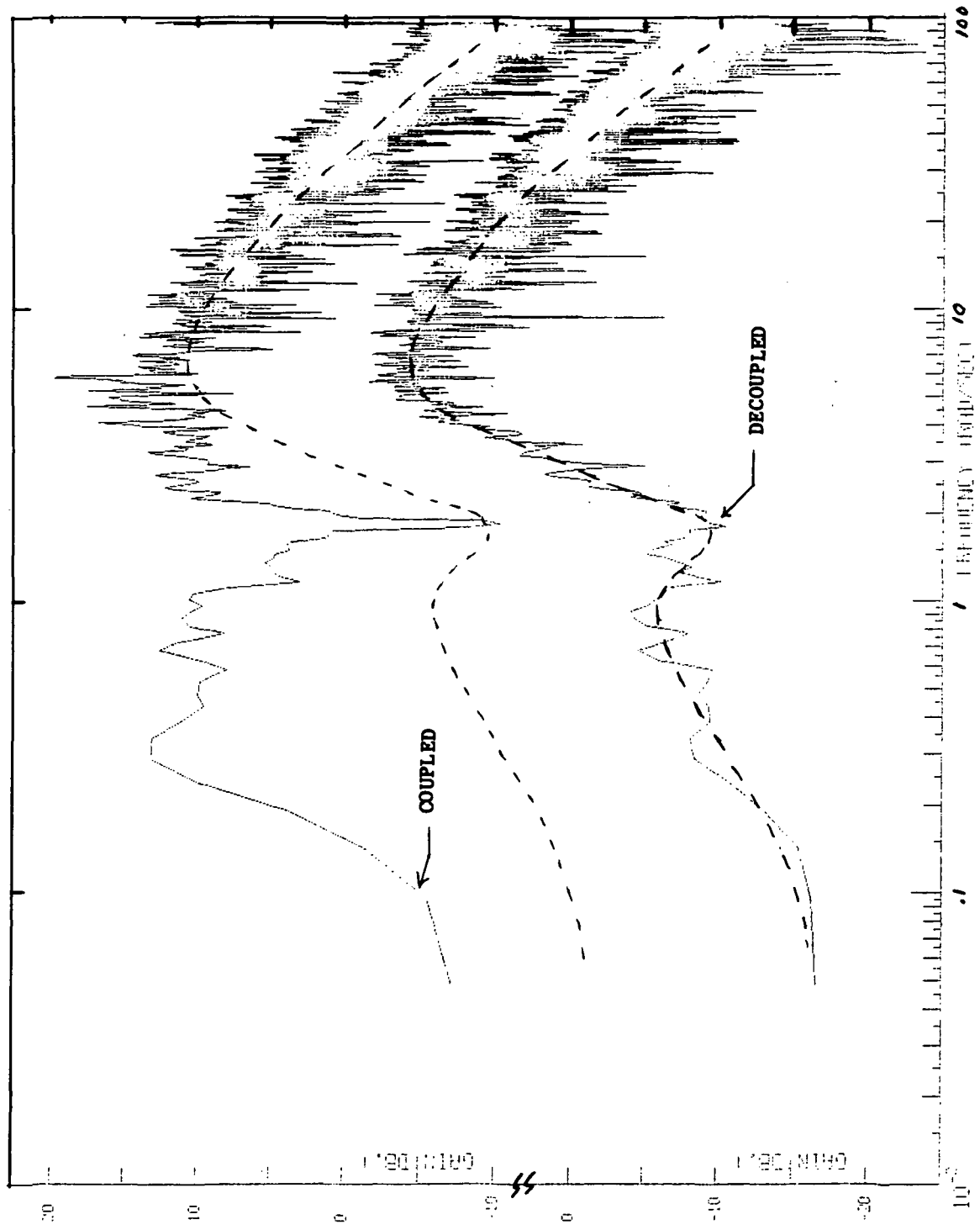

FIGURE 5.7. H_{21}: COUPLED AND DECOUPLED; θ, ψ

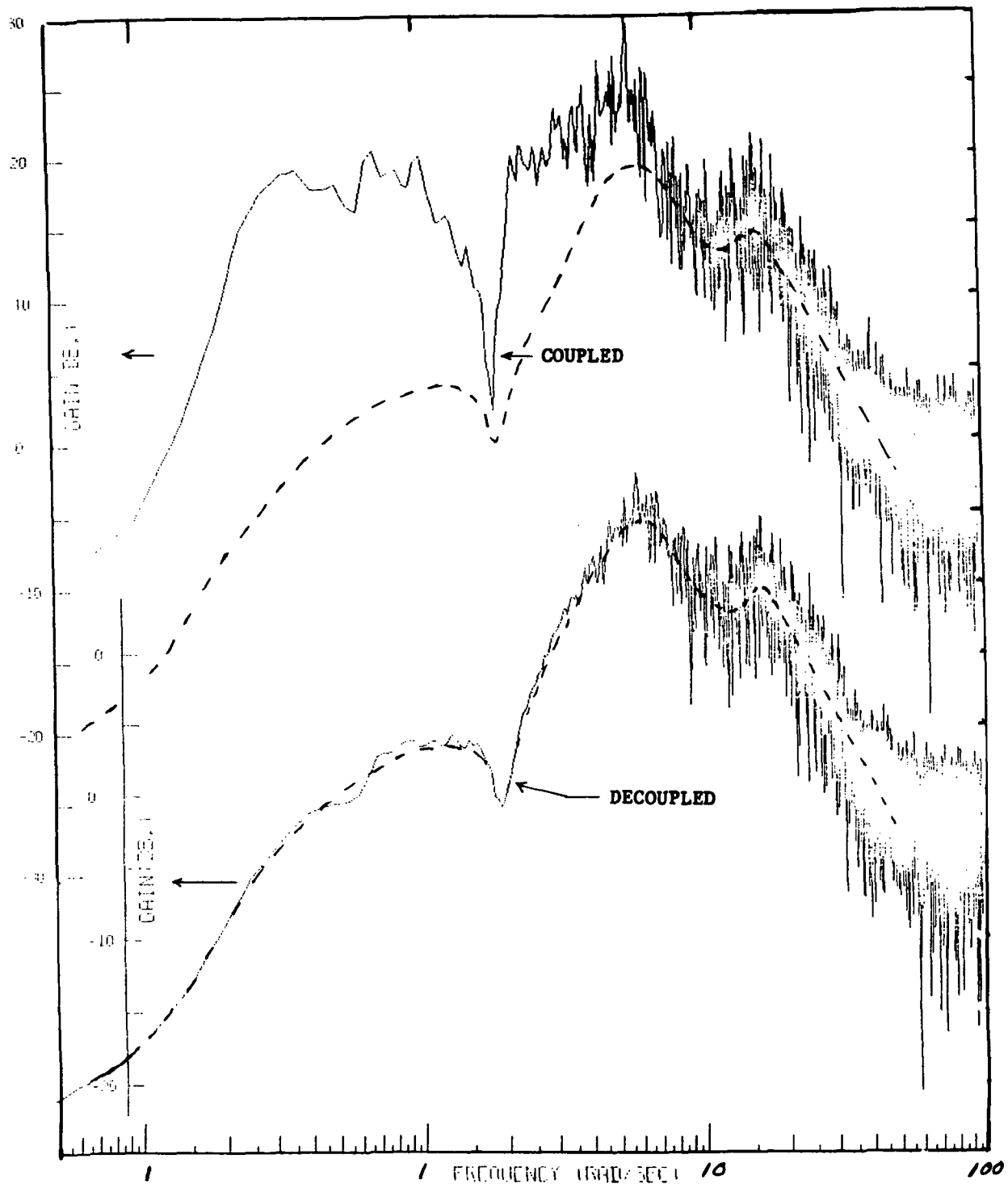

FIGURE 5.8. H_{22}; COUPLED AND DECOUPLED; θ, ψ

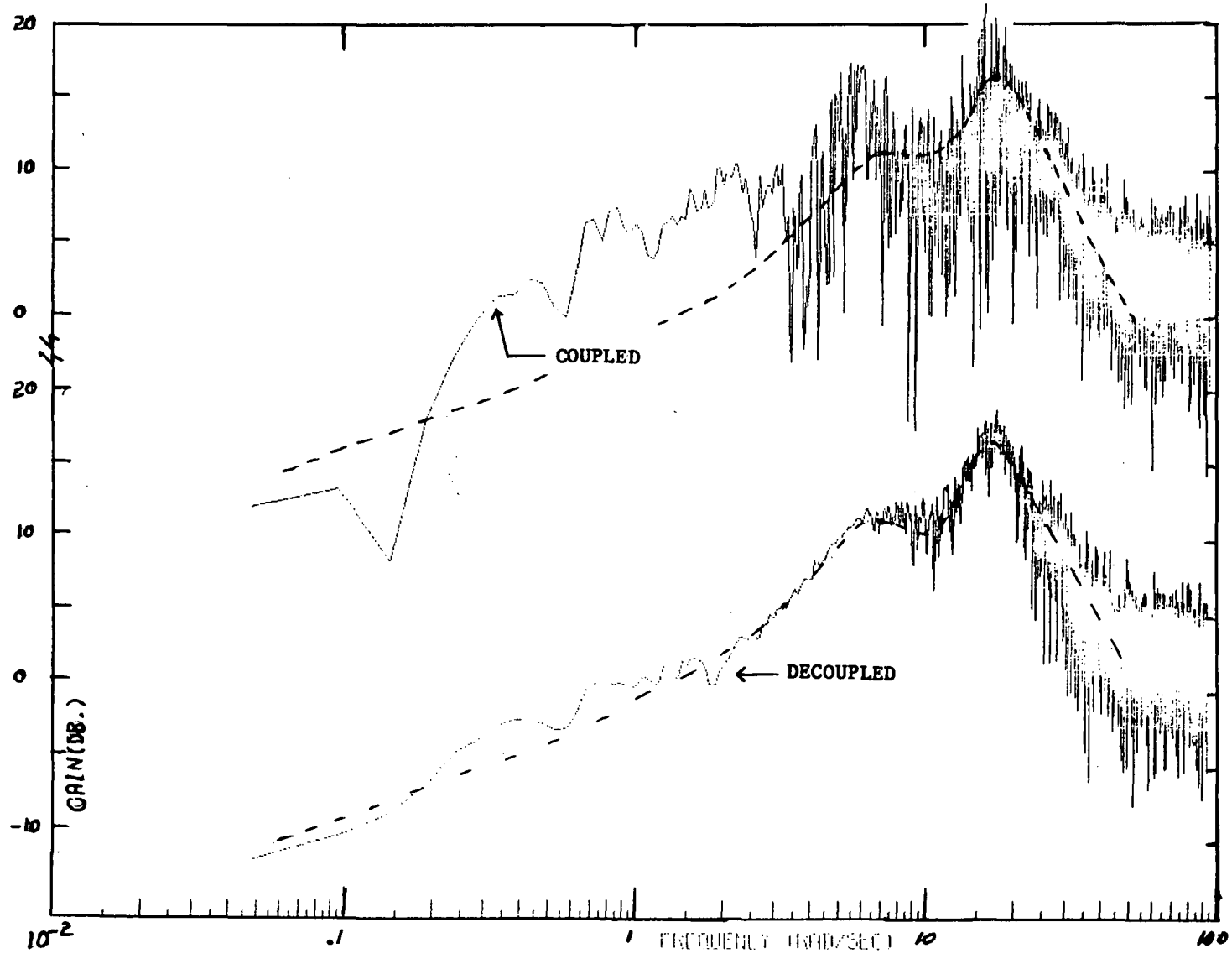

FIGURE 5.9. H_{11}; COUPLED AND DECOUPLED: e, ϕ

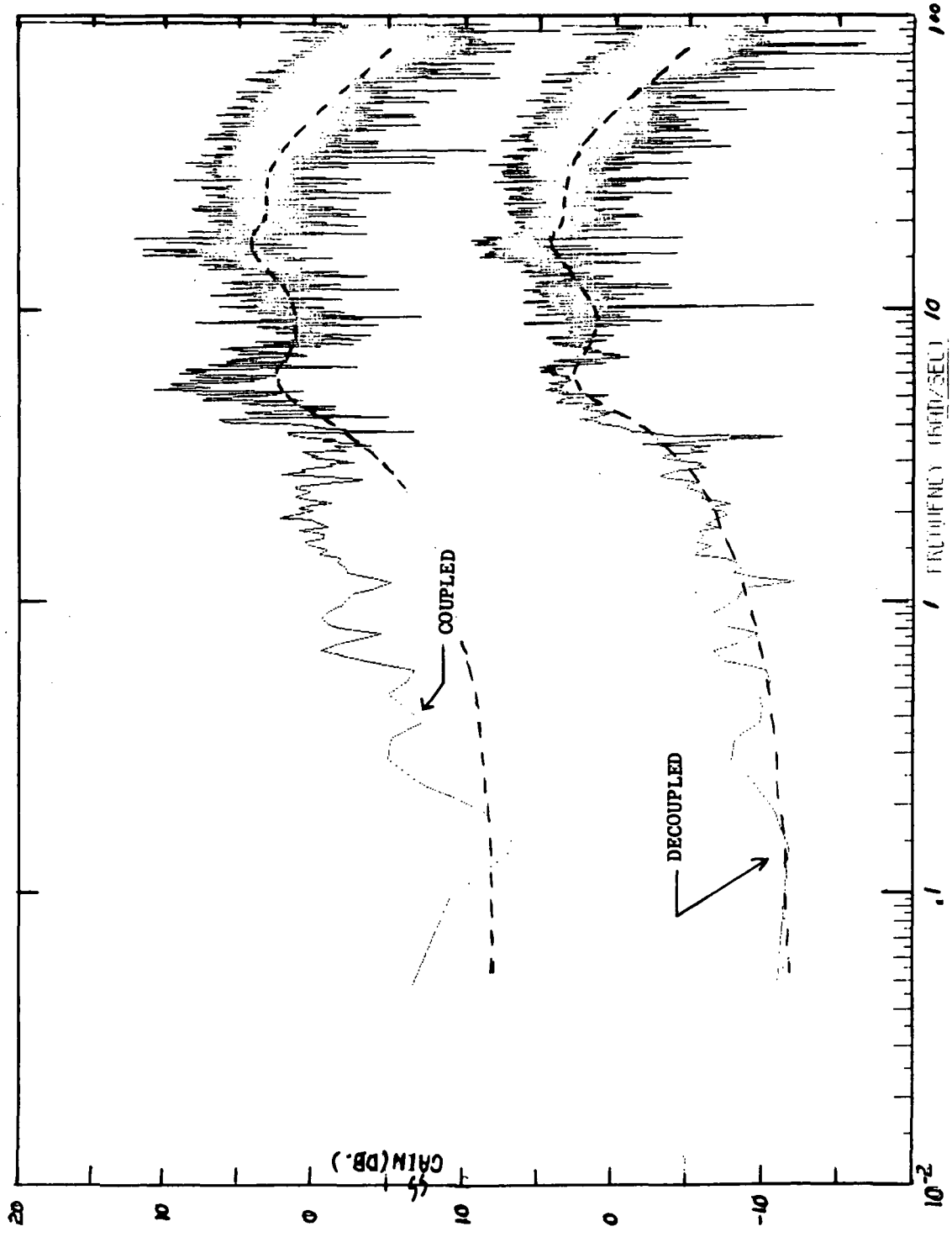

FIGURE 5.10. H_{12}; COUPLED AND DECOUPLED; θ, ϕ

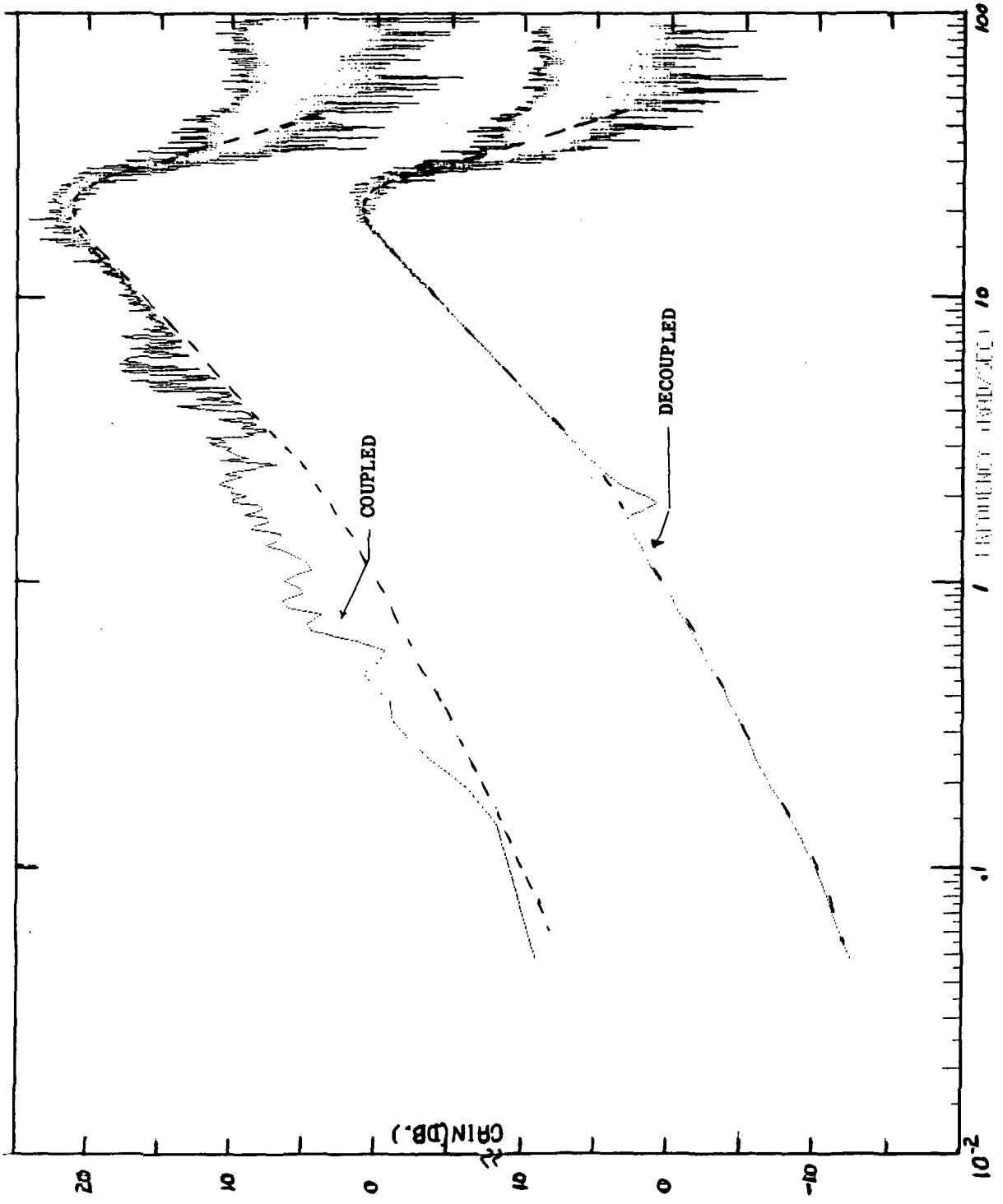

FIGURE 5.11. H_{21}; COUPLED AND DECOUPLED; ϵ, ϕ

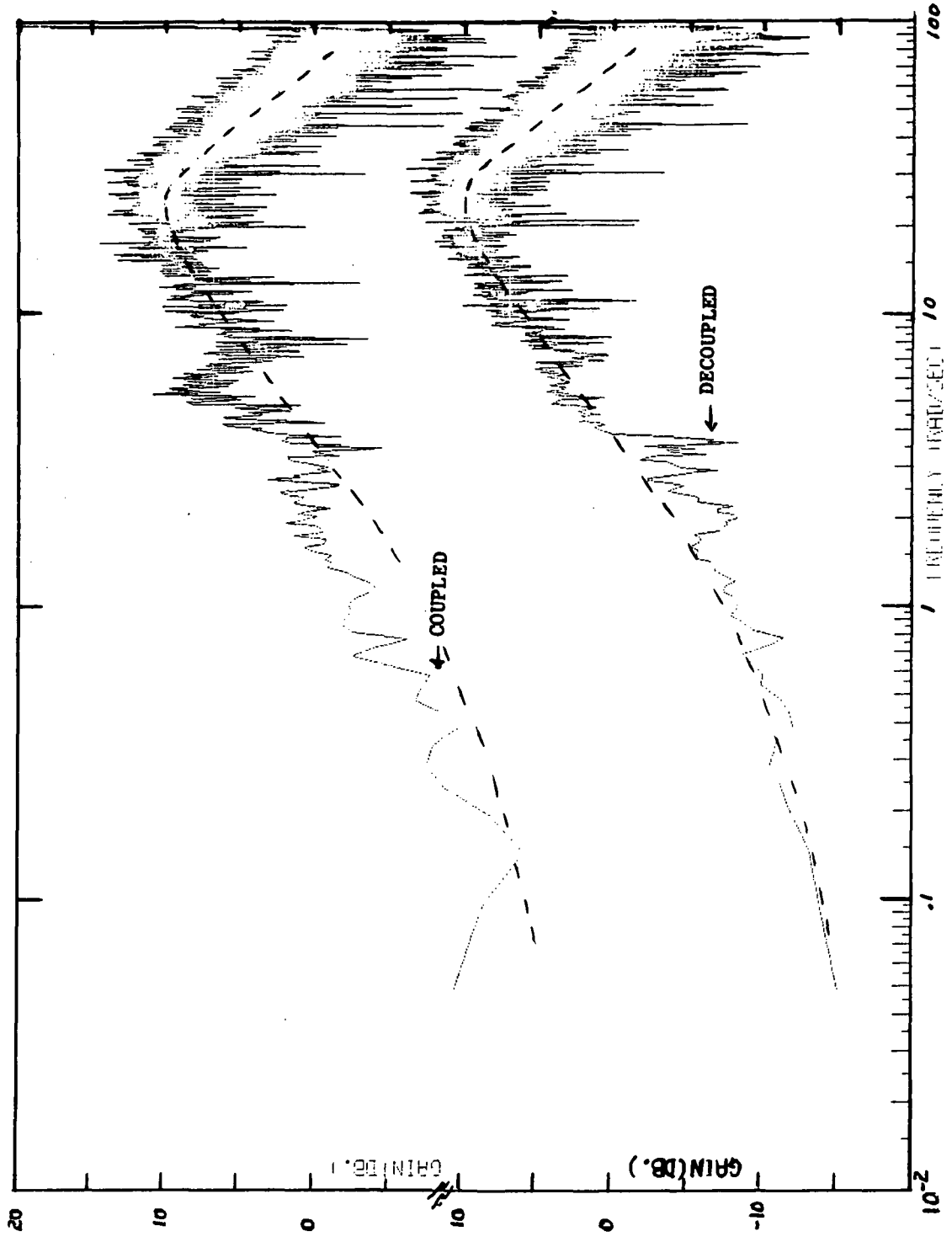

FIGURE 5.12; H_{22}; COUPLED AND DECOUPLED; θ, ϕ

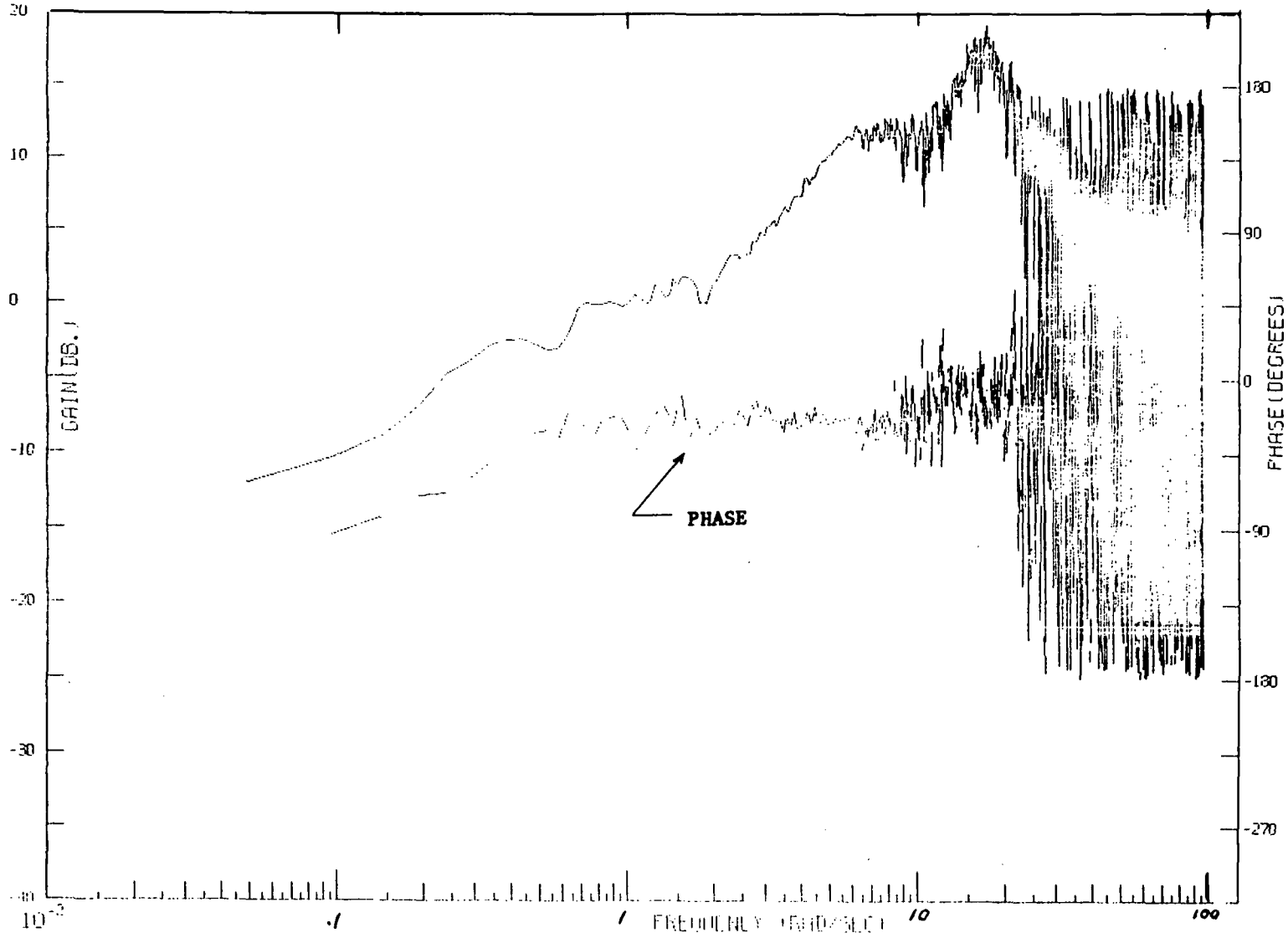

FIGURE 5.13. H_{11}; **DECOUPLED;** e, ψ ; **PHASE**

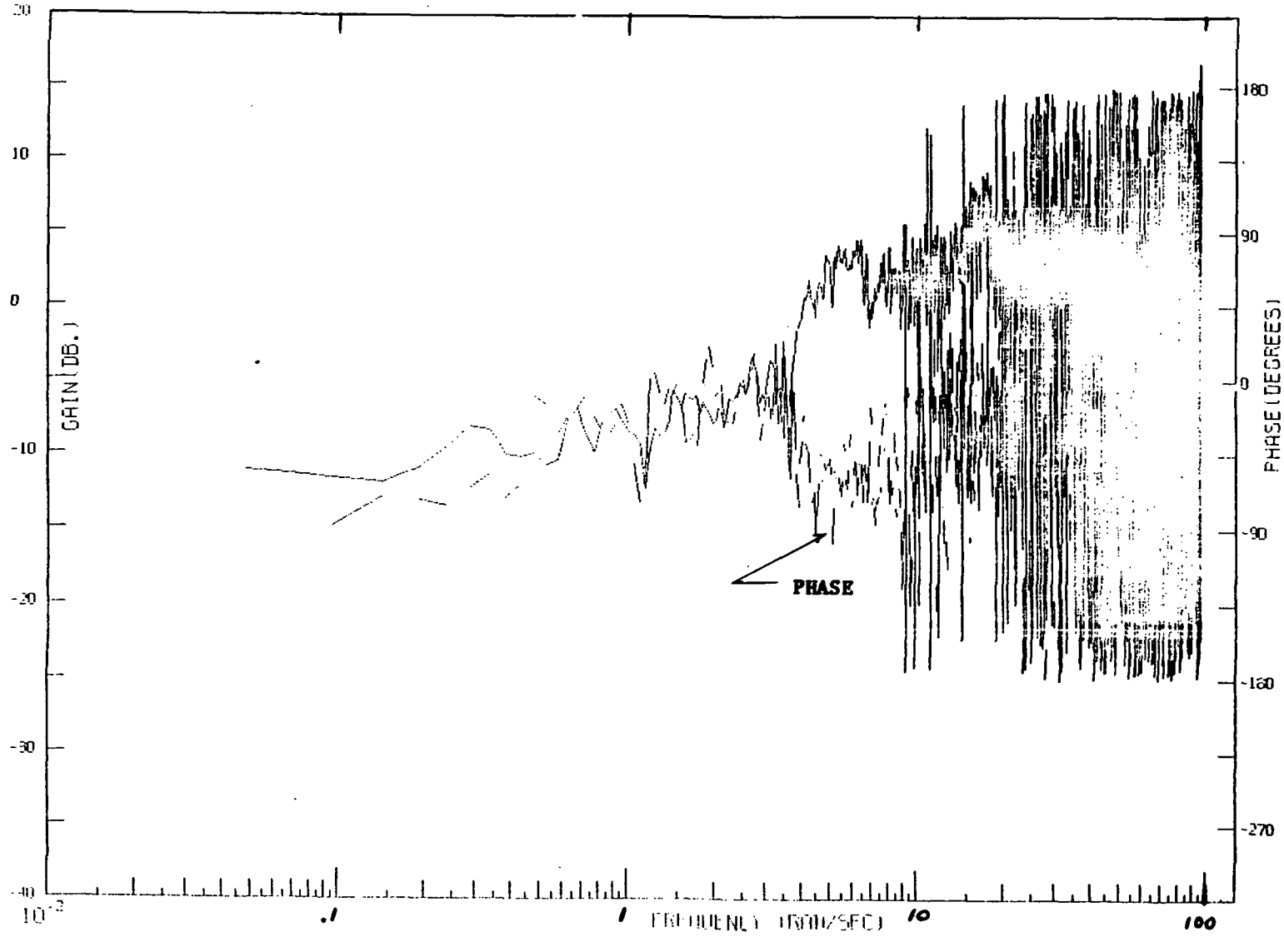

FIGURE 5.14. H_{12}; **DECOUPLED;** e, ψ ; **PHASE**

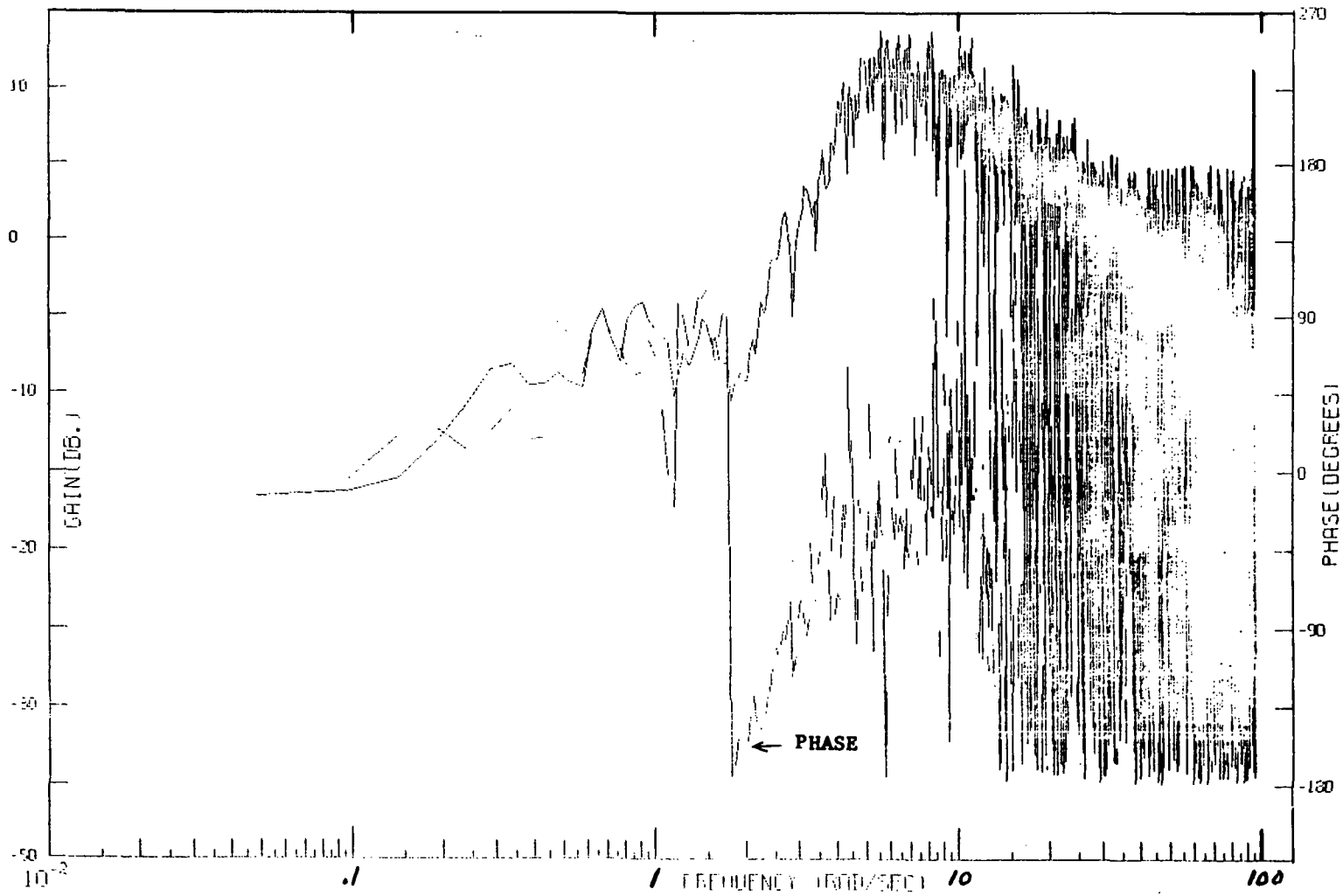

FIGURE 5.15. H_{21}; **DECOUPLED;** e , ψ ; **PHASE**

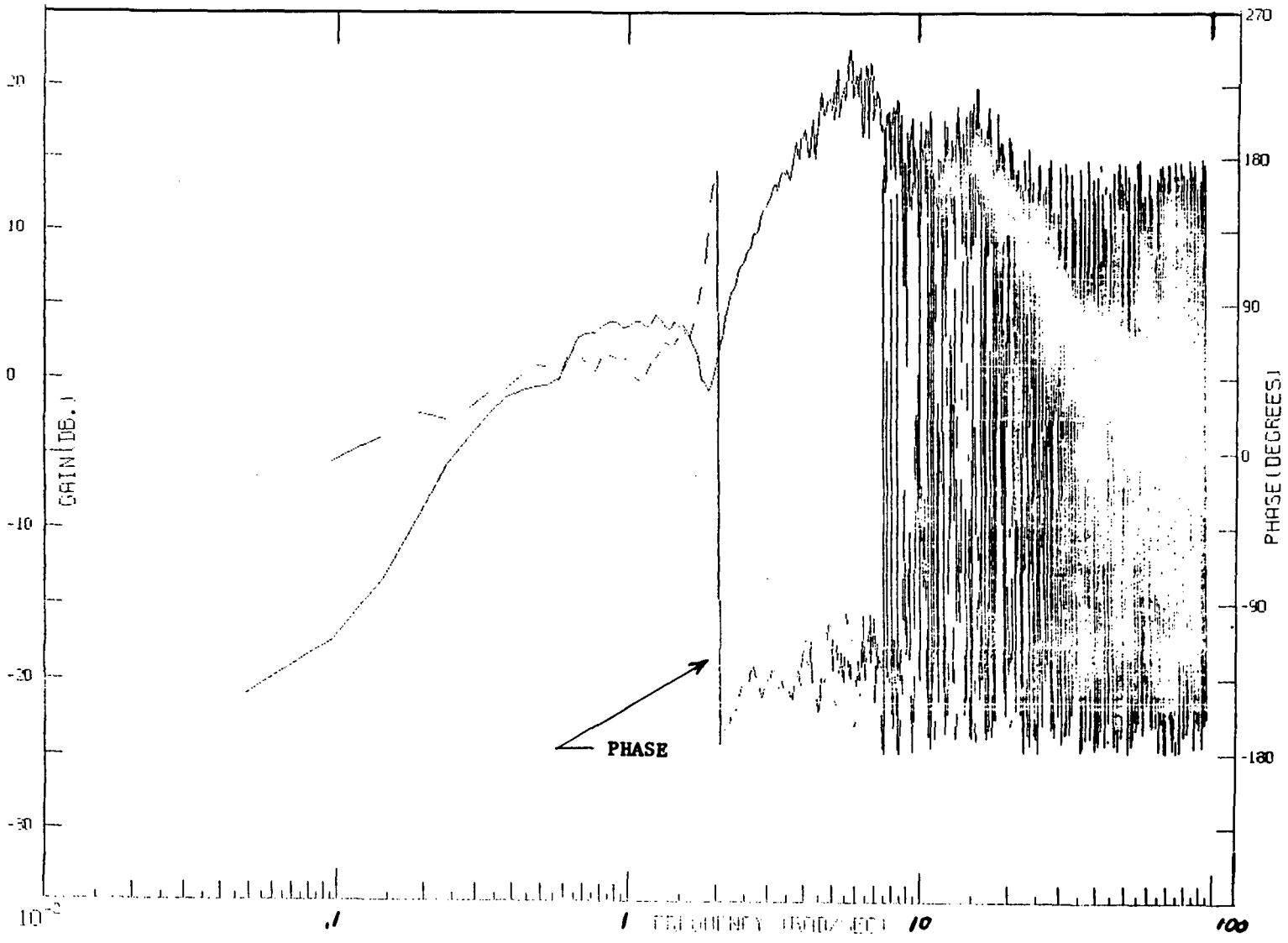

FIGURE 5.16. H_{22}; **DECOUPLED;** e, ψ ; **PHASE**

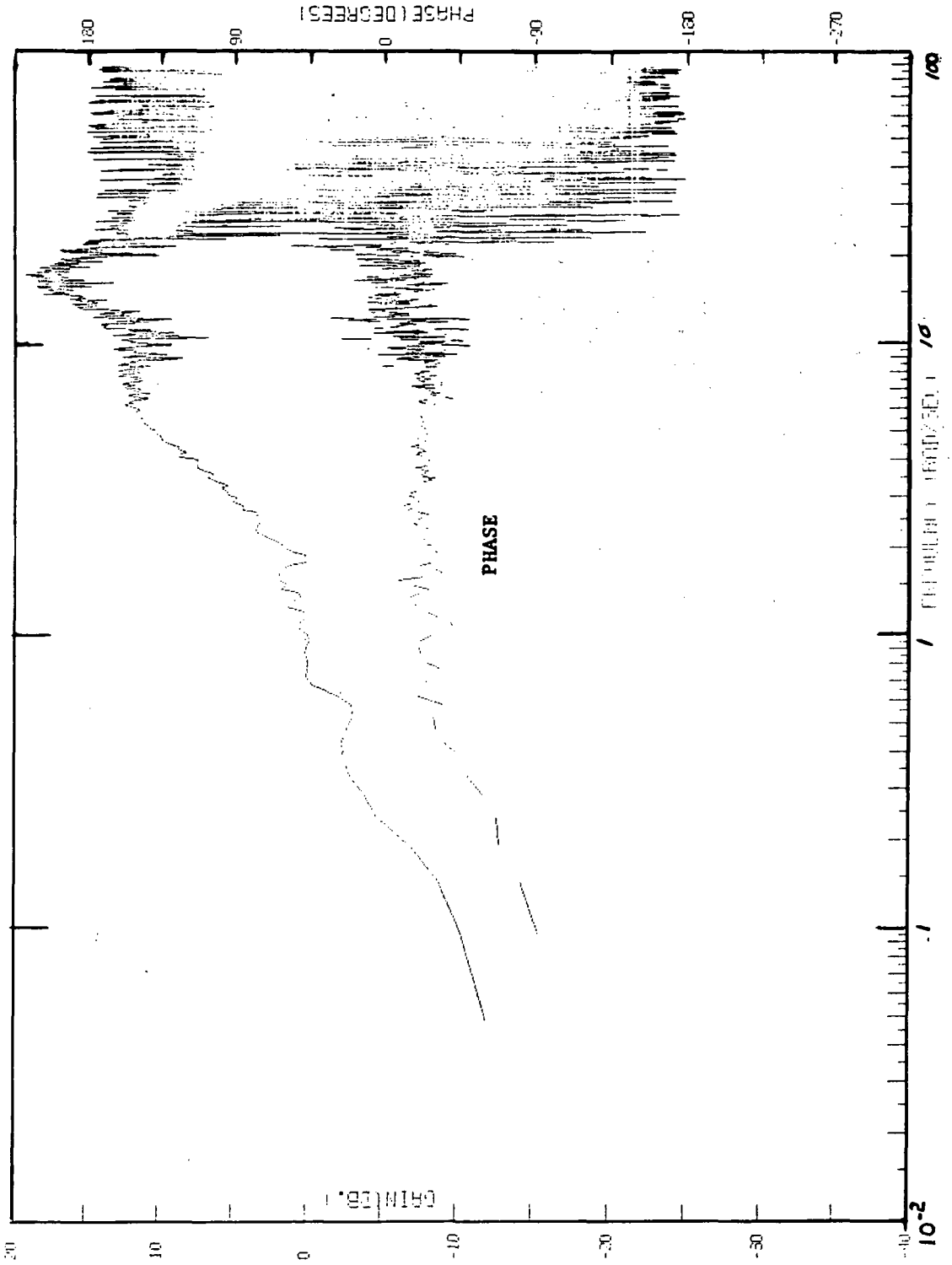

FIGURE 5.17. H_{11}; **DECOUPLED;** θ , ϕ ; **PHASE**

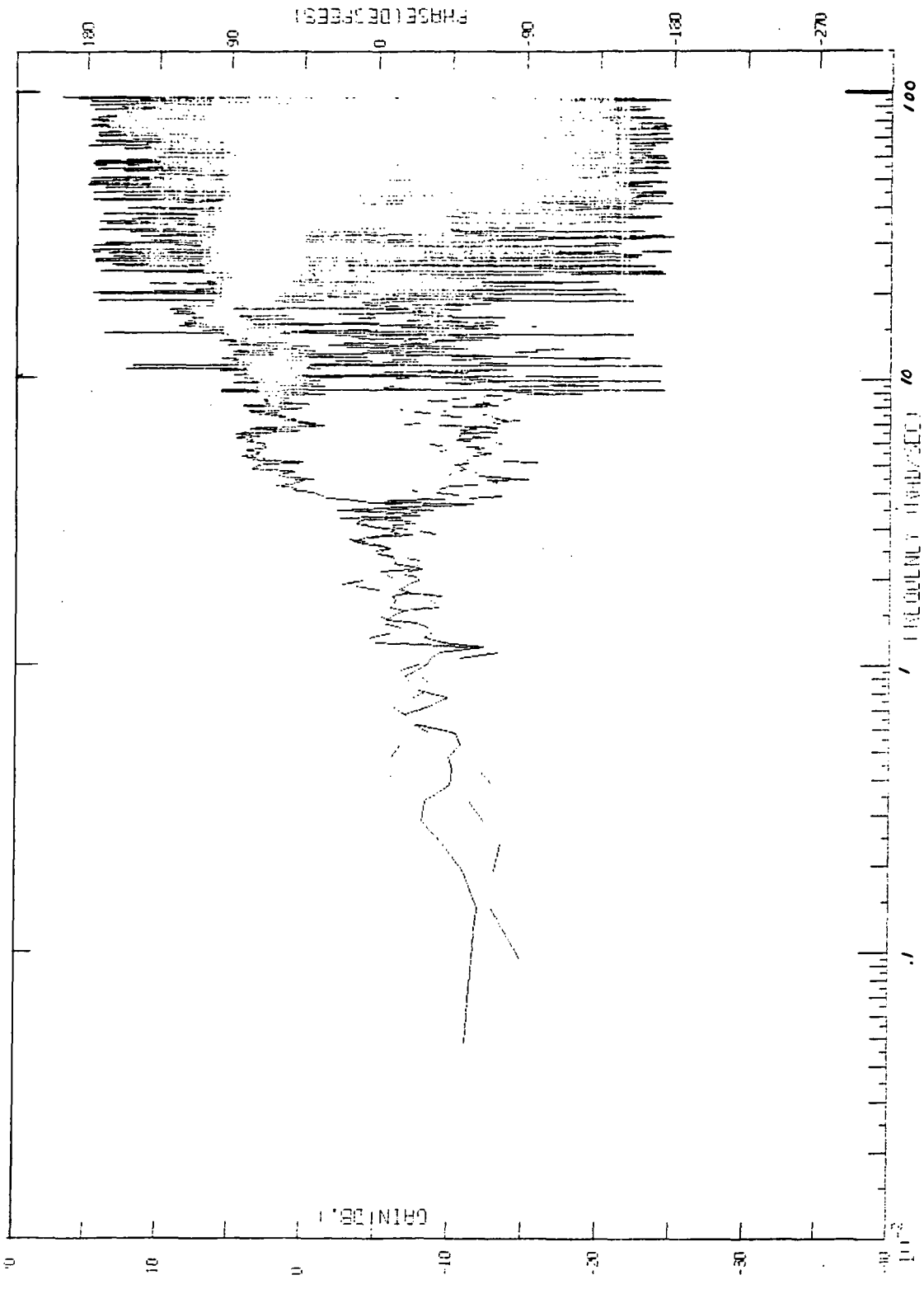

FIGURE 5.18. H_{12}; DECOUPLED; e, ϕ ; PHASE

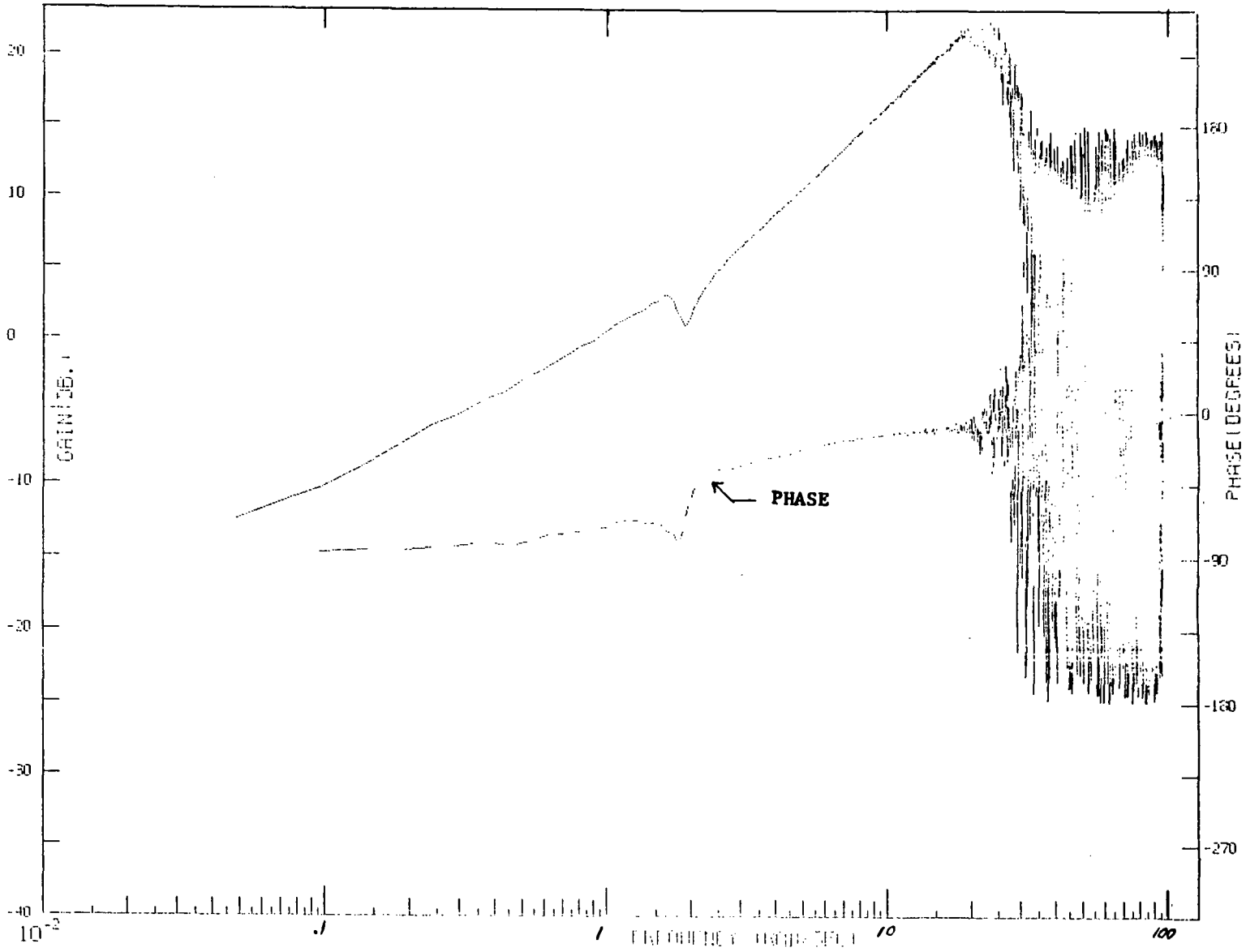

FIGURE 5.19. H_{21}; **DECOUPLED;** Θ , ϕ ; **PHASE**

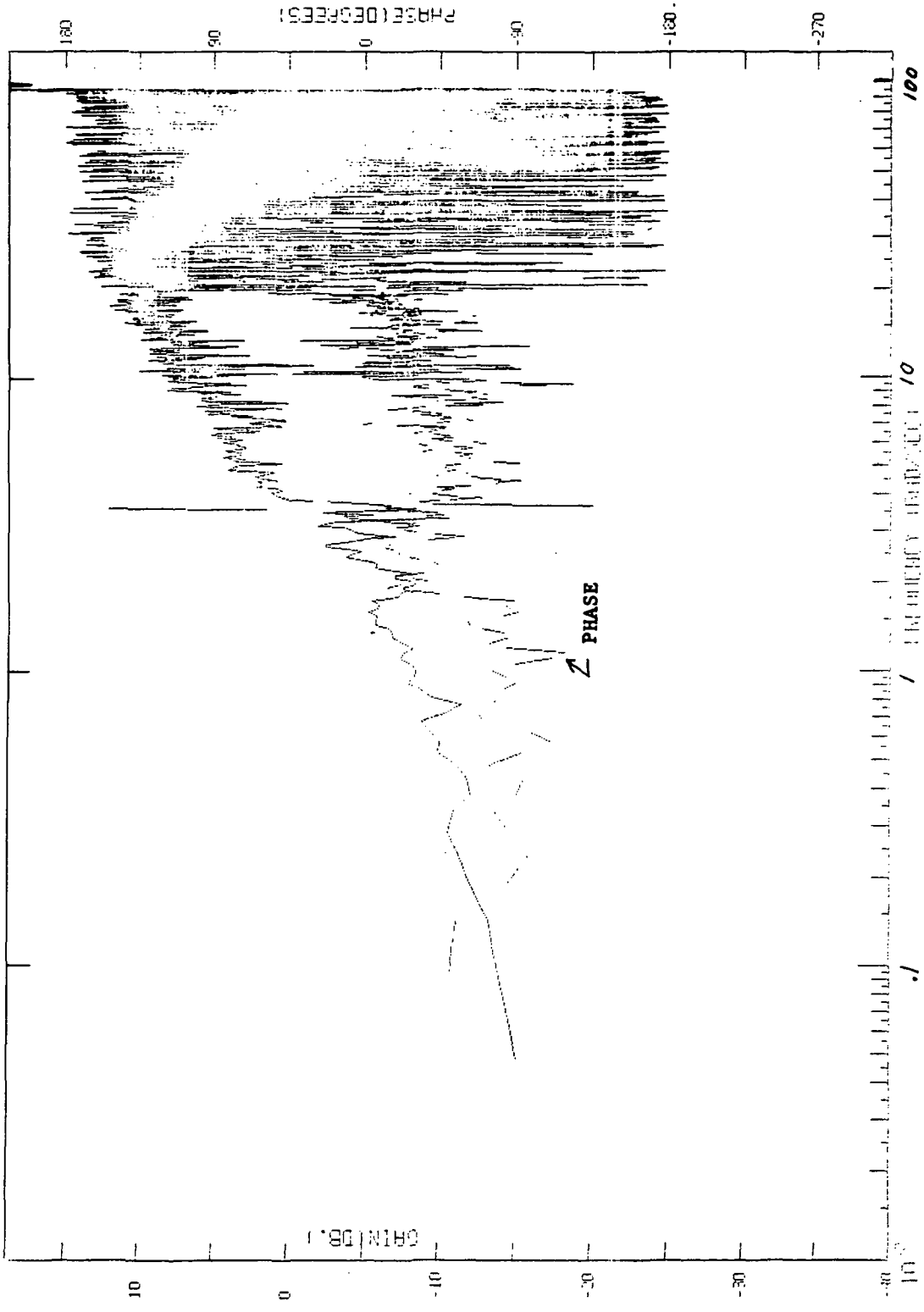

FIGURE 5.20. H_{22}; DECOUPLED; θ, ϕ ; PHASE

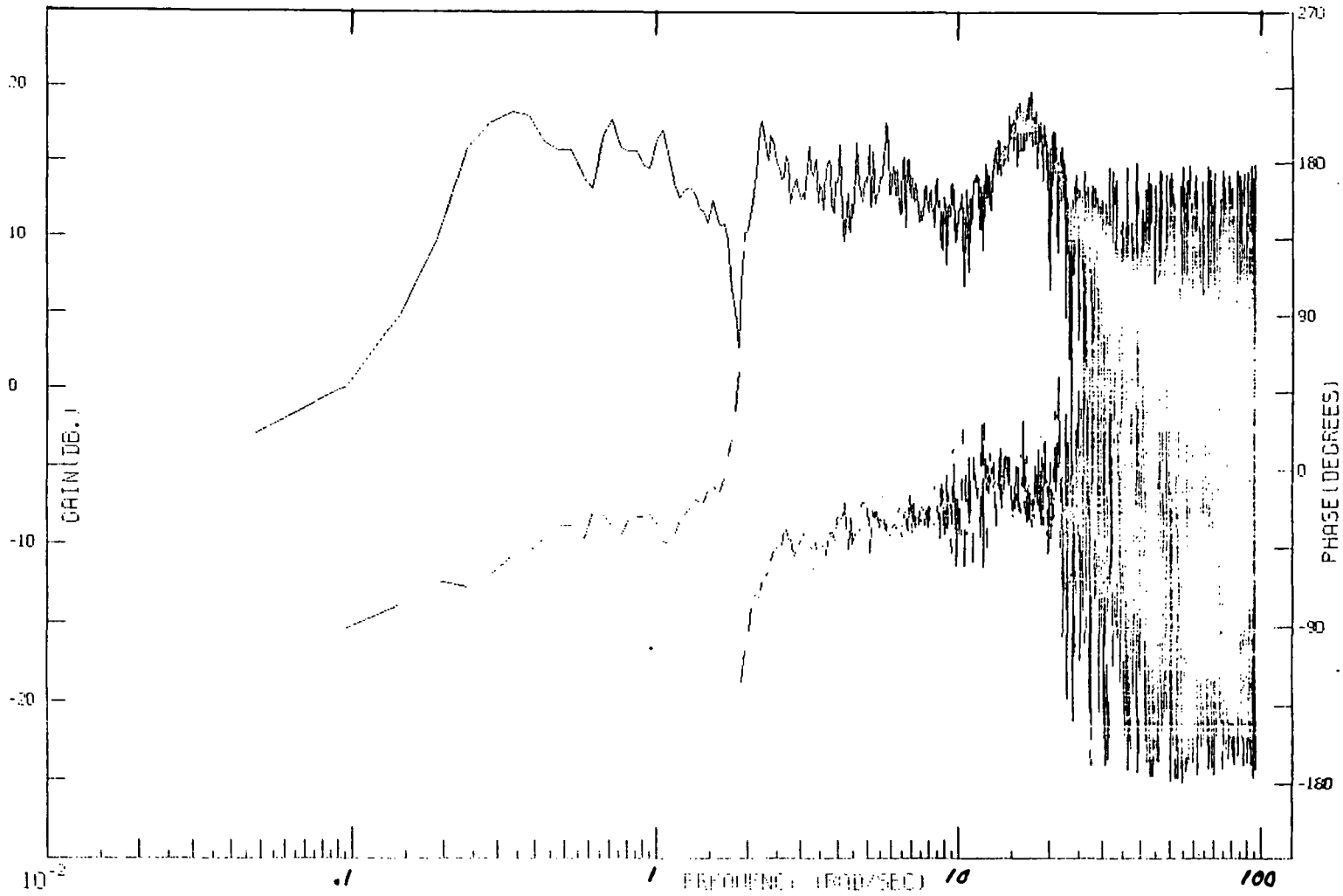

FIGURE 5.21. H_{11}; **COUPLED;** e , ψ ; **PHASE**

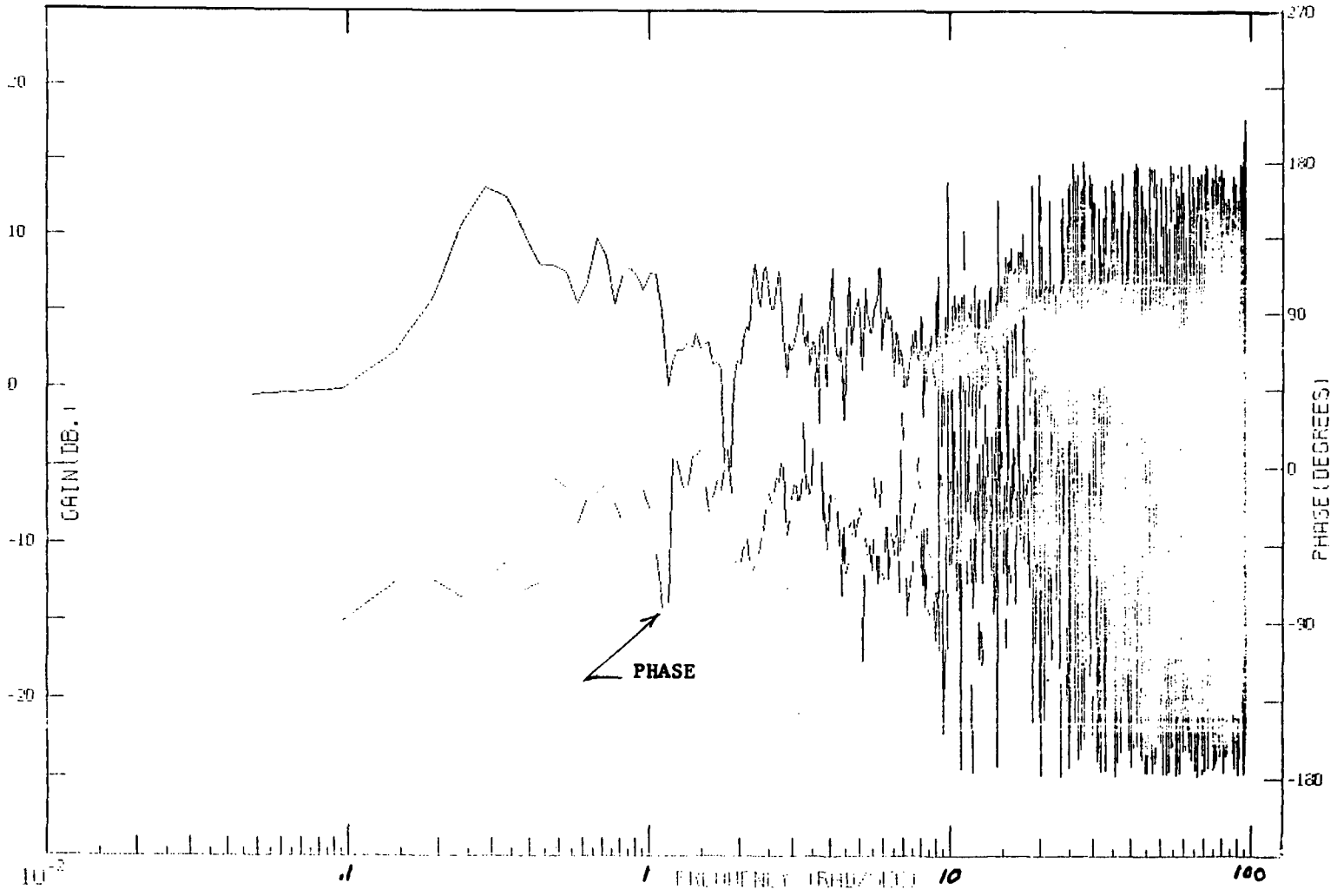

FIGURE 5.22. H_{12}; COUPLED; ϵ , ψ ; PHASE

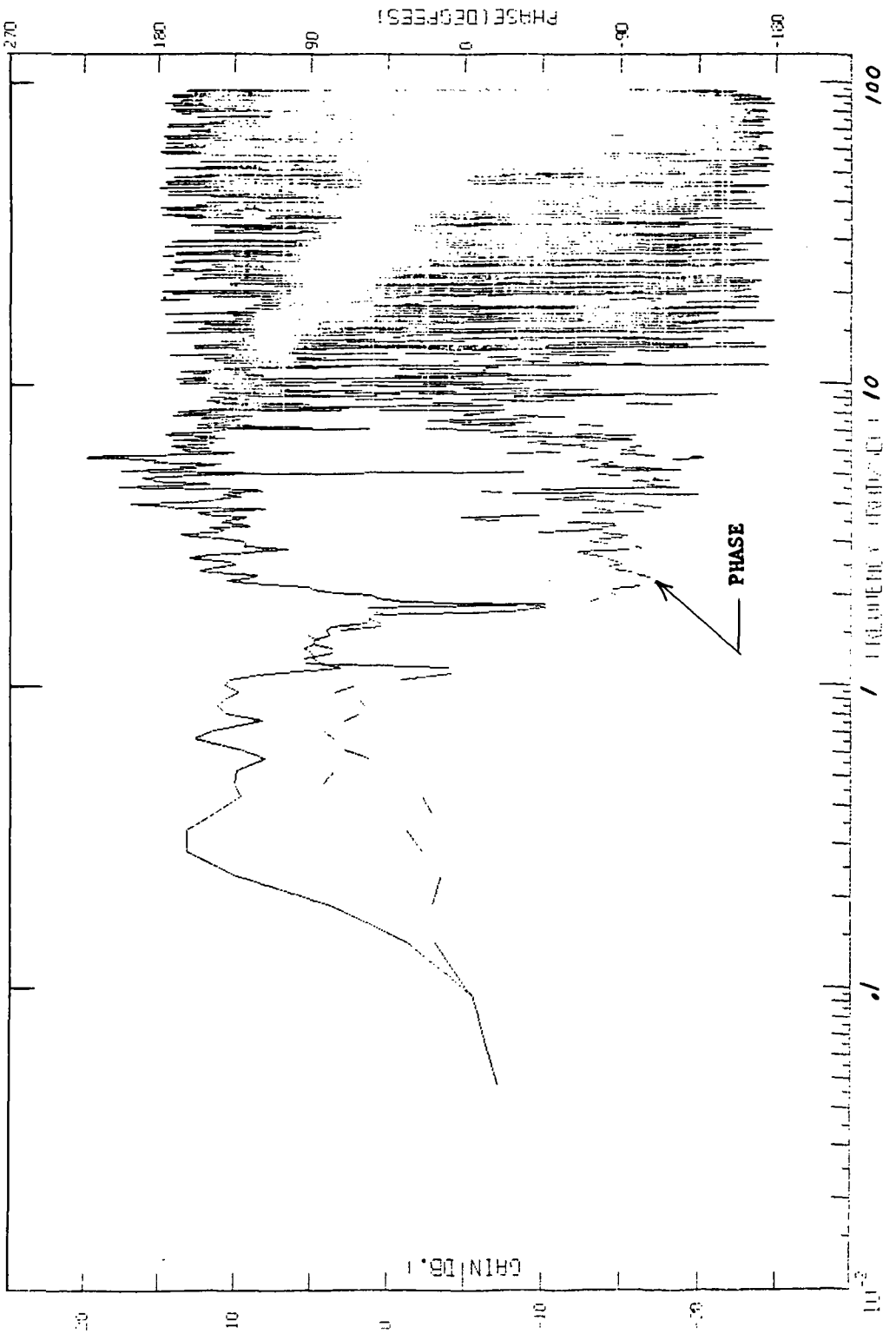

FIGURE 5.23. H_{21}; COUPLED; θ, ψ ; PHASE

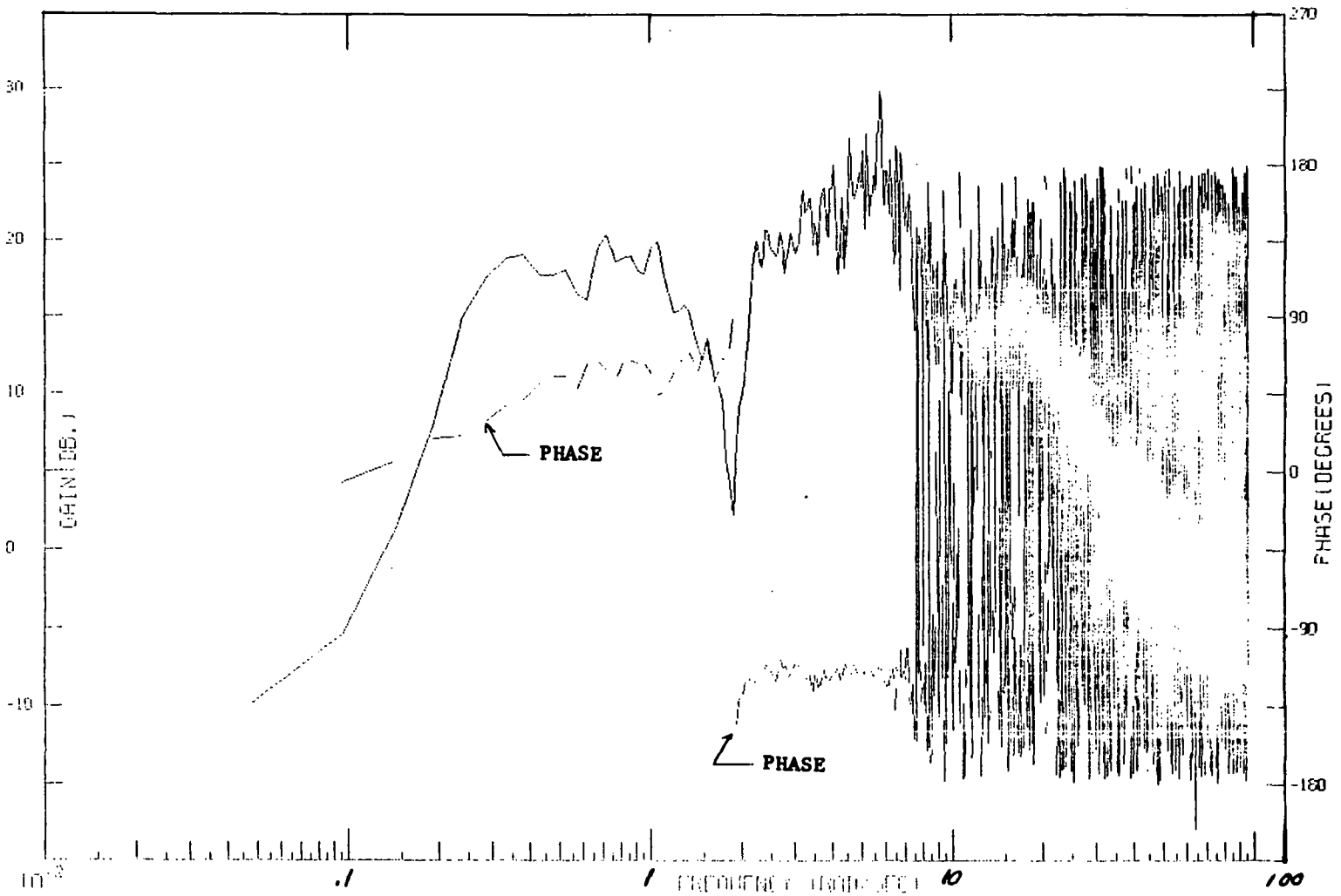

FIGURE 5.24. H_{22}; COUPLED; ϵ , ψ ; PHASE

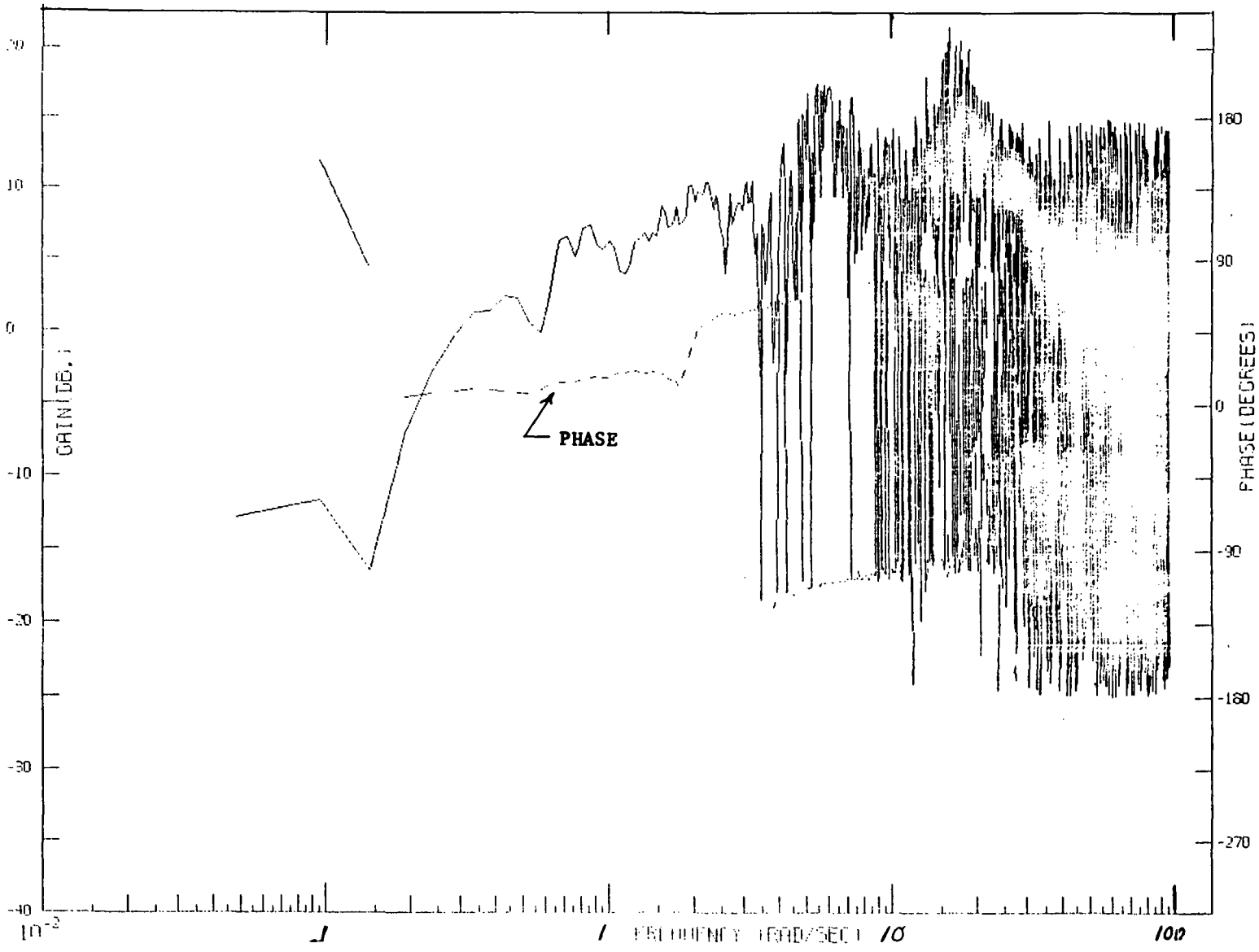

FIGURE 5.25. H_{11}; COUPLED; θ , ϕ ; PHASE

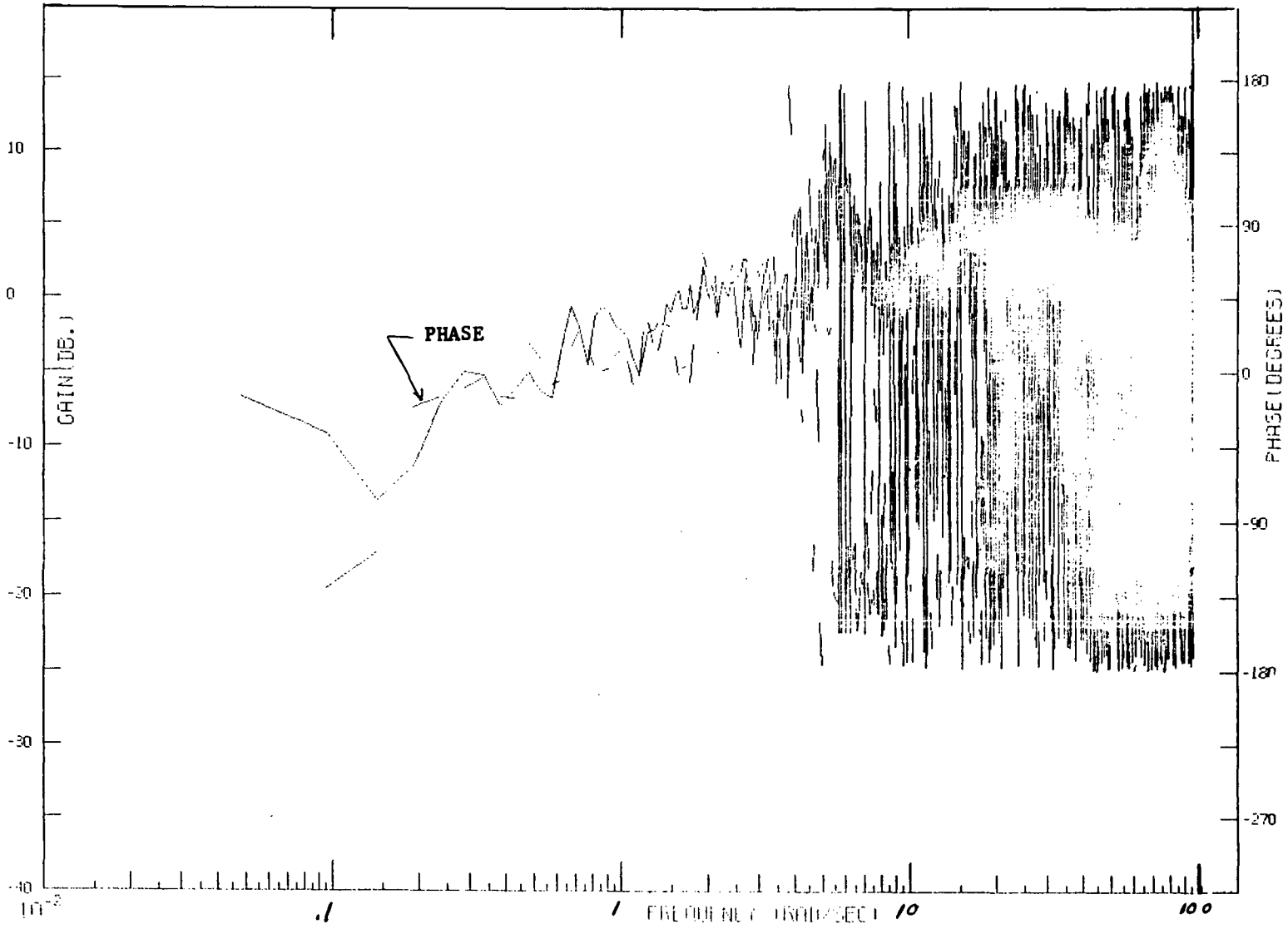

FIGURE 5.26. H_{12}; COUPLED; e , ϕ ; PHASE

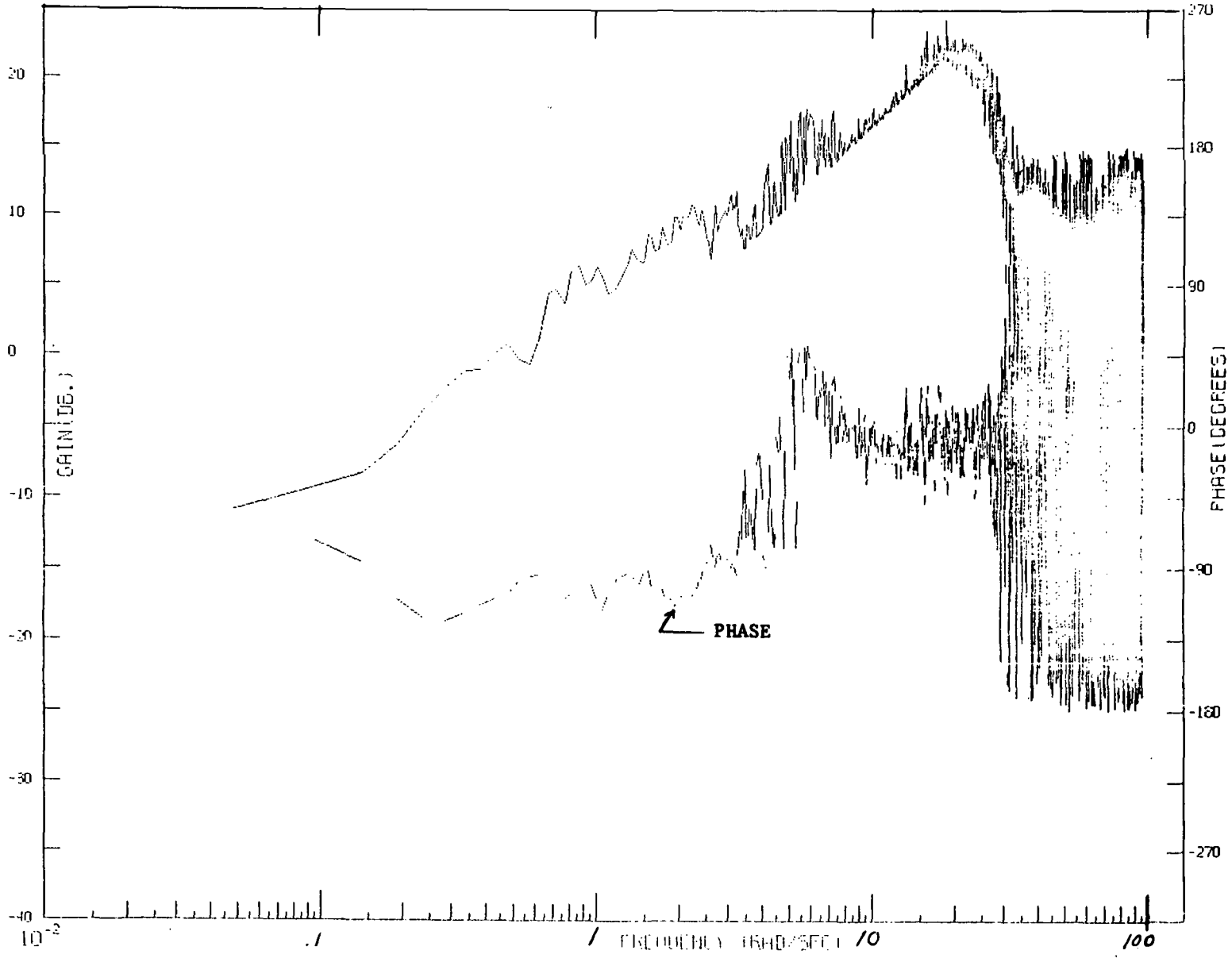

FIGURE 5.27. H_{21}; **COUPLED;** e , ϕ ; **PHASE**

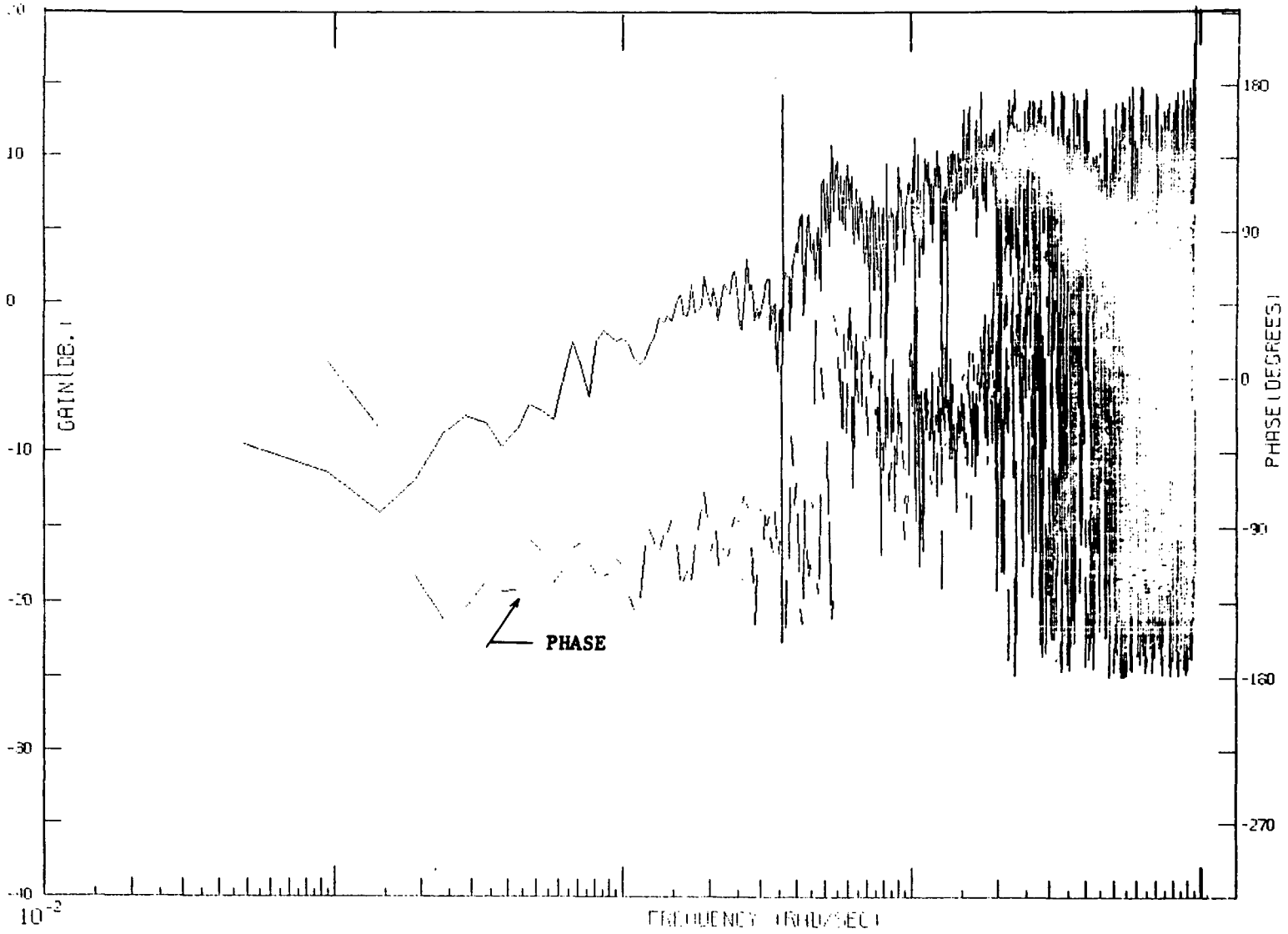

FIGURE 5.28. H_{22}; **COUPLED;** e , ϕ ; **PHASE**

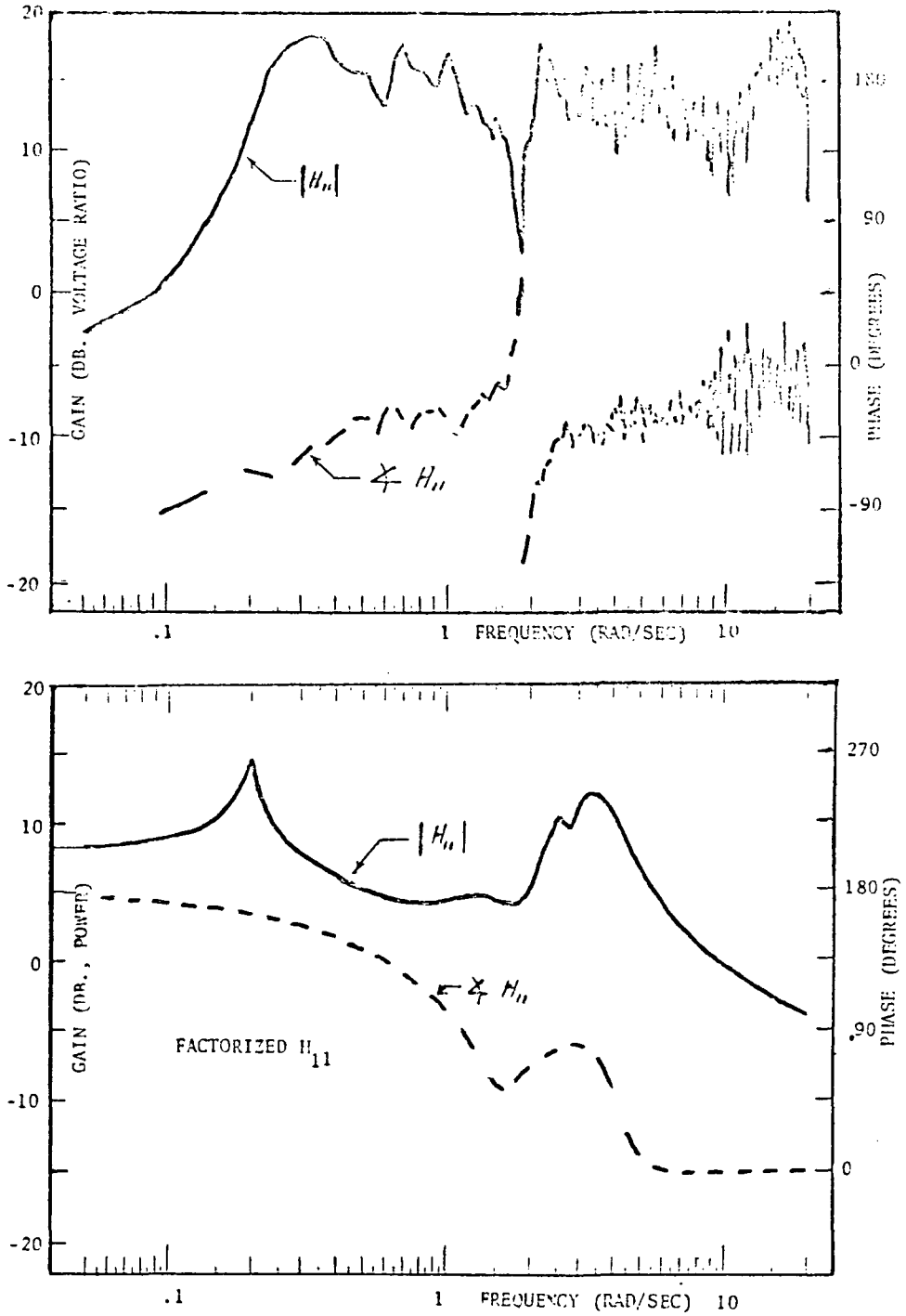

FIGURE 5.29. FACTORIZED H_{11} COMPARED TO NON-FACTORIZED H_{11}

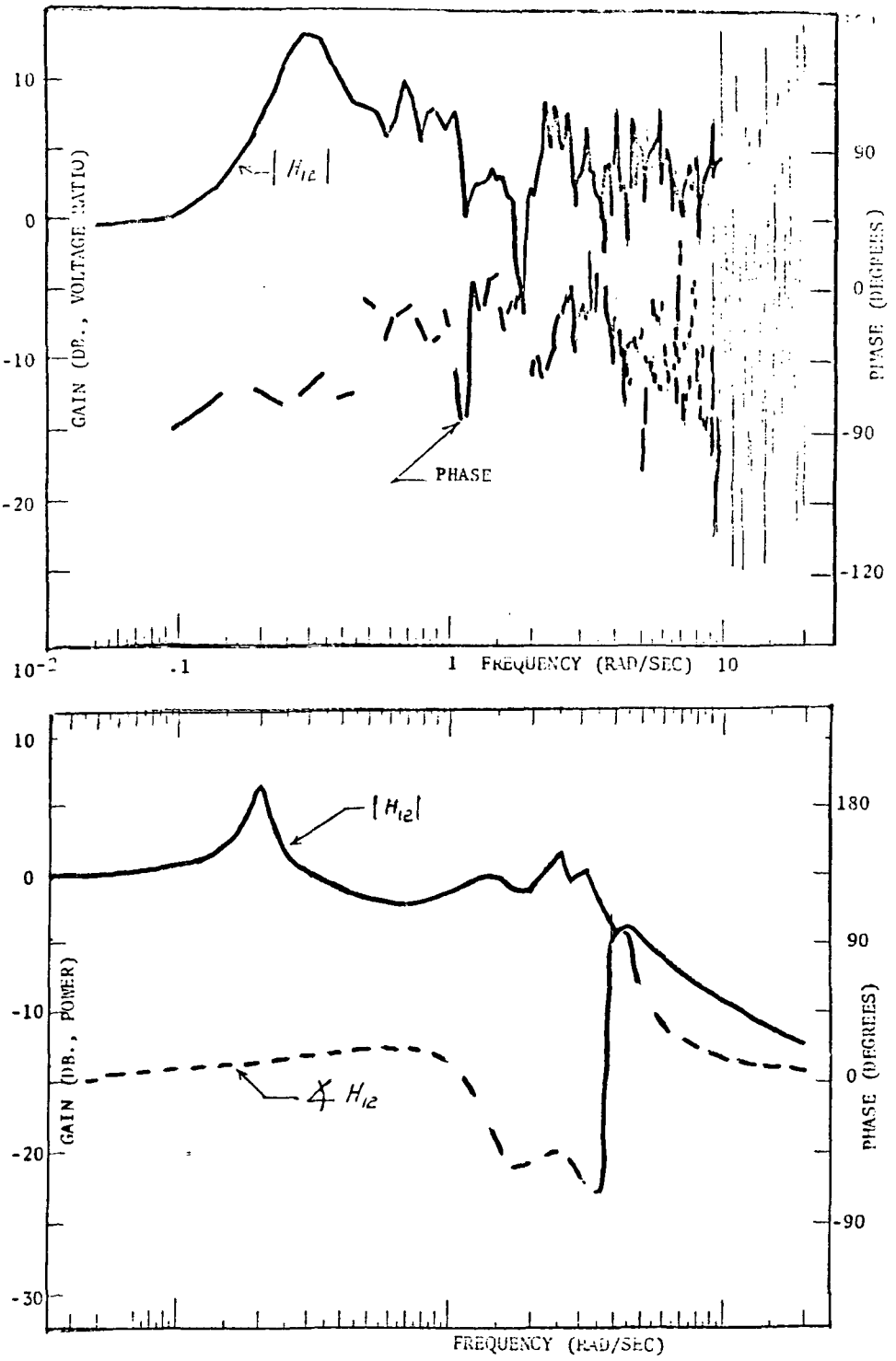

FIGURE 5.30. FACTORIZED H_{12} COMPARED TO NON-FACTORIZED H_{12}

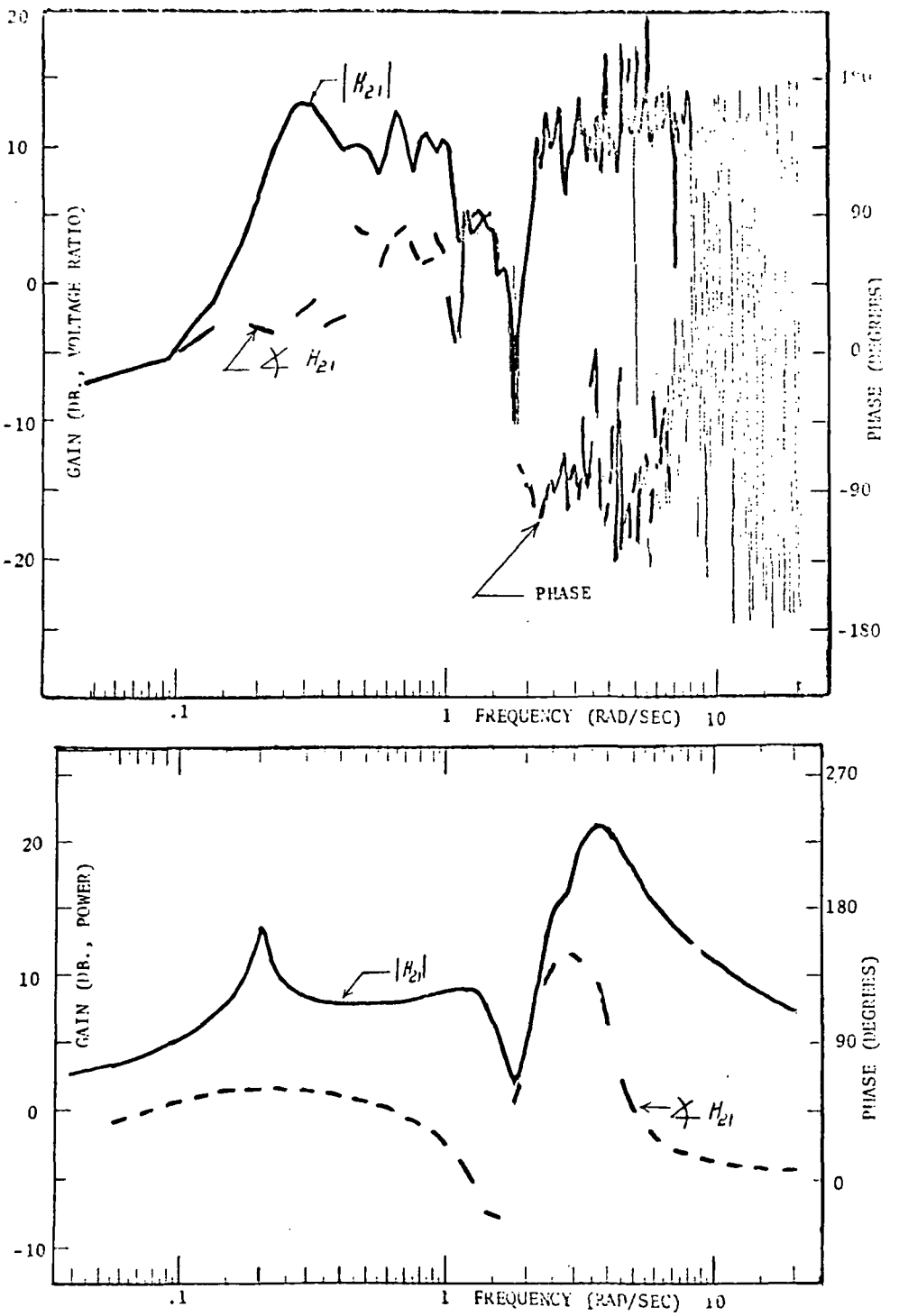

FIGURE 5.31. FACTORIZED H_{21} COMPARED TO NON-FACTORIZED H_{21}

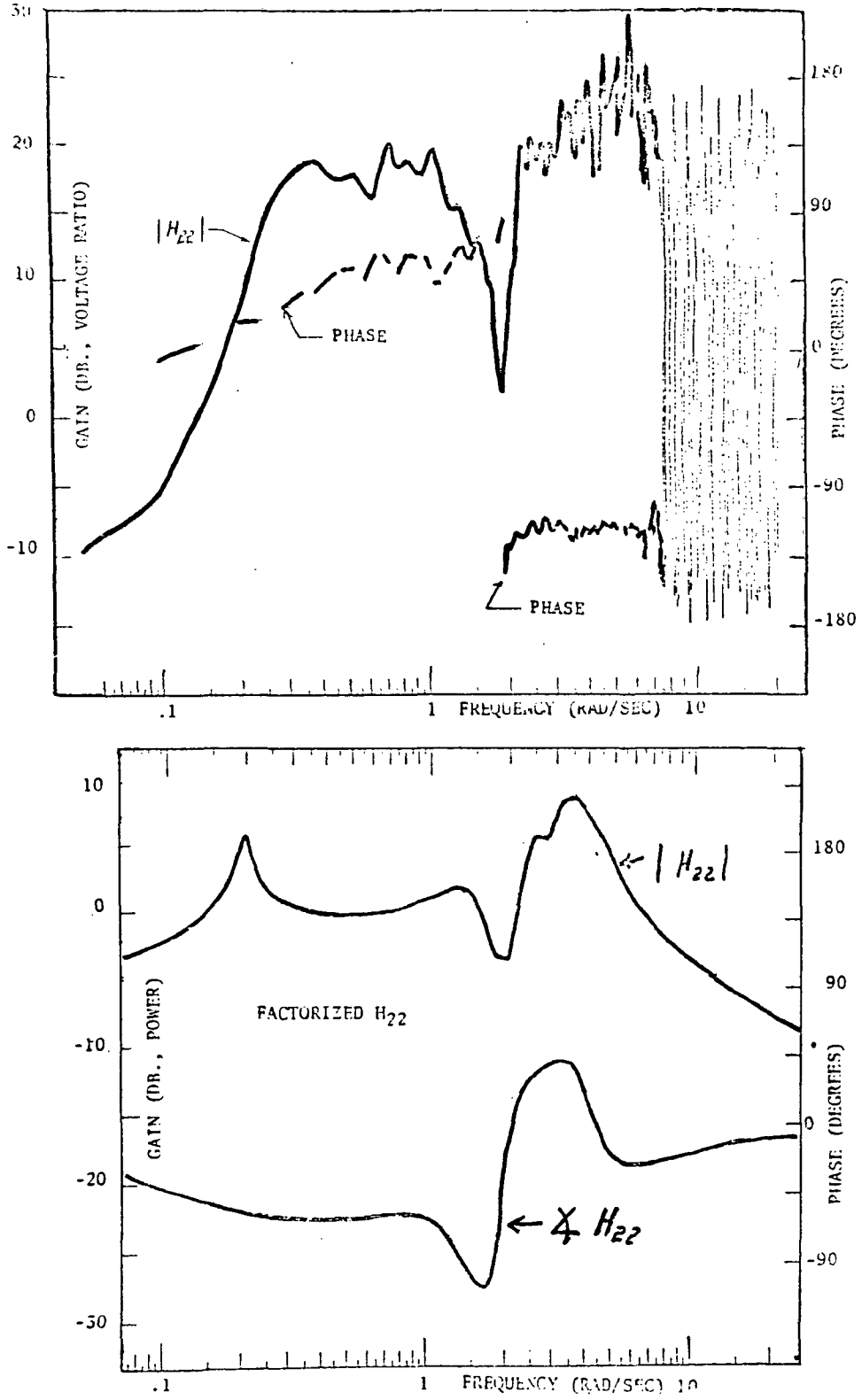

FIGURE 5.32 FACTORIZED H_{22} COMPARED TO NON-FACTORIZED H_{22}

6. CONCLUSIONS AND RECOMMENDATIONS

6.1 Introduction

The purpose of this program was to establish the practical usefulness of a matrix model of the human pilot. The ultimate objective was to run many variations on a two-controller roll tracking task in order to assess the effect, on the pilot model, of increasingly complex tasks. It was our intent that the degree of complexity attained would be governed by the success achieved as more and more complex situations were studied. The fundamental problems which surfaced in the early stages of the study ultimately restricted the effort, to only one configuration. However, the indications are that this particular roll tracking task is an excellent experiment for studying the two-controller task, since pilot activity with both the rudder and aileron was very significant.

The primary problem, which prevented a deeper penetration into the vector model, was the initial poor quality of the spectral estimates obtained in the scalar experiments. With time, we were successful in refining our algorithms to the point where high quality estimates were obtained over a limited frequency range. It was established that the limited frequency range was attributable to the presence of certain anomalies (roll up, break up, and roll down) in the estimates. It was theoretically demonstrated that these anomalies were due to the finite data length (coupled with the spectral properties of the (time domain) filtering algorithm) and not due to "noise", as was first suspected.

The useful frequency range achieved in the scalar cases was approximately $.2 < \omega < 60$ rad/sec. The power spectra used to compute the various transfer functions had a dynamic range on the order of 60 dB (power basis). However, when working with the higher-order aircraft equations of motion, the dynamic range was more on the order of 90 to 120 dB (power basis), resulting in a significant reduction in the useful frequency range. In the case of the pilot estimates generated using error and bank angle as the primary signals, the frequency range was approximately $.2 < \omega < 20$ rad/sec while the estimates for which error and yaw were the primary signals had a range of $.2 < \omega < 7$ rad/sec. It is apparent that even scalar tracking experiments, which work with realistic aircraft equations, will require improved computational algorithms if false results are to be avoided.

Preliminary estimates of the vector pilot model were generated for the two-controller experiment using assumptions which lead to a "decoupled" as well as a "coupled" model. These results were described in detail in Section 5. A primary result is that the coupled models had, in general, more power at lower frequencies than did the decoupled models. This was especially true in the case where the spectral matrix was generated using the error and yaw signals. Alternatively, in the case where the error and bank angles were used, one may take the position that there were no significant differences between the coupled and decoupled models.

There is a marked difference between the spectral factorized model and the non-factorized results. However, bear in mind that internal program checks on the factorization algorithm showed that the computer was having great difficulty in coping with the wide dynamic range of the input data. The explicit set of conclusions, drawn from the analytical analysis as well as the experimental results, are listed below. This is followed by a list of recommendations.

6.2 Summary of Theoretical Conclusions and Experimental Observations

(1) When working with finite lengths of data, the roll up, break up and roll down phenomena are to be expected.

(2) Ideally, knowing that the anomalies exist, one could use Equation (3.8) to predict the frequency band for which relatively undistorted estimates can be anticipated. In practice, the high order of the system dynamics makes this impractical.

(3) In general, one may anticipate distortion at a given frequency when the spectral window, which corresponds to a time domain filtering algorithm, is falling off more slowly than the true underlying spectral density.

(4) When ensemble averaging was used with no overt filtering (i.e., the square time window), the estimates obtained over as many as 134 estimates were considered unsatisfactory.

(5) The triangular filtering algorithm in time, which corresponds to a $\left(\frac{\sin \pi/2}{\pi/2}\right)^4$ spectral window, produced results which were an order of magnitude better when used in conjunction with ensemble averaging.

(6) Filtering alone, without ensemble averaging, also produced unsatisfactory results. However, with filtering, the number of ensembles necessary to produce acceptable results, was dramatically reduced. For example, the ensemble average across 5 with filtering produced an estimate of the K/S^2 dynamics which were noticeably superior to the ensemble alone estimate which used 134.

(7) Break up occurs if any of the cross and auto power spectra being estimated contain lightly damped modes.

(8) In general, the experimental variability in the estimation of cross spectral densities is greater than the variability observed in the estimation of auto spectra. For example, a typical observation is that ensemble averages across 5 or 10 on auto spectra have less variability than cross spectral averages across 100. Thus the estimation of dynamics and pilots variations of cross/cross, as opposed to ratios of cross/auto, are very likely to display more distortion (see Appendix B).

(9) Regardless of which time domain filtering algorithm is invoked, the estimate of the cross power between two independent random variables goes down only as $1/\sqrt{n}$, n being the number ensembled across.

(10) In the multi-controller case, a fundamental step is the computation of the determinant of the spectral matrix. It is imperative to recognize that all present computational algorithms automatically force a zero determinant if no ensemble average is employed. Thus, the number of ensembles necessary to reasonably approximate the determinant of the spectral matrix is a decisive factor in determining the utility of the vector approach for modeling the pilot. There is strong evidence that a diligent pursuit of the filtering - ensemble approach could get this number down to something on the order of 5.

(11) Using the $\left(\frac{\sin \pi/4}{\pi/4}\right)^8$ window, a useful frequency range of approximately $.2 < \omega < 60$ rad/sec. was achieved for the scalar tracking experiment. This range is not so much related to the scalar nature of the problem as it is to the dynamic range of the various spectra, which was as high as 60 dB in experiment 2.

(12) Using the $\left(\frac{\sin \pi/4}{\pi/4}\right)^8$ window, a useful frequency range of $.2 < \omega < 20$ rad/sec. was achieved in the vector roll tracking task when the input variables were error and roll angles. This was reduced to $2 < \omega < 7$ when the input variables were error and yaw. That is, the dynamic range of ψ seems to be far greater than that of roll.

(13) In general, the coupled models displayed more power at lower frequency than did the decoupled models. The decoupled models are computed by setting the off-diagonal terms in the spectral matrix equal to zero, resulting in a set of scalar definitions.

(14) In general, the coupled models which were generated using error and bank angle to specify the spectral matrix displayed far less power at low frequency than did the coupled models generated using error and yaw angle.

(15) The power in the transfer functions, making up the pilot model, are comparable in magnitude. In the case of the coupled models whose spectral matrix depends on error and yaw angle, the diagonal term (H_{11}, H_{22}) are slightly higher in power (5-10 dB) than are the off-diagonal terms (H_{12}, H_{21}).

(16) Along the lines of (17) above, there is less that can be said about the models which use error and bank angles as the input signals for the differences appear to be smaller. In fact, H_{21} produces a higher peak than any observed in the other three transfer functions.

(17) The differences between the various models appear to be quite significant. That is, it does make a difference whether one sets up decoupled or coupled models, spectral factorizes, or whether the model was generated using e , ψ as opposed to e , ϕ data.

(18) Care must be used in the experimental design in order to insure that the spectral matrix does not have a determinant which is identically equal to zero (see Section 5.3).

6.3 Recommendations

(1) The roll tracking experiment, as it was originally conceived, should be pursued. Consideration should be given to including turbulence inputs in the model in order to more closely approximate true flight conditions. Comparisons between the models produced by this vector approach should be compared with the results of other modeling approaches, using the roll tracking data in order to provide a common base.

(2) The algorithms for computing power spectra must be refined in order to cope with the increased dynamic range encountered when dealing with six degrees of freedom equations of motion. Ideally, we should strive for a usable frequency range of $.1 < \omega < 100$ rad/sec.

(3) The method for factorizing W-H equations given in Section 2.4 should be refined to the point where it can cope with the ill conditioned data associated with the wide dynamic ranges encountered using six degree of freedom aircraft equations of motion.

7. REFERENCES

1. Adams, J.J. and Bergeron, H.P., A Synthesis of Human Response in Closed-Loop Tracking Tasks, NASA Technical Note, NASA TND-4842, October 1968.

2. Schultz, W.C., Newell, F.D., and Whitbeck, R.F., A Study of Relationships Between Aircraft System Performance and Pilot Ratings, NASA Contractor Report NASA CR-1643 (CAL Report No. IH-2748-B-1), January 1970.

3. Chang, S.S.L., Synthesis of Optimum Control Systems, McGraw Hill Book Company, Inc., 1961.

4. Whitbeck, R.F., A Frequency Domain Approach to Linear Optimal Control, Journal of Aircraft, Vol. 5., No. 4, July-August 1968.

5. Youla, D.C., On the Factorization of Rational Matrices, IRE Transactions on Information Theory, July 1961.

6. Davis, M.C.. Factoring the Spectral Matrix, IEEE Transactions on Automatic Control, October 1963.

7. Meeker, J.I. and Hall, G.W., In Flight Evaluation of Lateral-Directional Handling Qualities for the Fighter Mission, AFFDL-TR-67-98, CAL Report No. BM-2238-F-2, July 1967.

Appendix A

THE RELATIONSHIP BETWEEN THE TIME AND SPECTRAL WINDOW

A.1 Introduction

This appendix gives a proof of Equation (3.8) of Section 3. The proof is simple and we were admittedly surprised not to find it in the literature. Since our search was not exhaustive we would not be surprised to find, at some future time, that such a proof already exists. However, in the event that it does not, the reason will probably be that most researchers have concentrated on the relationship between the lag window and the spectral window, ignoring the relationship between the time window and the spectral window.

As an introduction, the derivation is first given for the "square" time window, followed by the more general result.

A.2 Square Window

Given $x(t)$ and $y(t)$ are of finite length 2T:

$$\frac{1}{2T} X(-s)\, Y(s)\Big|_{s\to j\omega} = \frac{1}{2T}\int_{-T}^{T} x(t_2)\, e^{j\omega t_2}\, dt_2 \cdot \int_{-T}^{T} y(t_1)\, e^{-j\omega t_1}\, dt_1$$

$$= \frac{1}{2T}\int_{-T}^{T}\int_{-T}^{T} y(t_1)\, x(t_2)\, e^{-j(t_1-t_2)\,\omega}\, dt_2\, dt_1 \qquad \text{(A.1)}$$

Let $\tau = t_1 - t_2$ so that the domains of integration are as shown in the figure below.

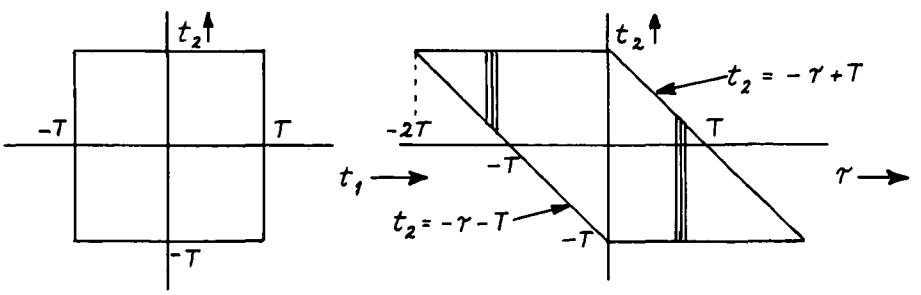

Figure A.1 DOMAINS OF INTEGRATION

$$\frac{1}{2T}\, X(-s)\, X(s) = \frac{1}{2T}\int_{-2T}^{0}\int_{-\tau-T}^{T} x(t_2)\, y(t_2+\tau) e^{-j\omega\tau}\, dt_2\, d\tau + \frac{1}{2T}\int_{0}^{2T}\int_{-T}^{-\tau+T} x(t_2)\, y(t_2+\tau) e^{-j\omega\tau}\, dt_2 d\tau$$

$$\frac{1}{2T}\, E\left\{X(-s)\, X(s)\right\} = \frac{1}{2T}\int_{-2T}^{0} (2T+\tau)\, R_{xY(\tau)}\, e^{-j\omega\tau}\, d\tau + \frac{1}{2T}\int_{0}^{2T} (2T-\tau)\, R_{xY(\tau)}\, e^{-j\omega\tau}\, d\tau \tag{A.2}$$

$$= \int_{-2T}^{2T}\left(1 - \frac{|\tau|}{2T}\right) R_{xY(\tau)}\, e^{-j\omega\tau}\, d\tau$$

However, the "lag window"

$$f(\tau) = \begin{cases} 1 - \frac{|\tau|}{2T} & |\tau| < T \\ 0 & |\tau| \geq T \end{cases}$$

can be found by convolving the square time window with itself, and, of course letting $t \rightarrow \tau$. This suggests that a more direct relationship between the time window and spectral window exists. This relationship will now be derived.

A.3 The General Time Window

Let

$$f(t) = \begin{cases} \text{even} & -T < t < T \\ 0 & |t| \geq T \end{cases} \tag{A.3}$$

and form

$$\frac{1}{2T}\, X_T(-s)\, X_T(s) = \frac{1}{2T}\int_{-T}^{T} y(t_1)\, f(t_1)\, e^{-j\omega t_1}\, dt_1 \cdot \int_{-T}^{T} x(t_2) f(t_2)\, e^{j\omega t_2}\, dt_2$$

$$= \frac{1}{2T}\int_{-\infty}^{\infty}\int_{-\infty}^{\infty} x(t_2)\, y(t_1)\, f(t_1) f(t_2)\, e^{-j(t_1-t_2)\omega}\, dt_2\, dt_1 \tag{A.4}$$

Let $\tau = t_1 - t_2$. Equation (A.4) becomes, after taking the expected value

$$\frac{1}{2T}\, E\left\{X_T(-s)\, X_T(s)\right\} = \frac{1}{2T}\int_{-\infty}^{\infty} R_{XY(\tau)} \left[\int_{-\infty}^{\infty} f(t_2)\, f(t_2+\tau)\, dt_2\right] e^{-j\omega\tau}\, d\tau \qquad (A.5)$$

$$= \frac{1}{2T}\int_{-\infty}^{\infty} R_{XY(\tau)} \left[\int_{-\infty}^{\infty} f(t)\, f(\tau - t)\, dt\right] e^{-j\omega\tau}\, d\tau$$

since $f(t)$ is an even function.

$$\therefore\ \frac{1}{2T}\, E\left\{X(-s)\, Y(s)\right\} = \frac{1}{2T}\int_{-\infty}^{\infty} R(\tau)\left[f(\tau) * f(\tau)\right] e^{-j\omega\tau}\, d\tau \qquad (A.6)$$

$$= \frac{1}{4\pi T}\int_{-\infty}^{\infty} \phi(\omega_1)\, F^2(\omega - \omega_1)\, d\omega$$

Appendix B

DEMONSTRATION OF ROLL UP, BREAK UP AND ROLL DOWN IN SPECTRAL ESTIMATES

B.1 Introduction

In Section 4, an experimental realization of the roll up, break up and roll down was demonstrated, for both Experiments 1 and 2. In this appendix, it will be demonstrated, via a series of illustrative examples that these phenomena are to be expected, and of course, can reduce considerably the frequency band over which acceptable spectral estimates are obtained.

The basic equation used in carrying through the analytical details is Equation 3.8 of Section 3. The examples are four in number. The first example demonstrates "roll-up," the second example demonstrates roll up, break up and roll down while the third example demonstrates the differences that can exist between estimation procedures which use only cross spectral densities as opposed to the more classic approach of a cross-to-an auto spectral density.

For convenience, the relationships which exist between the various domains, from Section 3, are repeated below.

$$\text{Let} \qquad f(t) = \begin{cases} \text{even} & -T < t < T \\ 0 & |t| \geq T \end{cases} \tag{B.1}$$

$$\hat{\phi}_{xY} = \frac{1}{2T} E\left\{X_T(-s)\, Y_T(s)\right\} = \frac{1}{2T}\int_{-\infty}^{\infty} R(\tau)\left[\int_{-\infty}^{\infty} f(t)\, f(\tau - t)\, dt\right] e^{-j\omega\tau}\, d\tau \tag{B.2}$$

$$= \frac{1}{4\pi T}\int_{-\infty}^{\infty} \phi_{(\omega_1)}\, F^2(\omega - \omega_1)\, d\omega \quad \text{when} \quad F(\omega) = \mathcal{F}\left[f(t)\right]$$

B.2 Example 1: Roll Up

Suppose we have the problem of estimating $\frac{1}{s+1}$, given two different input power spectra (Refer to Figure B-1). Let the input power spectra be

$$\phi_{1xx} = \frac{1}{-s^2+1} \qquad \text{or} \qquad \phi_{2xx} = \frac{1}{(-s^2+1)^2} \tag{B.3}$$

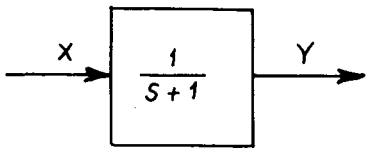

Figure B-1 ESTIMATION OF $\frac{1}{S+1}$

The estimate of $\frac{1}{S+1}$ is computed using the equation

$$\hat{H} = \frac{\frac{1}{2T} E\left\{X(-s)\, Y(s)\right\}}{\frac{1}{2T} E\left\{X(-s)\, X(s)\right\}} \tag{B.4}$$

That is, it is assumed that an infinite number of records, each of length $2T$, are available. The window used is the $\left(\frac{\sin x}{x}\right)^2$ window of Table I (Section 3). Carrying out the operation indicated in Equation B-4 after using Equation B-1 to compute the auto and cross power estimates, we obtain the Bode plots shown in Figure B-2. Observe that the estimate $\hat{H}$ looks like a zero over a pole for the $\frac{1}{-s^2+1}$ input while looking like a notch filter for the $\frac{1}{(-s^2+1)^2}$ input. This distortion is to be expected, since the true cross power, ϕ_{xy}, is dropping with a -3 slope at high frequencies while $\left(\frac{\sin x}{x}\right)^2$ spectral filter has only a -2 slope. For the $\left(\frac{\sin x/2}{x/2}\right)^4$ window of Table I, the estimate of $\hat{H}$ is quite precise for the $1/(-s^2+1)$ input. This input rolls off at -2 for high frequencies while $\left(\frac{\sin x/2}{x/2}\right)^4$ rolls off as -4 (ϕ_{xy} rolls off as -3). When the $\left(\frac{\sin x/2}{x/2}\right)^4$ spectral window is used with the $1/(-s^2+1)^2$ input (ϕ_{xy} rolls off as -5), the estimate $\hat{H}$ again contains a zero at about 200 rad/sec.*

This example clearly demonstrates the roll up phenomenon but does not show any breakup. The breakup does not occur because the dynamic modes in this particular example are associated with $\frac{1}{s+1}$, a well damped mode which leads to additional error terms like

$$\frac{e^{-2T}}{2T}\left[\sin 2\omega T - j\cos 2\omega T\right] \tag{B.5}$$

in the expression for $\hat{H}$. These terms, while present, do not show up in Figure B-2 since $e^{-2T}/2T \approx 10^{-63}$ when $2T = 100$ seconds. Thus the break up phenomenon will not be apparent when all the modes of the system are well damped (assuming reasonable record lengths like 100 seconds).

The next example will demonstrate the breakup in the estimator in addition to roll up and roll down.

---

* The results for the $\left(\frac{\sin x/2}{x/2}\right)^4$ window are not plotted.

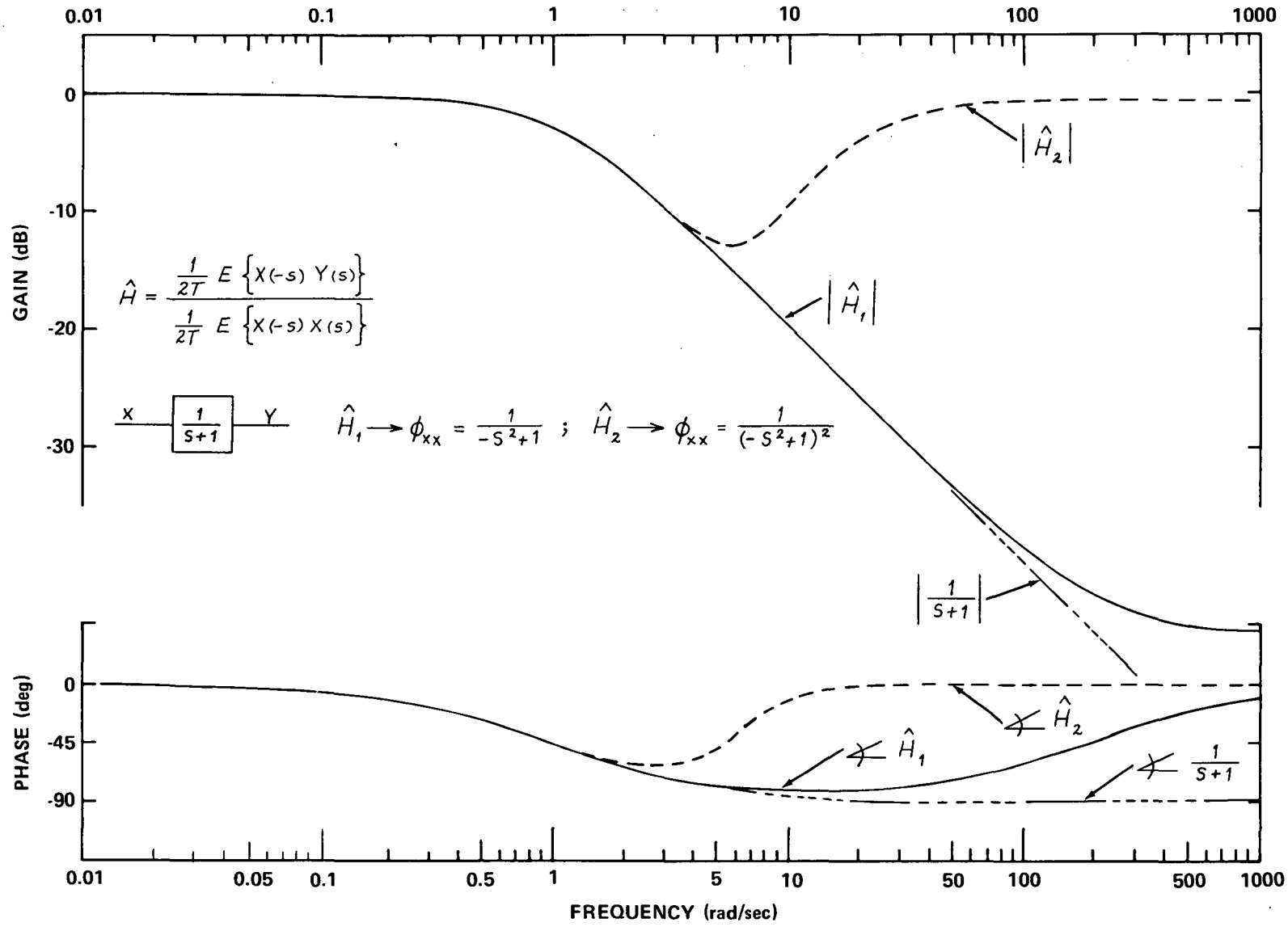

Figure B-2 ESTIMATION OF $\frac{1}{S+1}$ FOR RECORD LENGTHS OF 100 SECONDS

B.3 Example 2: Break Up, Roll Up and Roll Down

Estimate 1/S for $\phi_{xx} = \frac{1}{-s^2+1}$ (see Figure B-3)

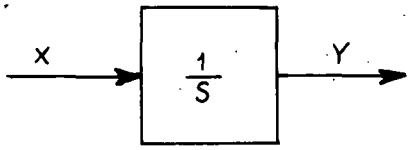

Figure B-3 ESTIMATION OF $1/S$

Again, using Equation B-1, the theoretical result for record lengths of $2T = 100$ seconds can be computed. The results are shown in the Bode plot of Figure B-4. Note the roll down at low frequency, where the $|\hat{H}|$ plot departs from the $\left|\frac{1}{S}\right|$ and approaches a constant as $\omega \to 0$. The breakup and roll up is shown by the envelope curves at high frequency, since the $\sin 2\omega T$ and $\cos 2\omega T$ terms cannot be conveniently plotted in the frequency range of interest. The breakup is most violent in the phase plot.

B.4 Example 3: Roll Down, Bandpass Input Spectra

The next example (see Figure B-5) demonstrate the presence of roll down without either the breakup or roll up phenomenon. The Bode plots are shown in Figure B-6. Even though we are estimating $1/S$, breakup is not apparent because the true auto and cross spectra,

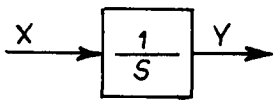

Figure B-5 ESTIMATION OF $1/S$ WITH A BANDPASS INPUT SPECTRA

$$\phi_{xx} = \frac{-16\,s^2}{(-s^2+1)(-s^2+9)}$$

$$\phi_{xy} = \frac{-16\,s}{(-s^2+1)(-s^2+9)} \qquad \text{(B.6)}$$

do not have any lightly damped modes.

Note that the $\left(\frac{\sin x/2}{x/2}\right)^4$ filter has decreased the roll down break frequency by about two octaves. The extremely pronounced roll down demonstrated in this example appear to be typical of what occurs when dealing with band pass input spectra. This band pass power spectra is representative of what is encountered at the various points of the block diagram which defines the subject "M" experiment (Experiment #2).

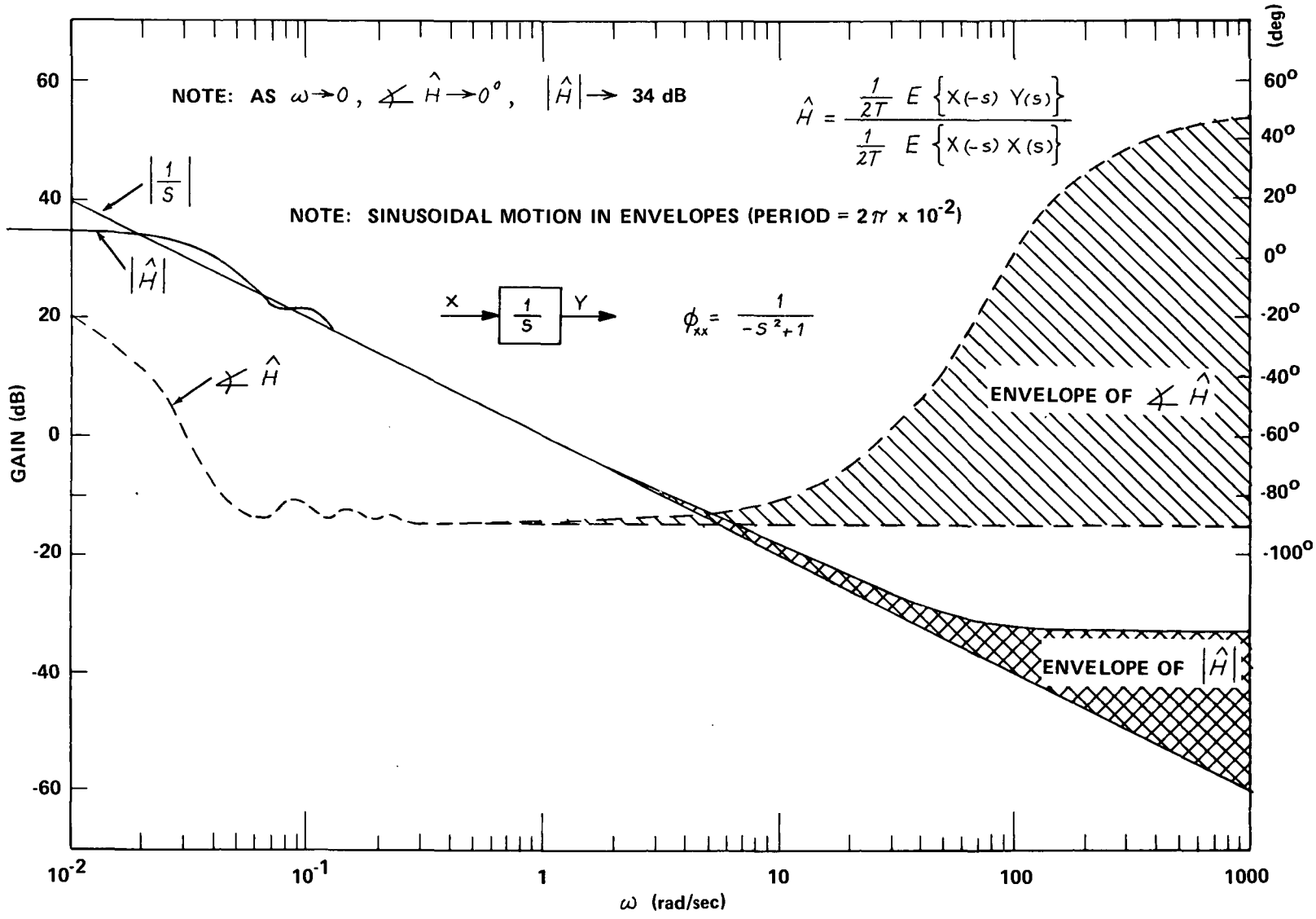

Figure B-4 ESTIMATION OF 1/S FOR RECORD LENGTHS OF 100 SECONDS

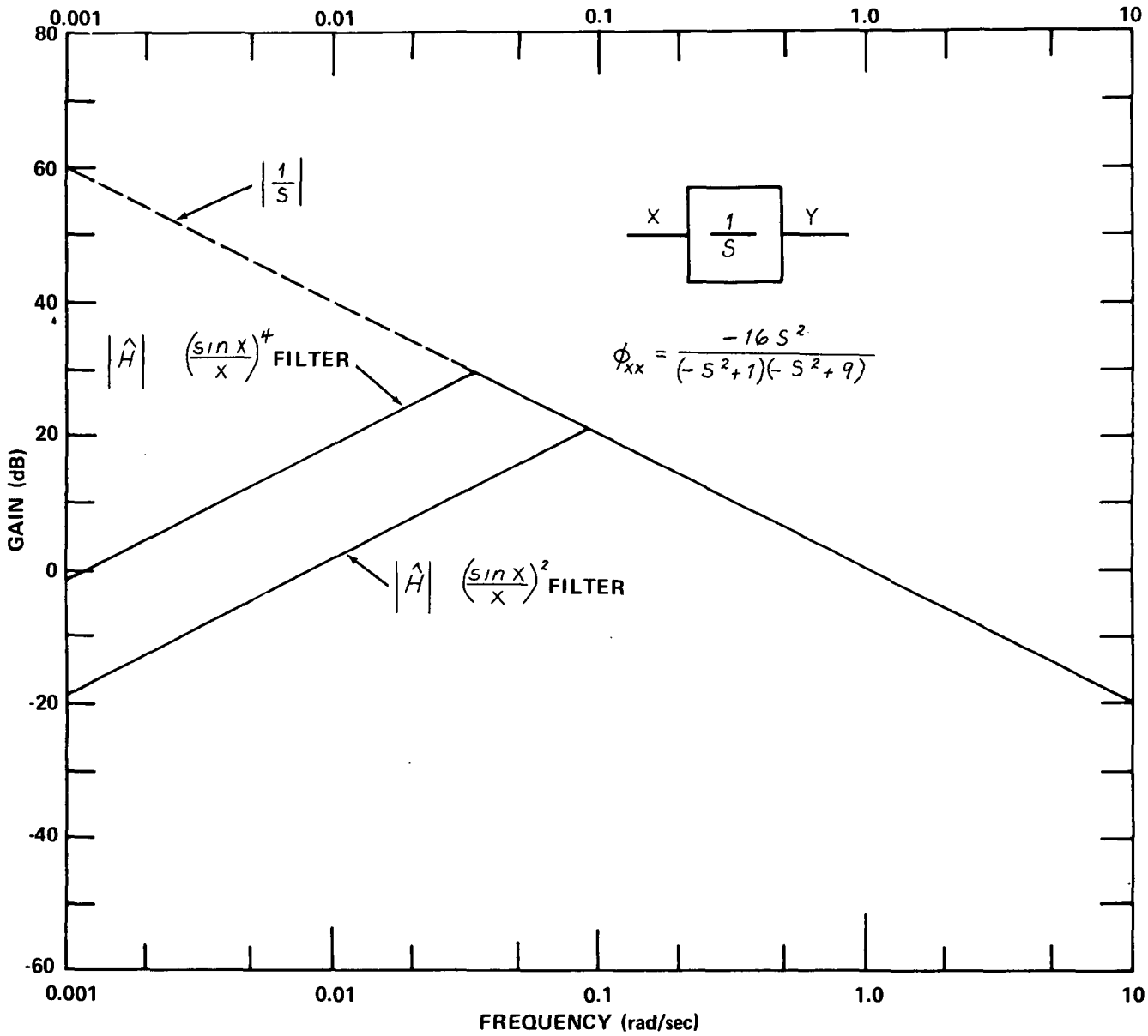

Figure B-6 ESTIMATION OF 1/S FOR BANDPASS INPUT SPECTRA

B.5 Estimation Using Ratios of Cross Spectra

The estimates given in these theoretical examples have been computed using the ratio of a cross-to an auto-spectra. As a general rule, it is the estimate of the cross spectra that introduces the greatest error into the modeling process. Hence one may expect the distortion to be greater in those estimators which are computed using only ratios of cross spectra, a fact which has been verified experimentally in the single controller roll tracking task (Experiment #1). In that experiment, the $\frac{K}{S(S+2)}$ dynamics were estimated using

$$\hat{H} = \frac{\phi_{\delta\phi}}{\phi_{\delta\delta}} \tag{B.7}$$

while the pilot was estimated using the equation

$$\text{Pilot} = \frac{\phi_{D\delta}}{\phi_{DE}} \tag{B.8}$$

The estimate of $\frac{K}{S(S+2)}$ is shown in Figure B-7 while the pilot estimate is shown in Figure B-8. Observe that break up and roll up occurs in the estimate of the pilot at around ω = 15 rad/sec, while it does not occur in the estimate of $\frac{K}{S(S+2)}$ until about 60 rad/sec. Also observe that the break up and roll up are nowhere near as severe in the estimate of $\frac{K}{S(S+2)}$ as it is in the estimate of the pilot, which is computed using the ratio of two cross spectras. Indeed, had we not known about the roll up and break up phenomonon, out fits to the pilot would probably have been something like the dashed lines in Figure B-8. That is, a zero at ω = 20 rad/sec and/or an added +2 break at ω = 60 rad/sec. Being aware of the possibility of roll up and break up, a more realistic estimate would be given by the solid line in Figure B-8.

B.6 Example #4: Estimation of $1/S$ In A Unity Feedback System

This difference in the estimation procedure, between ratio of cross/auto and cross/cross can also be demonstrated with a simple theoretical example. Consider the feedback system depicted in Figure B-9.

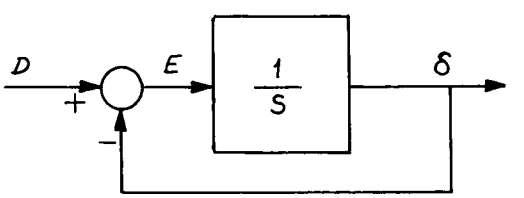

Figure B-9 ESTIMATION OF $1/S$ IN A FEEDBACK LOOP

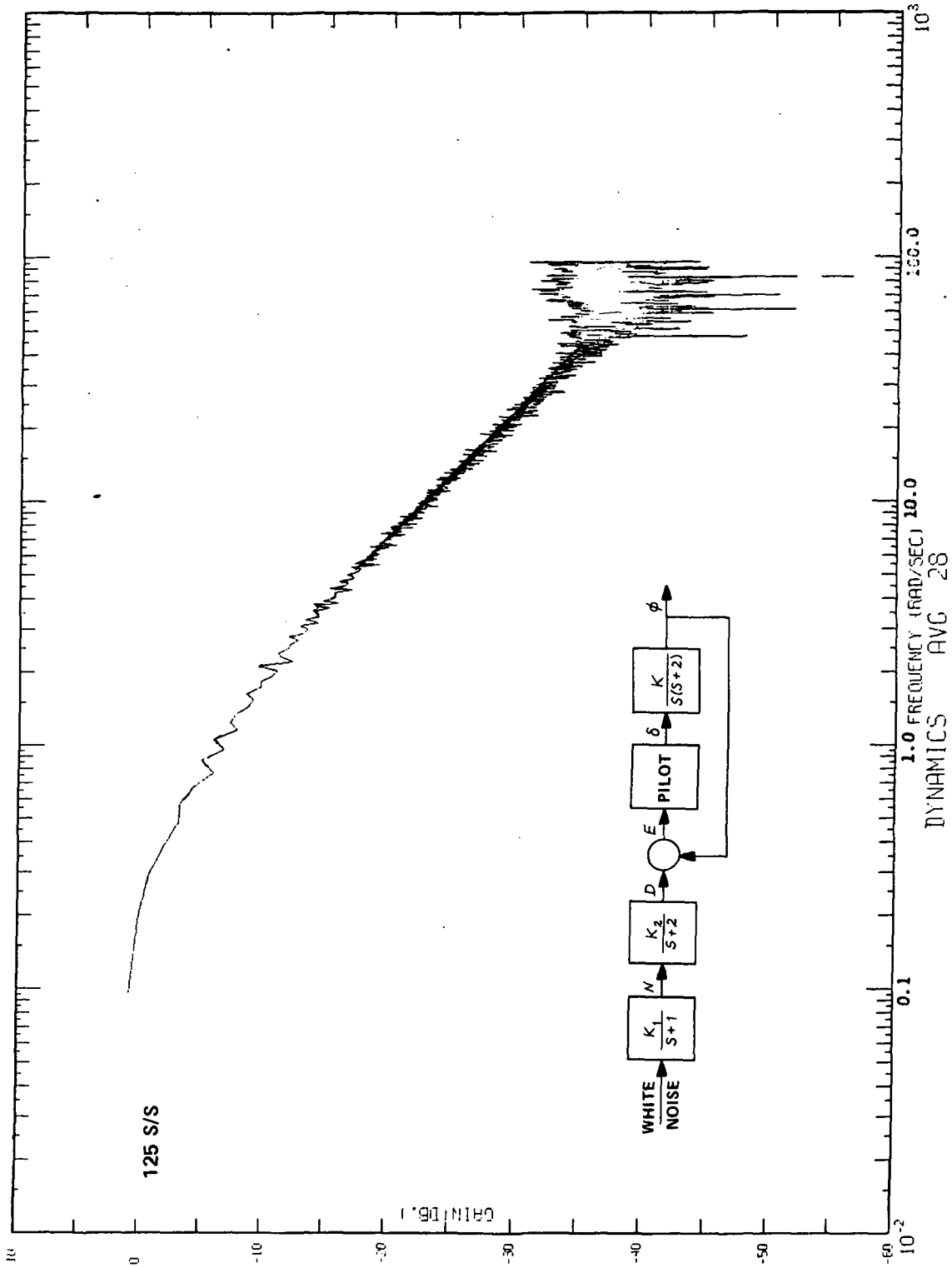

Figure B-7 SINGLE CONTROLLER ROLL TRACKING EXPERIMENT, FILTER AND ENSEMBLE AVERAGE

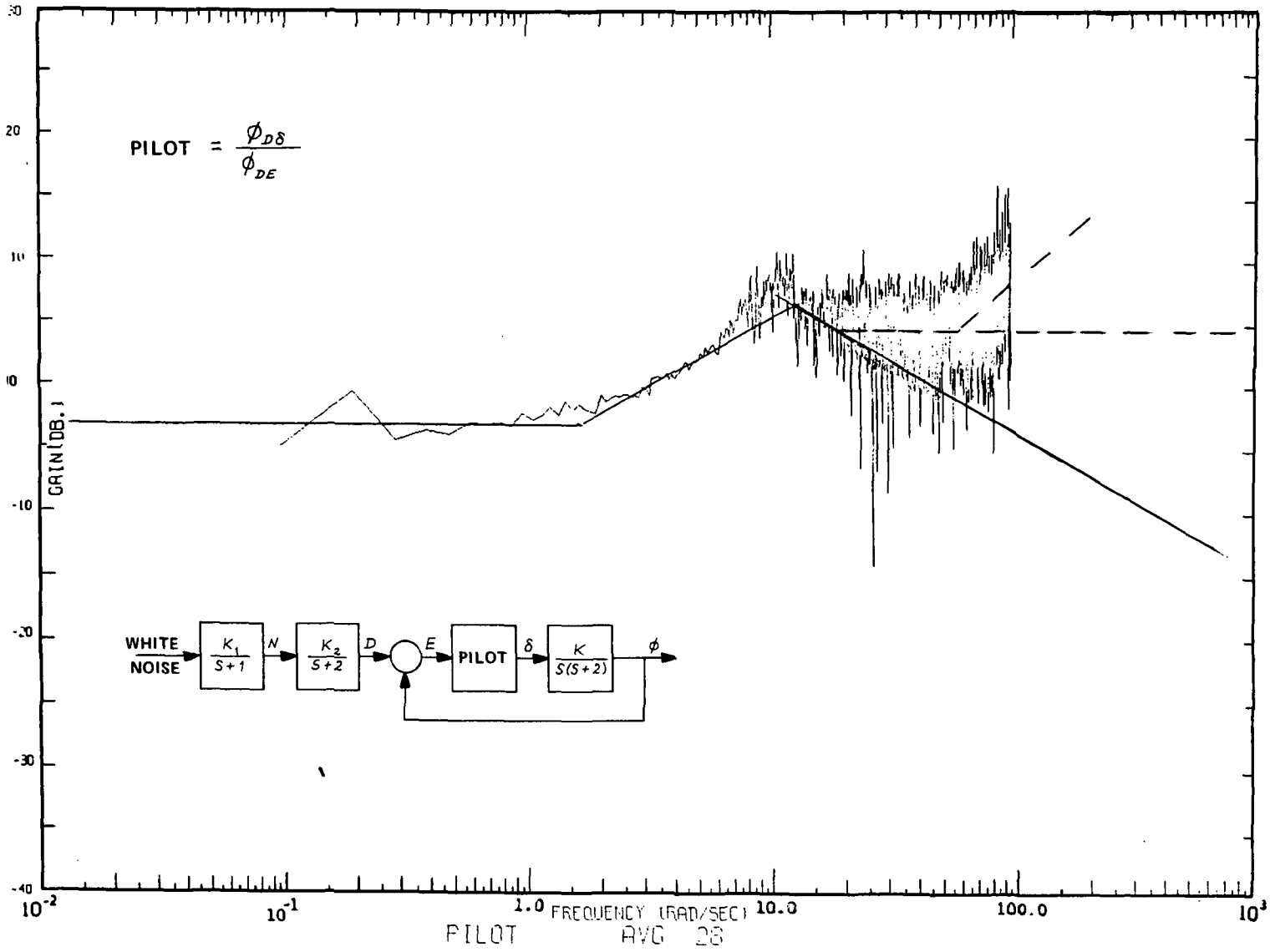

Figure B-8 SINGLE CONTROLLER ROLL TRACKING EXPERIMENT, FILTER AND ENSEMBLE AVERAGING

Suppose the task is to estimate $1/S$ in two different ways, using either

$$\hat{H}_1 = \frac{\phi_{E\delta}}{\phi_{EE}} \tag{B.9}$$

or

$$\hat{H}_2 = \frac{\phi_{D\delta}}{\phi_{DE}} \tag{B.10}$$

Let

$$\phi_{DD} = \frac{16}{-S^2+9} \tag{B.11}$$

then

$$\phi_{D\delta} = \frac{16}{(S+1)(-S^2+9)}, \qquad \phi_{DE} = \frac{16S}{(S+1)(-S^2+9)} \tag{B.12}$$

and

$$\phi_{E\delta} = \frac{-16S}{(-S^2+1)(-S^2+9)}, \qquad \phi_{EE} = \frac{-16S^2}{(-S^2+1)(-S^2+9)} \tag{B.13}$$

Using the $\left(\frac{\sin x}{x}\right)^2$ filter and Equation B-1, the theoretical estimates for $\hat{H}$ can be computed. Very good approximations to these estimates are shown in Figure B-10.

While the difference is not spectacular for this simple example, they are, nevertheless significant, in that low frequency roll down occurs later for $\hat{H}_2$ (a detriment) and, at the same time $\hat{H}_2$ has a high frequency roll up where $\hat{H}_1$ has none.

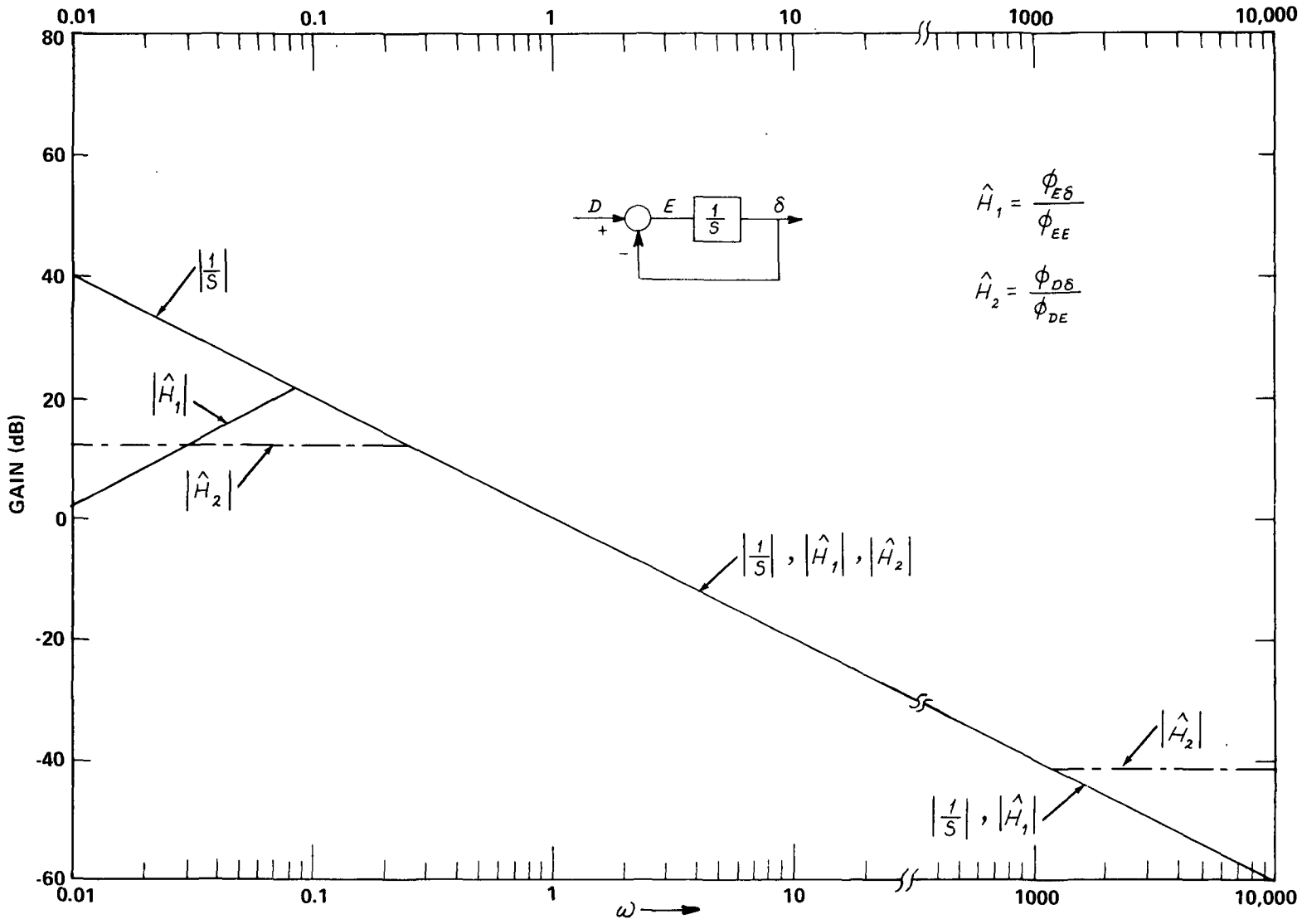

Figure B-10 ESTIMATION OF 1/S USING CROSS/AUTO AND CROSS/CROSS

Appendix C

THE MAGNITUDE OF THE CROSS SPECTRAL ESTIMATOR FOR TWO INDEPENDENT SIGNALS USING FINITE LENGTHS OF DATA

Reference has been made, in Section 4 of this report, to the fact that the magnitude of the cross power spectral estimator will be non zero even when the signals considered are independent. In this appendix, a relatively simple proof of that statement will be given. A more complete proof requires the use of vector notation and identities that would require a very lengthy development, and for that reason, will not be presented here.

Suppose there are two independent time signals $x(t)$ and $y(t)$ for which record lengths of reasonable lengths exist. Suppose further that the data is taken in the following manner:

(1) Take a record of the signal x which is 2T seconds long.

(2) After waiting a reasonable period of time, take another record 2T seconds long. It will now be assumed that record #1 and record #2 are decorrelated.

(3) Repeat the above procedure until n (essentially) decorrelated records, each of length 2T seconds, have been taken.

(4) Repeat the above steps for the $y(t)$ record.

(5) Using the Fast Fourier Transform, take the truncated Fourier transform of each record piece.

Thus

$$\mathcal{F}\left\{x_1(t)\right\} = X_1(\omega) = A_1(\omega) - j\,B_1(\omega) \tag{C.1}$$

For simplicity of presentation, the functional dependence on ω will be suppressed. Therefore a set of transformed signals of the form

$$\left.\begin{aligned} X_1 &= A_1 - j\,B_1, \quad X_2 = A_2 - j\,B_2, \quad \ldots, \quad X_n = A_n - j\,B_n \\ Y_1 &= C_1 - j\,D_1, \quad Y_2 = C_2 - j\,D_2, \quad \ldots, \quad Y_n = C_n - j\,D_n \end{aligned}\right\} \tag{C.2}$$

are available.

By hypothesis, the mean of each signal is zero. Therefore the mean values are

$$E\left\{A_i\right\} = E\left\{B_i\right\} = E\left\{C_i\right\} = E\left\{D_i\right\} = 0 \tag{C.3}$$

Further, the expressions for the variance are

$$V\left\{A_i\right\} = \sigma_A^2 \ , \quad V(B_i) = \sigma_B^2 \ , \quad V(C_i) = \sigma_C^2 \ , \quad V(D_i) = \sigma_D^2 \tag{C.4}$$

Because $x(t)$ and $y(t)$ are independent

$$E\left\{A_i B_j C_n D_m\right\} = E\left\{A_i\right\} \cdot E\left\{B_j\right\} \cdot E\left\{C_n\right\} \cdot E\left\{D_m\right\} = 0 \tag{C.5}$$

First consider only X_1 and Y_1, find $\hat{\phi}_{x_1 Y_1}$ and derive its statistics.

$$\begin{aligned} \hat{\phi}_{x_1 Y_1} &= \frac{1}{2T} X_1(-s) Y_1(s) = \frac{1}{2T}\left\{(A_1 + jB_1)(C_1 - jD_1)\right\} \\ &= \frac{1}{2T}\left\{(A_1 C_1 + B_1 D_1) - j(A_1 D_1 - B_1 C_1)\right\} \end{aligned} \tag{C.6}$$

or

$$\hat{\phi}_{x_1 Y_1} = \frac{1}{2T}\left\{\alpha_1 - j\beta_1\right\} \tag{C.7}$$

The magnitude of the cross spectral estimator is

$$\begin{aligned} \left|\hat{\phi}_{x_1 Y_1}\right| &= \sqrt{\frac{1}{2T} X(-s) Y(s) \cdot \frac{1}{2T} X(s) Y(-s)} = \sqrt{\frac{1}{4T^2}\left(\alpha_1^2 + \beta_1^2\right)} \\ &= \sqrt{\frac{1}{4T^2}\left(A_1^2 C_1^2 + B_1^2 D_1^2 + A_1^2 D_1^2 + B_1^2 C_1^2\right)} \end{aligned} \tag{C.8}$$

Since

$$\left.\begin{aligned} E\left\{\alpha_1\right\} &= E\left\{A_1 C_1 + B_1 D_1\right\} = 0 \\ E\left\{\beta_1\right\} &= E\left\{A_1 D_1 - B_1 C_1\right\} = 0 \end{aligned}\right\} \tag{C.9}$$

and

$$\left.\begin{aligned} V(\alpha_1) &= V(A_1) V(C_1) + V(B_1) V(D_1) \\ V(\beta_1) &= V(A_1) V(D_1) + V(B_1) V(C_1) \end{aligned}\right\} , \tag{C.10}$$

$$E\left\{\left|\hat{\phi}_{x_1y_1}\right|^2\right\} = E\left\{\hat{\phi}_{x_1y_1} \cdot \hat{\phi}_{y_1x_1}\right\} = \frac{1}{4T^2}\left(V(\alpha_1) + V(\beta_1)\right)$$

$$= \frac{1}{4T^2}\left(V(A_1)\,V(C_1) + V(B_1)\,V(D_1) + V(A_1)\,V(D_1) + V(B_1)\,V(C_1)\right) \tag{C.11}$$

Note that the expected value of the sum of the squares is easy to find. However, finding the expectation of the square root of the sum of the squares is extremely difficult. In a like manner, the variance of the sum of square or the square root of the sum of square are also difficult to find. We must be content, for the present, with the one statistic readily available, namely,

$$E\left\{\left|\phi_{x_1y_1}\right|^2\right\} = \frac{1}{4T^2}\left[V(\alpha_1) + V(\beta_1)\right] \tag{C.12}$$

Before proceeding to the statistics for an average across n, a short diversion, in order to express $\left|\hat{\phi}_{x_1y_1}\right|$ in terms of $\hat{\phi}_{x_1x_1}$ and $\phi_{y_1y_2}$, is in order.

Consider

$$\frac{1}{2T}\,X_1(-s)\,X_1(s) = \frac{1}{2T}\left(A_1^2 + B_1^2\right) \tag{C.13}$$

$$\frac{1}{2T}\,Y_1(-s)\,Y_1(s) = \frac{1}{2T}\left(C_1^2 + D_1^2\right) \tag{C.14}$$

so that

$$\sqrt{\phi_{x_1x_1} \cdot \phi_{y_1y_1}} = \sqrt{\frac{1}{4T^2}\,X_1(-s)\,X_1(s)\,Y_1(-s)\,Y_1(s)}$$

$$= \sqrt{\frac{1}{4T^2}\left(A_1^2C_1^2 + B_1^2C_1^2 + B_1^2D_1^2 + A_1^2D_1^2\right)} = \left|\hat{\phi}_{x_1y_1}\right| \tag{C.15}$$

Equation (C-15) says that, with no averaging, the magnitude of the cross spectral estimator is simply the square root of the product of the auto spectral estimators.

Returning to the problem of averaging across n estimates, generate

$$\alpha_1 - j\beta_1 \,, \quad \alpha_2 - j\beta_2 \,, \quad \ldots \,, \quad \alpha_n - j\beta_n \tag{C.16}$$

and form

$$\bar{\alpha} = \frac{1}{n}\sum_{i=1}^{n} \alpha_i \quad , \qquad \bar{\beta} = \frac{1}{n}\sum_{i=1}^{n} \beta_1 \tag{C.17}$$

Since $x(t)$ and $y(t)$ are independent, and if we assume that the "decorrelated" pieces of $x(t)$ (and $y(t)$) are pairwise independent, then

$$E\{\bar{\alpha}\} = 0 \,, \quad E\{\bar{\beta}\} \tag{C.18}$$

$$V(\bar{\alpha}) = \frac{V(\alpha_1)}{n} \,, \quad V(\bar{\beta}) = \frac{V(\beta_1)}{n} \tag{C.19}$$

Therefore, using Equation (C-18) and (C-19),

$$E\left\{\left|\phi_{\frac{1}{n}\sum x_1 Y_1}\right|^2\right\} = \frac{E\left\{\left|\hat{\phi}_{x_1 Y_1}\right|^2\right\}}{n} \tag{C.20}$$

The implication of Equation (C-20) is that the square of the magnitude of the cross spectral estimator goes down as $1/n$, where n is the number of estimates ensembled across. It is further implied that the magnitude of the cross spectral estimator should go down as $1/\sqrt{n}$, but this cannot be proven (or disproved) without first finding the statistics for the magnitude of $\hat{\phi}_{\frac{1}{n}\sum x_1 Y_1}$. This is a difficult task involving higher order moments than the second (a further complication is that the joint probability density function of the α's and β's is required and presently, the only density functions available to us are the marginals).

At any rate, the important point is that the magnitude of the cross spectral estimator will be non-zero for finite data lengths even when the random signals are independent, going down roughly as $1/\sqrt{n}$.

Using vector notation and identities, one can prove the $1/\sqrt{n}$ result, given that the sum of certain non gaussian variables approach a gaussian (a reasonable assumption).

Appendix D

DIGITAL SPECTRAL ANALYSIS PROCEDURE

D.1 Introduction

In this study, digital algorithms which represent the following continuous equations were used.

$$\hat{\phi}_{xx} = \frac{1}{N}\sum_{i=1}^{N} X_i(-j\omega)\, X_i(j\omega) = \frac{1}{N}\sum_{i=1}^{N} \hat{\phi}_{i\,xx} \tag{D.1}$$

$$\hat{\phi}_{xY} = \frac{1}{N}\sum_{i=1}^{N} X_i(-j\omega)\, Y_i(j\omega) = \frac{1}{N}\sum_{i=1}^{N} \hat{\phi}_{i\,xY} \tag{D.2}$$

where

$$X_i(j\omega) = \int_{-T}^{T} x_i(t)\, e^{-j\omega t}\, dt \tag{D.3}$$

$$Y_i(j\omega) = \int_{-T}^{T} y_i(t)\, e^{-j\omega t}\, dt \tag{D.4}$$

That is, the discrete auto spectral estimator is given by

$$\hat{\phi}_{i\,xx}(f_k) = \frac{\Delta}{N}\left|\sum_{\ell=-n}^{n-1} x_\ell\, e^{-j2\pi f_k \Delta \ell}\right|^2 \tag{D.5}$$

where $2\pi f_k \Delta \ell = \frac{2\pi k}{N}\ell$ (there are $2n = N$ samples).

The cross spectral estimator is given by

$$\hat{\phi}_{i\,xY}(f_k) = \frac{\Delta}{N}\left[\sum_{h=-n}^{n-1} x_h\, e^{+j2\pi f_k h\Delta}\right]\left[\sum_{\ell=-n}^{n-1} x_\ell\, e^{-j2\pi f_k \Delta \ell}\right] \tag{D.6}$$

D.2 Vector Notation

Equation (D-5) and (D-6) can be expressed more compactly using vector notation.

Let

$$\left.\begin{array}{lll} \cos\frac{2\pi k}{N}(-n)=\lambda_1 & \sin\frac{2\pi k}{N}(-n)=\alpha_1 & x_{-n}=X_1 \\ \cos\frac{2\pi k}{N}(-n+1)=\lambda_2 & \sin\frac{2\pi k}{N}(-n+1)=\alpha_2 & x_{-n+1}=X_2 \\ \vdots & \vdots & \vdots \\ \cos\frac{2\pi k}{N}(n-1)=\lambda_N & \sin\frac{2\pi k}{N}(n-1)=\alpha_N & x_{n-1}=X_N \end{array}\right\} \quad (D.7)$$

Equation D-5 becomes

$$\hat{\phi}_{xx_i} = X'\left[\frac{\Delta}{N}(\lambda\lambda' + \alpha\alpha')\right]X \quad (D.8)$$

where

$$\lambda' = \left[\lambda_1 \lambda_2 \ldots \lambda_N\right], \quad \alpha' = \left[\alpha_1 \alpha_2 \ldots \alpha_N\right], \quad X' = \left[x_1 x_2 \ldots x_N\right]$$

In a like manner, Equation (D-6) can be expressed as

$$\hat{\phi}_{xy_i} = X'\left[\frac{\Delta}{N}(\lambda\lambda' + \alpha\alpha')\right]Y - jX'\left[\frac{\Delta}{N}(\lambda\alpha' - \alpha\lambda')\right]Y \quad (D.9)$$

where

$$Y' = \left[y_1 y_2 \ldots y_N\right]$$

Equations (D-8) and (D-9) are computationally implemented through the use of the Fast Fourier Transform.

D.3 Computation Procedure

The data was collected in both analog and digital form, being recorded on BRUSH MARK 200 pen recorders and, simultaneously in digital format via the CAL digital recording facility (COREC).

The hardware of COREC consists of 3 data acquisition units and 4 tape transports.

The data acquisition units accept analog or digital inputs and produce digital outputs suitable for recording on the digital tape transports. The analog inputs are sampled sequentially and converted to digital signals by a high speed A/D converter.

Various combinations of tape speeds and packing densities determine the rates at which the transports can accept data from the data acquisition units. These rates, combined with the number of variables determine the permissible sampling rates for each variable. For 5 variables plus a digital count channel, the choices of sampling rates near 100 samples/second are 58 S/S, 125 S/S and 350 S/S. The rate of 125 S/S was selected.

The steps in the data handling procedure are

(1) Record data on digital tape using COREC hardware.

(2) Use blocking program (part of COREC software) to break tape into lengths that can be handled by normal computer I/O subroutines (32,760 bytes is the maximum physical record for normal tapes on IBM 370 computers, our data records were around 203,000 bytes).

(3) Convert the data to normal floating point numbers while checking for errors in the input data (missed bytes because of bad spots on tape or hardware problems). This step uses the general purpose COREC program.

(4) Special program to arrange data into arrays by variable, for efficient I/O.

(5) Multiply each piece of record, of length $2T$ seconds, by the desired time window.

(6) Use Fast Fourier Transform.

(7) Sum real and imaginary parts of each spectral estimate with values for these variables and frequency from previous records (ensemble average).

(8) Compute magnitude and phase for bode plots.

D.4 Amount of Data

A typical experiment No. 2 run produced the following amount of data:

16,384 samples from each of 5 analog channels,
plus count for error detecting.

$\therefore$ 6(16,384) = 98304 data words recorded.

Since there are 2 bytes/word, this gives 196,608 bytes of data per record or, since 27 records were recorded, 5,238,416 bytes recorded. Since there are 6 bits/byte, the total number of bits is 31,430,496.